A Computer Simulation of ST Segment Shift in Myocardial Ischaemia

Chuan Yong Li

BSc., MSc.

Submitted in fulfilment of the requirements for the degree of

Doctor of Philosophy

Division of Clinical Sciences

University of Tasmania

April 7, 1998

Declaration

The investigations described in this thesis constitute my own work. This thesis contains no material which has been accepted for the award of any other higher degree or graduate diploma in any tertiary institution. To the best of my knowledge and belief, this thesis contains no material previously published or written by another person, except where due acknowledgement and reference are made in the text of the thesis.

Signed: 

Date: October, 1997

This thesis may be made available for loan and limited copying in accordance with the Copyright Act 1968.

Signed: 

Date: October, 1997

Abstract

This thesis presents a computer simulation of electrocardiographic ST segment shift in myocardial ischaemia to elucidate the source of ST changes in both subendocardial and transmural ischaemia.

A realistic torso model was constructed, in which the myocardium was represented by the bidomain model. In a normal heart, there is no current source during the ST segment and there is a minimal ST potential field. With myocardial ischaemia, the transmembrane potential of ischaemic cells changes, allowing current to flow between the ischaemic and nonischaemic regions, which generates ST segment shift. The ischaemic regions included in the model were those measured using fluorescent microspheres in a sheep model, and the transmembrane potentials were generated from values extracted from the literature.

Subendocardial ischaemia in the territory supplied by either the left anterior descending coronary artery (LAD) or left circumflex coronary artery (LCX) was simulated, showing that the current source is produced at the ischaemic boundary, with the positive source at the ischaemic and the negative source at the normal side of the boundary. At the intramural boundary, the current flow is highly localised around the boundary, while at the lateral boundary normal to the endocardium, current flows both by crossing the boundary and through the intracavity blood. Epicardial ST depression is seen over the lateral boundary while endocardial ST elevation appears over the ischaemic region. The source in the septum is not seen on the epicardium because it is surrounded by highly conductive blood. LAD and LCX ischaemia share the lateral boundary and produce a similar pattern of epicardial ST depression on the left free wall.

Transmural ischaemia of varying size was studied. Transmural ischaemia of a small region produces localised ST elevation over the ischaemic region with little ST depression elsewhere on the epicardium and a similar pattern on the endocardium with a much lower amplitude. Ischaemia in either the LAD or LCX territory produces a strong dipole on the epicardium over the left lateral region, with ST elevation on the ischaemic region and ST depression on the nonischaemic region. ST depression in transmural ischaemia is generated with ST elevation and is an integral part of the source, thus it is inevitable that ST depression on the body surface will be generated during ischaemia of a large region of myocardium.

The effect of the myocardial anisotropy on ST potentials was also studied. The inclusion of myocardial anisotropy produces results somewhat closer to measured results in animal models.

In conclusion, the bidomain model is successful in modelling the ST potential and the simulation in this study successfully explains the observations of ST segment shift during myocardial ischaemia. It provides useful guidance for the clinical interpretation of ST segment shift.

Acknowledgements

I wish to sincerely thank my supervisor, Professor David Kilpatrick, for his constant guidance, invaluable advice and encouragement throughout the whole project.

I also wish to thank my husband Mr. Desheng Han and my son Li Han for their continuous support and encouragement during these years, without which this task would have been much more difficult.

I am grateful to Dr. Danshi Li and Dr. Timothy Gale for their kind help in providing the related data used in this thesis.

Grateful thanks are also extended to:
Dr. Peter Johnston for his technical assistance.

Dr. Ah Chot Yong, Dr. Yong-shun Xiao, Mr. Kevin Pullen, Mrs Julia Greenhill, Mr. Malcolm Johnson, Mrs Sue Johnson and Mrs Margaret Wright for their language aid and proof-reading.

Professor G. W. Boyd and Dr. Janet Vial for providing the opportunity to undertake this work in the Discipline of Medicine, and also my colleagues and staff in this Department and Clinical School for providing a congenial and friendly atmosphere to work.

Tianjin Medical University and the Ministry of Education in China for providing the opportunity to study in Australia.

I would like to acknowledge the financial support received from the Australian Agency for International Development (AusAID).

Special thanks go to my parents and my parents in-law for their support and understanding.

To my husband, Desheng, and my son, Li

Publications

Full papers

- C. Y. Li, W. K. Pluta and D. Kilpatrick, **Field Programmable Gate Array in a fast 256-channel data acquisition system**, *Australasian Physical & Engineering Sciences in Medicine*, Vol. 20, No. 1, P47-52, 1997

Short papers/Abstracts

- C. Y. Li, D. S. Li, D. Kilpatrick and P. R. Johnston, **A computer model of ST depression in transmural ischaemia**, *45th Annual Scientific Meeting of the Cardiac Society of Australia and New Zealand*, Hobart, Tasmania, Australia, 10-13 August, 1997, P229

- C. Y. Li, D. S. Li, D. Kilpatrick and P. R. Johnston, **An explanation for ST depression in subendocardial ischaemia**, *45th Annual Scientific Meeting of the Cardiac Society of Australia and New Zealand*, Hobart, Tasmania, Australia, 10-13 August, 1997, P230

- L. Wang, C. Y. Li, A. C. Yong and D. Kilpatrick, **Determination of mean ventricular fibrillation intervals as an index of ventricular refractoriness: fast Fourier transform analysis versus time averaging technique**, *45th Annual Scientific Meeting of the Cardiac Society of Australia and New Zealand*, Hobart, Tasmania, Australia, 10-13 August, 1997, P272

- L. Wang, C. Y. Li, A. C. Yong and D. Kilpatrick, **The effect of acute myocardial ischaemia on ventricular refractoriness and its dispersion in sheep**, *45th Annual Scientific Meeting of the Cardiac Society of Australia and New Zealand*, Hobart, Tasmania, Australia, 10-13 August, 1997, P47

- C. Y. Li, D. Kilpatrick, P. R. Johnston, and D. S. Li, **A bidomain model of ST changes during subendocardial ischaemia**, *18th Annual International Conference of the IEEE Engineering in Medicine and Biology Society*, 1996, Track 5.4.1, Paper number:1083

- C. Y. Li, W. K. Pluta and D. Kilpatrick, **A fast 256-channel data acquisition system**, *Engineering and Physics in Medicine*, Queenstown, New Zealand, 20-24 November, 1995, P199

- C. Y. Li, W. K. Pluta and D. Kilpatrick, **The role of 3D myocardial anisotropy in electrocardiogram during ischaemia**, *Engineering and Physics in Medicine*, Queenstown, New Zealand, 20-24 November, 1995, P163

Abbreviations

3D	three dimensional
AP	action potential
BSPM	body surface potential maps
DC	direct current
CT	computerised tomography
ECG	electrocardiogram
EMF	electromotive force
FDM	finite difference method
FEM	finite element method
FIDAP	fluid dynamics analysis package
LAD	left anterior descending coronary artery
LCX	left circumflex coronary artery
LV	left ventricle
LVC	left ventricular cavity
LVW	left ventricular wall
MRI	magnetic resonance imaging
OM	obtuse marginal branch of the left circumflex coronary artery
PDA	posterior descending coronary artery
PTCA	percutaneous transluminal coronary angioplasty
RCA	right coronary artery
RMBF	regional myocardial blood flow
RMS	root mean square
RV	right ventricle
SI	spatial intracellular
SPT	septum
VCG	vectorcardiogram

Contents

Chapter 1

Introduction

Electrocardiographic ST segment shift is a marker of myocardial ischaemia, and is generated by electrical currents flowing across the ischaemic boundary due to changes in the transmembrane potential of the ischaemic muscle. It provides some information about the location and the severity of the ischaemic injury, but its clinical usefulness is limited because some of the clinical and experimental observations can not be explained by the classic models of ST segment shift.

It is well known that ST depression can not localise the underlying ischaemic region in subendocardial ischaemia [1, 2, 3, 4], but the mechanism is unclear [5]. There are also controversial reports regarding the distribution pattern and the amplitude of ST potential varying with the ischaemic size during transmural ischaemia (infarction) [6]. Small regions of transmural ischaemia tend to produce uniform epicardial ST elevation over the ischaemic region with little ST depression over the adjacent non-ischaemic region [7, 8, 9]. Large regions of ischaemia produce epicardial ST elevation with its amplitude not correlating with the underlying ischaemic region [10, 11, 12, 13], and ST depression over the non-ischaemic region [14, 7, 15]. ST depression on the body surface also occurs in patients with acute infarction [16, 17, 18, 19]. However, the mechanism which causes this ST depression in infarction remains controversial [20]. A study in which simultaneous endocardial and epicardial ST potentials were mapped in sheep was conducted by Li in our laboratory [21]. Ischaemia was produced by atrial pacing and coronary artery ligation,

and confirmed by blood flow measurement using the fluorescent microsphere technique. In Li's study, mapping was performed in the following five types of ischaemia: subendocardial ischaemia in the territory of either the left anterior descending coronary artery (LAD) or the left circumflex coronary artery (LCX), and transmural ischaemia in the territory of the obtuse marginal branch (OM) of the LCX, the LAD and the LCX.

The aim of this thesis is to simulate ST potentials in ischaemia and to derive current paths which will elucidate Li's experimental results and related clinical observations. Three different models, a 3D block, an isolated heart and a torso, were developed in which the myocardium was represented by the bidomain model. ST potential is governed by a Poisson's equation where the current source arises in the ischaemic boundary and is directly associated with the intracellular conductivity and the spatial gradient of the transmembrane potential. The ischaemic boundary for the above five types of ischaemia followed the results of blood flow measurements using fluorescent microspheres [21]. Transmembrane potentials were based on the measurements by Kleber *et al.* [8] and the blood flow measurements mentioned above. A realistic torso model was used to study the relationship between ST potential on the epicardium and that on the body surface, and to explain the clinical observations. The governing equation was numerically solved by a finite element method. ST potentials on the endocardium, epicardium and the body surface were extracted to compare with Li's experimental and relevant clinical observations. In addition, the effects of myocardial anisotropy on ST potentials were studied.

This thesis consists of eight chapters. Chapter one is an introduction and Chapter 2 provides the background knowledge of the genesis and mathematical models of the normal ECG. Chapter 3 presents the literature review on the occurrence of ischaemia, the ischaemic boundary, ischaemic cellular electrophysiology and ST segment shift. Chapter 4 outlines methods and relevant parameters used in the simulation. Chapters 5 & 6 provide the results of simulations of subendocardial ischaemia and transmural ischaemia of small and of large regions. The effects of the myocardial anisotropy are discussed in Chapter 7. Chapter 8 concludes this study and puts forward proposals for future work.

Chapter 2

Background of electrocardiogram

2.1 Introduction

This chapter presents background material on the electrocardiogram (ECG), and covers cardiac cellular electrophysiology, genesis of the ECG, mathematical simulation and physical source models of the ECG.

2.2 Cellular electrophysiology

There are five different types of cardiac muscle cells: sinoatrial (SA) node, atrioventricular (AV) node, His-Purkinje system, atrial muscle and ventricular muscle. These cells are involved in two primary physiological events: mechanical function and electrical activity. The pacemaker cells, located at the SA node, are characterised by self-excitation. The second and third types play prominent roles as conductive tissues, and the remaining two types are primarily contractive tissues. Consistent with its different functions, each type has different electrophysiological properties. Cardiac function depends partly on the physiological properties of individual cells and partly on the arrangement and interaction of those cells in the heart as a whole. The ordinary myocardium that makes up the bulk of the heart consists of elongated, single nucleus cells about 10-20μm in diameter and 50-100μm long.

The cells are branched and attached to adjacent cells in an end-to-end manner by intercalated discs. Like other excitable cells, myocardial cells are surrounded by a plasma membrane whose main function is to control the movement of ions in and out of the cell. The cellular electrical properties derive from the membrane's ionic behaviour and the transmission of electrical impulses from cell to cell occurs through the intercalated discs. The basic cellular electrical properties of the heart muscle include the resting potential and the action potential. The following material is based on Berne and Levy [22].

2.2.1 Ionic basis of the resting potential

Cardiac cells at rest show a significant voltage difference across their membranes, with the inside being negative with respect to the outside (-90mV). This means that the membranes of myocardial cells are polarised. The concentration of interior potassium ions (K^+), $[K^+]_i$, significantly exceeds exterior potassium ions, $[K^+]_o$, with a concentration ratio of 35:1. A reverse concentration gradient exists for sodium ions (Na^+) and calcium ions (Ca^{++}). At the resting state, the cell membrane is highly permeable to K^+ and is less so to Na^+ and Ca^{++}. This high permeability to K^+ produces a net outflow of K^+ from the cell, leaving the anions inside, thus causing the inside of the cell to become electro-negative. The force moving K^+ out of the cell, based on the concentration gradient, is called the chemical force. Meanwhile, an electrostatic force produced by interior negative potential attracts K^+ into the cell. If the system comes into equilibrium, both the chemical and the electrostatic forces will be equal. This equilibrium can be expressed by the Nernst equation as the transmembrane potential for K^+ (E_k) at 37^0C:

$$E_k = \frac{RT}{nF} \ln \frac{[K]_o}{[K]_i} = 0.0615 \lg \frac{[K]_o}{[K]_i}(V) \tag{2.1}$$

Here n is the valence of K^+; $[K]_i$ and $[K]_o$ are the intra- and extracellular concentrations of K^+ in moles per litre; R is the universal gas constant; T is the absolute temperature in K; and F is the Faraday constant. With the measured concentration of $[K^+]_i$ (4mM) and $[K^+]_o$ (135mM) substituted into equation (2.1), E_k is about -90mV to -100mV, which is close to but slightly more negative than the actual

measurement.

The chemical and electrostatic forces acting on Na^+ are completely different from those acting on K^+ for cardiac cells at rest. Both forces attract extracellular Na^+ into the cell. However, the quantity of Na^+ moving into the cell is small due to the low permeability of the resting membrane to Na^+. It is mainly this small inward current which causes the resting membrane potential to be slightly less negative than the prediction from the Nernst equation. This steady inward flow of Na^+ would slowly depolarise the resting cell membrane if it were not for the metabolic pump which continuously pushes Na^+ out of the cell and attracts K^+ into the cell. The quantity of Na^+ expelled by the pump exceeds that of K^+ moved into the cell by a ratio of 3:2.

2.2.2 Cellular action potential

Another property of cardiac cells is called the action potential, which relates to a rapid and complete depolarisation caused by a sudden change in the membrane resting potential. The cardiac action potential reflects a phasic and repetitive electrical event and follows a characteristic time course. The changes in the action potential are divided into five stages, i.e. phases 0-4 (Figure 2.1). Each phase of the action potential is related to changes in the permeability of the cell membrane to sodium, potassium and calcium ions. Such changes alter the rate of ion transfer across the membrane.

- Phase 0: When the cell is activated, the transmembrane potential (V_m) is suddenly changed to a threshold level of about -65mV and the permeability of the membrane to Na^+ becomes very high, thus allowing the movement of Na^+ into the cell. The movement of Na^+ is controlled by two gates, the m gate and the h gate. The former has the tendency to open the Na^+ channel as V_m becomes less negative and is thus called an activation gate. The latter tends to close the channel as V_m becomes less negative and is hence called an inactivation gate. When the cell is at rest, the m gates are closed and the h gates are fully open and almost no Na^+ moves into the cell. As Vm becomes

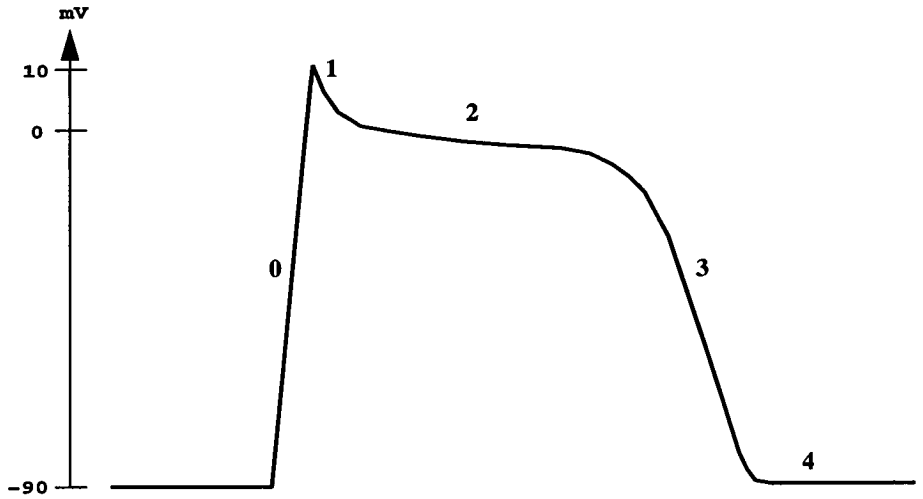

Figure 2.1: *Waveform of transmembrane action potential of a normal ventricular muscle cell.*

less negative, more and more m gates open. When the threshold value of about -65mV is reached, the remaining m gates rapidly open, activating the fast Na^+ channels. The inward Na^+ current causes the inside of the cell to become positive relative to the outside, thus causing a rapid up-stroke to a positive peak of the action potential. The inward Na^+ current eventually stops when the h gates close. Phase 0 is terminated when the h gates have closed and so have inactivated the fast Na^+ channels.

- Phase 1: A brief period of limited repolarisation between the end of the up-stroke and the beginning of the plateau. This initial rapid return to an action potential of 0mV is due largely to the abrupt closure of the sodium channels and the outward current of K^+. It has been suggested that chloride ions enter the cell during this phase.

- Phase 2: A plateau phase of refractoriness. The transmembrane potential remains almost constant for a considerable period of time, slowly repolarising. At the beginning of the action potential, the intracellular Ca^{++} concentration is much less than the extracellular concentration, therefore with an increase of the permeability to Ca^{++}, Ca^{++} ions move into the cell during the plateau. Meanwhile, the chemical force acting on K^+ greatly exceeds the electrostatic force, thus moving K^+ out of the cell. It tends to repolarise the cell membrane,

thus terminating the plateau. As a consequence of the reduced permeability to K^+ in an outward direction, there is a small outflow of K^+ during the plateau, which tends to balance the slow inflow of Ca^{++} and Na^+ and thus helps to maintain a prolonged plateau at a V_m close to 0mV.

- Phase 3: Final repolarisation. It depends on two principal processes: an increase in the permeability to K^+ and inactivation of the slow inward Ca^{++} and Na^+ currents. The increase of the permeability to K^+ is induced in part by the elevation in intracellular Ca^{++} during the plateau, leading to an outflow of K^+ from the cell. This voltage dependent K^+ channel produces the outward current of K^+ to exceed the slow inward currents of Ca^{++} and Na^+. The outflow of K^+ during phase 3 rapidly restores the resting level of the transmembrane potential.

- Phase 4: Restoration of the resting state. The $Na-K$ pump becomes effective, and moves Na^+ that has moved into the cell mainly during phases 0 & 2 out of the cell, at the same time moves K^+ which has moved out chiefly during phases 2 & 3 back into the cell with a ratio of 3:2.

In fact, the ionic currents during different phases of the action potential are far more complicated. Their detailed description is beyond the scope of this thesis and can be found elsewhere [23].

2.3 Genesis of ECG

2.3.1 Genesis of ECG

Each heartbeat, or cardiac cycle, is an intricate sequence of electrical and mechanical events. Myocardial contraction is triggered by electrical signals that originate in one part of the heart and travel to all cardiac chambers. The stimulus for electrical signals is generated by a group of pacemaker cells in the right atrial wall, and the excitation spreads in an orderly sequence through the atria and ventricles. The spread of the excitation is accompanied by mechanical contraction. The period of

active contraction (systole) is followed by an interval of relaxation (diastole) before the next cycle.

Cardiac activation is accompanied by electrical activity associated with the movement of ions across cell membranes during the phases of the action potential. Since body tissues conduct electricity, these sources of cellular current produce currents flowing through the body. Therefore potential differences can be detected at the body surface as a result of electrical activity of the heart muscle. The standard 12-lead system used to record the ECG is comprised of three bipolar limb leads: Lead I (the left arm minus the right arm), Lead II (the left leg minus the right arm) and Lead III (the left leg minus the left arm); three augmented unipolar limb leads: aV_L, aV_R and aV_F; six unipolar chest leads $V_1 - V_6$. The unipolar leads are relative to the Wilson's central terminal which is a terminal constructed by averaging three limb electrodes. The ECG signal measured on the body surface during one cycle of cardiac activation in lead II is shown in Figure 2.3. The typical components of the ECG are:

- P wave: The cardiac impulse originating at the SA node spreads radially throughout the right atrium and directly to the left. The potential difference in the action potential between the activated and non-activated tissues in the atrium produces the P wave, so indicating the activation of the atria.

- PR interval: In the normal heart, the atrial excitation initiates the excitation of the atrioventricular (AV) node, which in turn initiates the excitation of the ventricular conduction system (the bundle of His, right and left bundle branches, and the Purkinje fibres). This specialised conduction system conducts the activation to the subendocardial surfaces of both ventricles. As the diameter of the fibres of the AV node is small, the conduction velocity through these fibres is slow. Thus there is a delay between the atrial and ventricular excitation. PR interval represents the times for intra-atrial, AV node, and His-Purkinje conduction.

- QRS complex: The QRS complex arises from the excitation of the ventricular muscle which relates to phase 0 of the action potential in the ventricular

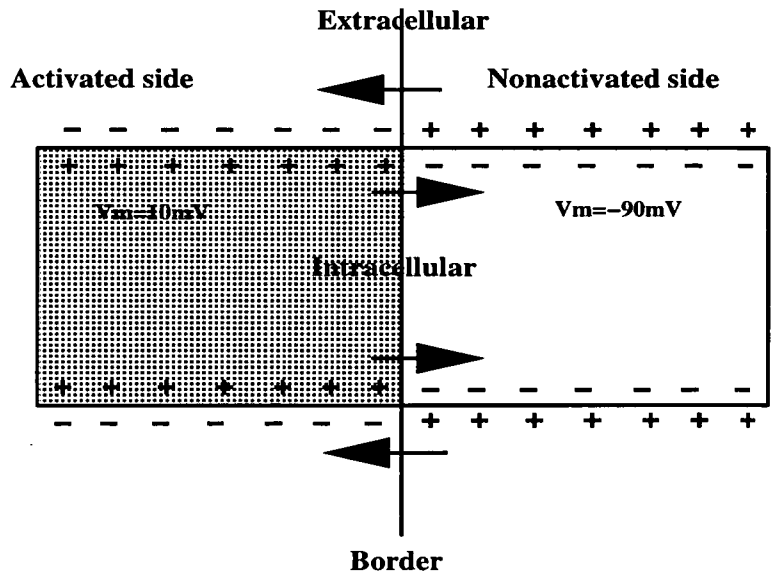

Figure 2.2: *Intracellular and extracellular currents at the border between the activated (hatched) and non-activated sections of a myocardial fibre during QRS. Vm represents the transmembrane potential. The arrows represent the direction of current flow. (Modified from Berne and Levy [22]).*

cells. In normal excitation, the wave of activation generally spreads from the conduction system into the septum, depolarising both the left and right endocardial surfaces, and through the ventricular free walls from the endocardium to the epicardium. The difference in transmembrane potential between activated ventricular and non-activated cells gives rise to intracellular current flowing from the activated to the resting cells, meanwhile extracellular current flows in opposite direction (Figure 2.2). These currents tend to depolarise (activate) the region of the resting fibre adjacent to the border. The extracellular current produces a positive potential at the non-activated region relative to that at the activated region. As the excitation proceeds, activation of the right ventricle ends before the left ventricular activation because the right ventricle is thinner than the left. Thus, the earlier part of QRS deflection normally reflects a combination of left and right ventricular activity, while the latter part reflects mainly left ventricular activation. The J point of the ECG is identified as the time when the slope changes suddenly at the end of the S wave, and is frequently used as a marker for the end of ventricular excitation.

- ST segment: Following the QRS complex, the ECG has a quiet period in which all ventricular cells are activated (in phase 2), and minimal current is produced. This isoelectric segment is called the ST segment.

- TQ segment: It is commonly referred to as the baseline for the ECG, and its interval covers the duration of the resting period.

- T wave: Repolarisation of the ventricular muscle. The T wave is produced in the phase 3 of the action potential. The polarity of the T wave is due to the ventricular gradient in which the duration of the action potential at the endocardial sites is longer than that at the epicardial sites. As phase 3 is a slow process, there is not a repolarisation wavefront like the activation wavefront. Thus the T wave is not as sharp as QRS complex. Also the difference in transmembrane potential between early and late repolarised cells is not as large as that between depolarised and non-depolarised cells during phase 0, hence producing a lower amplitude of the T wave. In fact, the spatial and temporal characteristics of ventricular repolarisation are far more complicated. The sequence of the repolarisation is geographically non-uniform; the difference in the duration of repolarisation in different regions may result from anisotropic property of the myocardial fibres or from the environmental influence. That is, the normal sequence of ventricular repolarisation and the anatomic sites with potential differences for the T wave are still unclear. However, this topic is outside the scope of this thesis.

- U wave: The U wave appears as a separate deflection of relatively low amplitude, usually detectable at slow or moderate heart rates. The presence, genesis and significance of the U wave is still controversial.

2.3.2 Mathematical simulation of ECG

There are two aspects involved in producing the ECG. One is the cardiac electrical source which represents the electrical activities of the heart. The other is the volume conductor which is composed of all the tissues inside the torso. Various

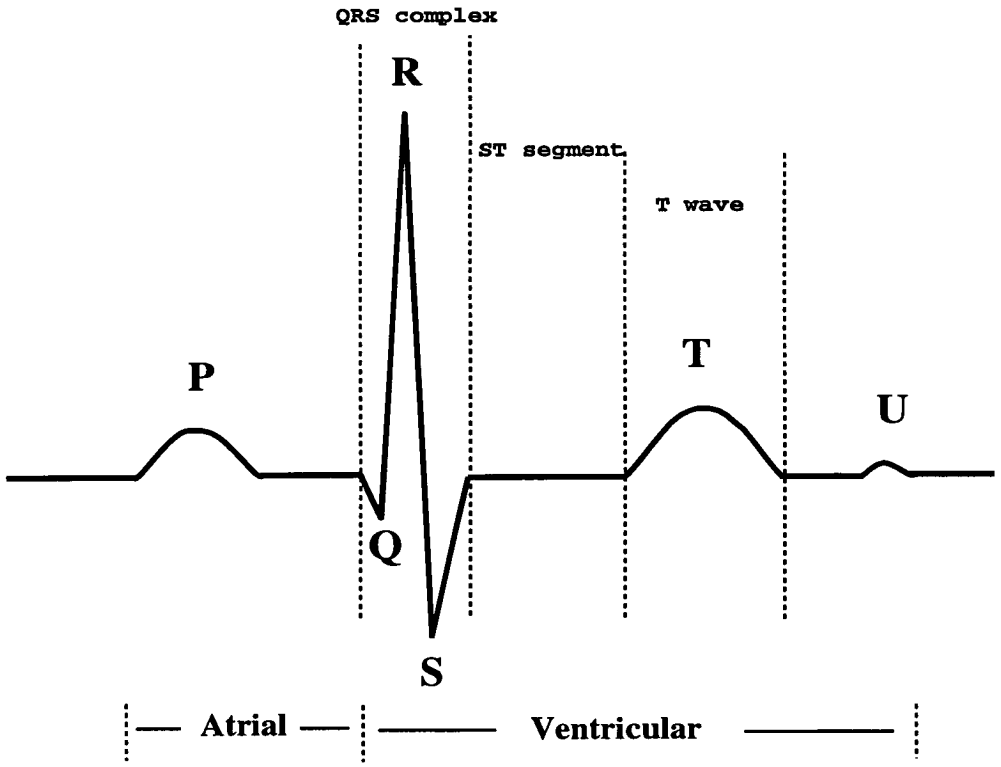

Figure 2.3: *Waveform of the normal ECG on lead II which represents the potential of the left leg relative to that of the right arm.*

models have been proposed to describe the electrical source and the volume conductor in which the source is embedded to understand the nature of ECG. There are two problems involved in electrocardiography. The computation of the torso or epicardial potentials resulting from the electrical source in the heart is known as the forward problem of electrocardiology [24, 25, 26]. The estimation of cardiac sources from measured body surface potentials is defined as the inverse problem of electrocardiography. There are mathematical problems in solving the inverse problem [27] however further discussion of the inverse problem is not within the scope of this review.

Electrocardiographic signals change slowly with time, having the frequency content from nearly direct current (0Hz) to 100Hz [28, 29]. Therefore the forward problem of the ECG can be degenerated to a quasi-static volume conductor problem [30]. The electric field $\vec{E}$ and the current density $\vec{J}$ in each region of the volume conductor may be represented by

$$\vec{E} = -\nabla\Phi \tag{2.2}$$

$$\vec{J} = \sigma\vec{E} + \vec{J^i} \tag{2.3}$$

where $\vec{J^i}$ is the impressed source current density in the heart, σ represents the conductivity tensor of the region, and Φ denotes the potential. Since $\vec{J}$ is solenoidal,

$$\nabla \cdot \vec{J} = 0 \tag{2.4}$$

$$\nabla \cdot (\sigma \nabla \Phi) = \nabla \cdot \vec{J^i} \tag{2.5}$$

$$\nabla \cdot (\sigma \nabla \Phi) = -I_v \tag{2.6}$$

where

$$I_v = -(\nabla \cdot \vec{J^i}) \tag{2.7}$$

is the representation of the current density, and has a dimension of current per unit volume. Equation (2.6) is the governing equation for the forward problem of ECG.

The forward problem requires the use of appropriate models for the heart's electrical source and for the volume conductor. Basically there are three different methods for solving the forward problem in terms of the representation of the torso geometry. The first is the physical approach which measures the potentials produced by an assumed source (e.g. a single current dipole) in a physical torso model (e.g. an electrolytic tank). The second is to use an idealised mathematical heart or torso model (e.g. a sphere) and a simplified current source, to solve the governing equation analytically. The third is the numerical method such as the finite element method (FEM), finite difference method (FDM) and integral equation, which solves the equation with realistic numerical torso models. The numerical method chosen because of its more realistic geometries and the availability of affordable powerful computers.

There are two different classes of cardiac source description. The first is that of equivalent generators of physics which are normally located inside the heart and produce a similar body surface ECG to that observed. The equivalent generators include a single dipole, multiple dipoles, multipole and uniform dipole layer. The second is that of the macroscopic source description which links the cardiac source with the cellular electrophysiology. This macroscopic approach uses the syncytial nature of the heart muscle, and treats a large number of individual cardiac cells as

a packed, macroscopic structure (in the order of mm) with the properties of a single cell. The bidomain model is a typical macroscopic generator.

2.4 Source models of ECG

The current source for QRS complex has been widely studied in terms of equivalent current generators [31, 32, 33] or macroscopic generators [34, 35].

2.4.1 Dipole

From Einthoven's postulates [36], the electromotive force (source) created during myocardial depolarisation is equivalent to a single dipole, which has the positive pole on the non-activated side and the negative pole on the activated side. The dipole's magnitude, direction and possible location are chosen so that it generates the same potentials on the body surface as that from a real heart. This 'dipole' can generate ECG patterns if the body surface is sufficiently far from the heart. Vectorcardiography (VCG) is based completely on an evaluation of the behaviour of the heart dipole during the heart cycle, assuming that the heart's electrical activity may be approximated by a fixed-location, variable-amplitude, variable-orientation current dipole within a finite homogeneous torso.

It is well known that there is a double layer existing in the wavefront of depolarisation with the positive potential at the non-activated side and the negative potential at the activated side [31, 32]. A gross approximation to the double layer could be found from the sum of all the dipole elements. The approximated result is a single dipole. Such a process ignores entirely all spatial features, since it treats all dipole elements as if their points of action were the same. The validity of such an approximation depends on the ratio of the extent of the source distribution to the source-field distance. It has been proven mathematically that this conception is valid only when the distance between the recording electrodes and the heart is large in comparison with the electrically active boundaries of the heart, and when the volume conductor is homogeneous [37, 38]. As the cardiac surface is close to the chest, the theory may

only be applied as a first approximation. Although useful, this highly simplified model is only the first step in understanding the relationship between ECG potentials and myocardial electrical activities. More accurate models need to be developed to better understand this relationship and provide more detailed diagnoses.

2.4.2 Multiple dipoles

Experiments, particularly from body-surface maps [39, 40], have demonstrated that no single dipole can be 'equivalent' in the sense of accurately reproducing the body-surface observations [41, 42]. As a result, several more realistic and sufficiently simple models have been proposed. One model represents the cardiac source by a number of discrete dipoles, namely, multiple dipoles [43, 44, 40].

Selvester *et al.* used a 20-dipole model [44, 45, 40] to simulate the VCG and ECG on the body surface. In their work, 20 current dipoles, each representing a segment of the heart, were located spatially at the centroid of the myocardial segment which they represented. Each dipole of the cardiac generator had a different time-history of current dipole strength based on activation sequences. The dipole magnitudes were assumed to follow a smoothed trapezoidal time course, with onset and offset times based on the activation data of Scher and Young [46]. The amplitude of each trapezoid was proportional to the maximum surface area of the myocardium in the region perpendicular to the regional dipole. The direction of each dipole was assumed to be perpendicular to the average wave front of depolarisation as it passed through that segment. Initially, the entire assembly of 20 dipoles was assumed to be placed in a homogeneous sphere and the VCG leads were calculated using analytical equations for the surface potentials due to eccentric dipoles in a conducting sphere. The sphere was later replaced by a realistic human torso model that included lungs, and the entire body surface potential map was calculated using the Gelernter-Swihart integral equation for the charge [47]. It was found that the simulated maps matched Taccardi's measured maps [39] to the limit of resolution of these maps through most of the ventricular depolarisation. Also the simulated body surface maps contained considerable information unaccounted for by an equivalent

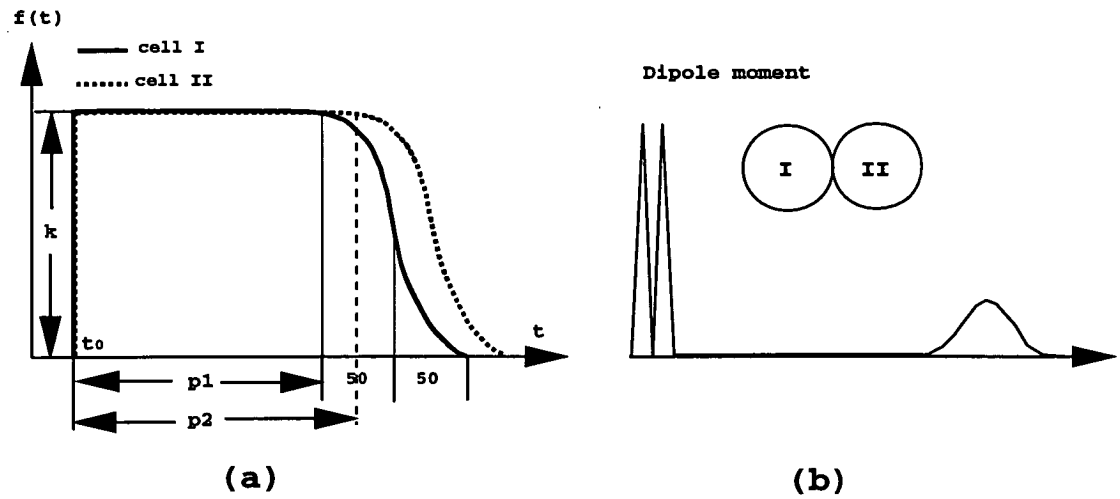

Figure 2.4: *Mathematical representation of the transmembrane action potential for the two contiguous cells (a) and their dipole moment (b) by Thiry and Rosenberg [46]. The solid line represents the first cell and dotted line the second cell. The action potential duration for cell I is represented by p1 and cell II by p2.*

dipole during the middle and terminal portions of the QRS.

Thiry and Rosenberg [48] combined the activation and recovery modelling techniques and developed a multiple dipole model to simulate the corresponding QRS complex and T waves in a standard 12-lead ECG. In their model, the heart was divided into 11 components, each being modelled by a dipole of fixed location and direction. The assumed action potential was given in Figure 2.4; the corresponding mathematical expressions for a cell (e.g. cell I) were:

$$f(t) = \begin{cases} 0 & 0 < t < t_0 \\ k > 0 & t_0 < t < t_0 + p1 \\ k(1 - \frac{(t-t_0-p1)^2}{5000}) & t_0 + p1 < t < t_0 + p1 + 50 \\ k\frac{(t_0+p1+100-t)^2}{5000} & t_0 + p1 + 50 < t < t_0 + p1 + 100 \end{cases} \tag{2.8}$$

and the excitation sequence was taken from the data of Durrer *et al.* [49]. When the action potential propagated over the surface of a spherical cell, the resultant dipole for the cell at any time t was obtained by integrating the dipole per unit area $\vec{f}(t)$ over the cell surface, and the moment of $\vec{f}(t)$ at each point is proportional to the transmembrane action potential with the direction normal to the cell surface. The resultant dipole for the single cell was diphasic (showing a negative T wave). When

the two cells were contiguous and had different duration in the action potential, there was a positive component during repolarisation because of the transmembrane potential difference (Figure 2.4). This positive component would be absent if the cells were not contiguous. When computing the body surface potentials, the body was regarded as a homogeneous, infinite volume conductor. The simulated 12 lead ECGs reproduced the main features of the clinical ECG.

Cuffin and Geselowitz [50] also used the isochrone data from Durrer *et al.* [49] to develop a 20-dipole heart model. The magnitudes and orientations of the dipoles were determined from the vector integration of the isochrone surface within the corresponding heart region. Surface potentials were computed using the technique of Barnard *et al.* [51] for both a homogeneous torso and an inhomogeneous torso with lungs. They found that the limb leads could be accurately simulated using only the dipole terms of the dipoles, but the precordial leads required the higher orders of the dipole. Cuffin and Geselowitz [50] reached a similar conclusion to that of Selvester *et al.* [40], i.e. the addition of lungs revealed little change in the body surface ECG map. Furthermore, considerable differences occurred in simulated ECGs between the fixed- and the variable-orientation dipole models, suggesting that variable-orientation models are imperative for an accurate forward transformation of the ECG.

2.4.3 Multipole

Another approach was the multipole model, in which higher moments of a dipole were taken into account [41, 52, 53, 50]. The multipole components could be determined from the surface ECG potential distribution. In the study of Cuffin and Geselowitz [50], they found that the multipole model, using dipole plus quadrupole plus octopole terms, could accurately represent the actual 20-dipole model in the homogeneous torso in terms of the body surface potentials. For the limb leads, the ECGs were accurately represented by the dipole terms alone, while for the precordial leads, the quadrupole and octopole terms were required for an accurate representation.

Arthur and co-workers [54] had determined the dipole and quadrupole components based on detailed measurements of the torso surface geometry and body surface potential, and found that the addition of the quadrupole contribution gave a better fit to the surface ECG. The root mean square (RMS) error during QRS was 0.091mV for the dipole alone and 0.054mV for dipole plus quadrupole, representing 23% and 14% of the total RMS value of the recorded ECGs respectively.

Savard *et al.* [55, 56] computed the location, orientation and magnitude of a single moving dipole from the body surface potentials. They concluded that 15 multipoles, including three dipoles, five quadrupole and seven octopole components, could produce a better presentation of the ectopic wavefront.

2.4.4 Uniform dipole layer

The uniform dipole layer model, or uniform double layer model, was first introduced in 1933 by Wilson *et al.* [31] and has been used in explaining ECG waveforms qualitatively [32, 33, 57]. According to this model, the electromotive force during ventricular depolarisation at the boundary could be represented by a uniform dipole layer, with the negative layer on the activated side and the positive layer on the resting side.

In the studies [32, 57], a spherical geometry was used to represent the torso in which a double layer spherical cap was chosen to be an idealised activation wavefront. The analytic solution for the potential at any point on the sphere surface was obtained in the form of a double series in Legendre polynomials with the known uniform dipole moment.

The solid angle theory, derived from the classical electrostatic field theory is another method to obtain the potential produced by a uniform double layer. It states that the potential produced by a uniform dipole layer in an infinite, isotropic and homogeneous volume conductor is equal to the product of the solid angle (Ω) of the exploring point subtended by the source surface and the double layer strength when the exploring point is far away from the source [38] (Figure 2.5). Van Oosterom [33]

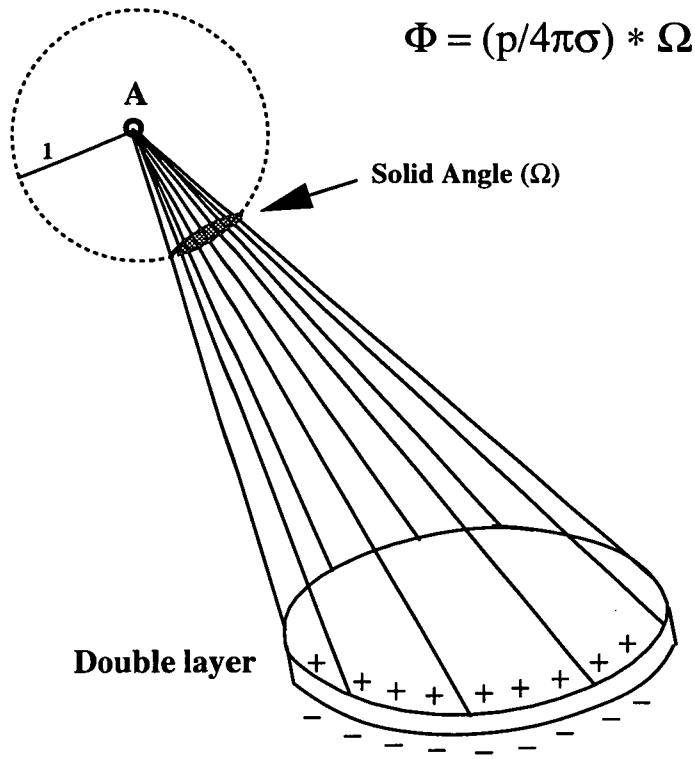

Figure 2.5: *Illustration of solid angle theory. The potential at point A (Φ) produced by the uniform double layer with the strength p in an infinite medium is proportional to the double layer strength and the solid angle (Ω) of point A subtended by the double layer boundary. (From Haus and Melcher [36]).*

further assumed that the potential difference at the boundary was proportional to the double-layer strength, i.e.

$$\Phi = \frac{p}{4\pi\sigma}\Omega = V_D\frac{1}{4\pi}\Omega \tag{2.9}$$

where p denotes the current dipole density and V_D the potential jump over the double layer. The potential distribution at the activation boundary showed an S-shaped curve rather than an abrupt jump noted by Solomon and Selvester [58]. The following function was used to describe the source potential distribution by van Oosterom [33].

$$S(x) = \frac{x}{(x^2 + W^2)^{1/2}} \tag{2.10}$$

where W is a measure of the width of the source distribution (Figure 2.6). Consequently, the potential $\phi(x)$ at the wavefront due to the local sources could be given by

$$\phi(x) = \frac{1}{2}V_D\frac{x}{(x^2 + W^2)^{1/2}} \tag{2.11}$$

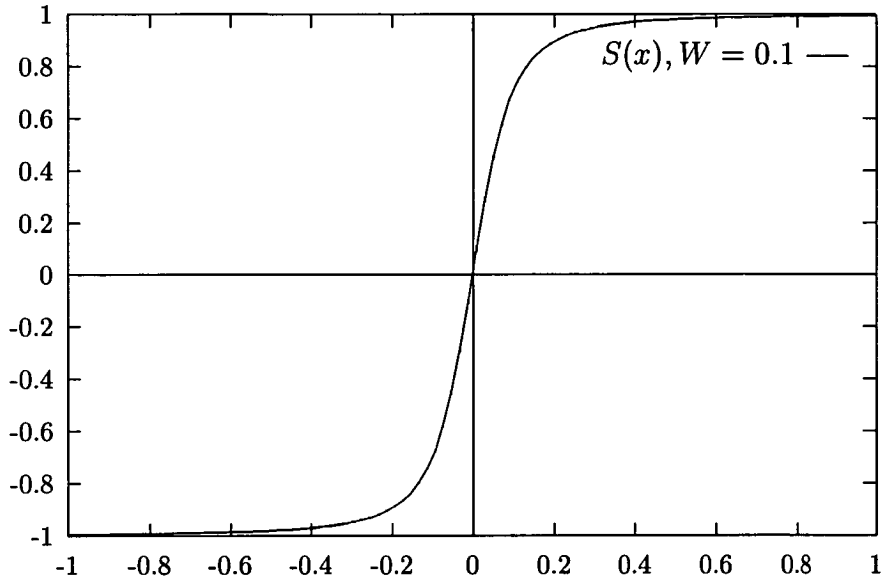

Figure 2.6: *The shape of the potential distribution over the activation boundary used by van Oosterom [31].*

It was assumed that V_D = 40mV during depolarisation and W = 0.8mm following the recordings with multi-terminal intramural electrodes in dogs [59, 33]. A number of triangles were used to approximate the activation wavefront at each time instant considered. The positions of these triangles were based on the data of Durrer *et al.* [49]. A triangulated representation of the torso surface was used. Plonsey [30] calculated the body surface potential using integral equation formulation, which calculated the potentials at the torso surface from the known strength of a uniform double layer in a homogeneous and bounded medium. The simulated body surface potentials for 11 time instants at 5ms intervals during depolarisation were in a similar order of magnitude to those recorded in healthy subjects.

Solid angle theory was widely used to study ST segment changes in myocardial ischaemia by Holland's group [60, 61] in which the source at the ischaemic boundary was represented by the difference in the action potential between the normal and ischaemic cells ($\Delta\Phi_m$).

$$\Phi = \frac{K}{4\pi} * \Delta\Phi_m * \Omega \tag{2.12}$$

The details of this approach will be discussed in the next chapter.

2.4.5 Bidomain model

The bidomain model, in which myocardium is represented by two superimposed but distinct continuous domains, intracellular and extracellular, separated everywhere by the cell membrane, was first derived in the late 1970s by Tung [62] and Miller and Geselowitz [34]. The model describes the average behaviour of the bioelectric fields of cardiac muscle over distances that are large compared with the size of a single cell. If $\vec{J}$ is the current density, Φ the potential and σ the conductivity, then

$$\vec{J}_i = -\sigma_i \nabla \Phi_i \tag{2.13}$$

$$\vec{J}_e = -\sigma_e \nabla \Phi_e \tag{2.14}$$

where the subscripts i and e represent intracellular and extracellular spaces respectively. The charges moving from one domain to the other must cross the membrane and hence represent membrane current per unit volume (I_m). The fundamental equation describing the potentials in cardiac tissue is the conservation of the current [62]. Mathematically

$$\nabla \cdot \sigma_i \nabla \Phi_i = I_m \tag{2.15}$$

$$\nabla \cdot \sigma_e \nabla \Phi_e = -I_m \tag{2.16}$$

$$\nabla \cdot (\vec{J}_i + \vec{J}_e) = 0 \tag{2.17}$$

By definition, the transmembrane potential

$$\Phi_m = \Phi_i - \Phi_e \tag{2.18}$$

Combining these equations yields equations for both intracellular and extracellular potentials:

$$\nabla \cdot \sigma \nabla \Phi_e = -\nabla \cdot \sigma_i \nabla \Phi_m \tag{2.19}$$

$$\nabla \cdot \sigma \nabla \Phi_i = \nabla \cdot \sigma_e \nabla \Phi_m \tag{2.20}$$

where $\sigma = \sigma_i + \sigma_e$ is the bulk conductivity of the heart muscle. Equation (2.19) is of the form of Poisson's equation and may then indicate that the term $\nabla \cdot \sigma_i \nabla \Phi_m$ is the source of the extracellular potential Φ_e.

The bidomain model has been applied extensively in cardiac electrophysiology. It has been used to compute intracellular and extracellular potentials when the action potential is known [63, 64, 65] and to calculate the transmembrane potential induced in passive tissue in response to applied currents [66, 67, 68, 69].

Miller and Geselowitz [34] applied the bidomain model in a slightly different context. Combining equations (2.15) and (2.16) gives

$$\nabla \cdot \sigma_i \nabla \Phi_i = -\nabla \cdot \sigma_e \nabla \Phi_e \tag{2.21}$$

which is reduced to

$$\nabla^2 \Phi_e = -(\sigma_i/\sigma_e)\nabla^2 \Phi_i = \frac{1}{\sigma_e} \nabla \cdot \vec{J}_i \tag{2.22}$$

when the two domains are assumed to be isotropic. From equation (2.13), the intracellular current density ($\vec{J}_i$) can be interpreted as the current dipole moment per unit volume, and is proportional to the spatial gradient of the intracellular potential distribution. It is evident from equation (2.22) that the potential Φ_e can be considered to arise from a cardiac current generator which can be represented by the intracellular current density ($\vec{J}_i$).

Miller and Geselowitz [34] represented the ventricular anatomy with a 3-D array of approximately 4000 points, which was assumed to be located in a homogeneous volume conductor with the shape of an adult torso. An assumed action potential shape was used with a ventricular gradient, in which depolarisation was modelled by a step change from the resting value of -90mV to 10mV at the activation time and repolarisation by a series of six linear segments (Figure 2.7). Isochrones were specified at each point on the basis of the human heart data of Durrer *et al.* [49], and the simulated intracellular potential at each point in the heart model was calculated using the assigned activation times and action potential data. The current dipole at each point was approximated by the discrete difference of the potentials at its six nearest neighbours. The moments of 23 dipoles were obtained by summing the moments of the dipoles at all the points within the corresponding regions of the heart model. Then the potentials on the surface of the torso were calculated from the set of 23 dipoles using the transfer coefficient previously obtained by Cuffin and Geselowitz [50].

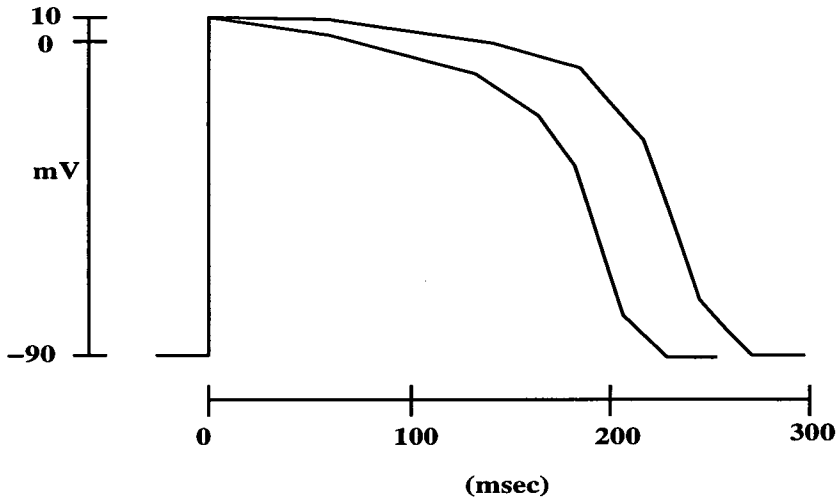

Figure 2.7: *The cellular action potential model with the longest and shortest action potentials used in the normal heart simulation. (From Miller and Geselowitz [32]).*

The simulation results from Miller and Geselowitz [34, 70] appeared to provide an excellent simulation of the body surface ECG for the normal and abnormal hearts. However, it is not clear how the intracellular potentials were simulated with the known transmembrane potential and activation times. It is extremely difficult to measure the spatial distribution of intracellular potentials. Also, endocardial and epicardial potentials were not addressed in the study, and thoracic inhomogeneity and myocardial anisotropy were ignored in the model.

In another model [71], the ventricles together with bundle branches and Purkinje fibres, were composed of approximately 50000 cubic cell units. The action potential waveforms with different durations in the plateau phase were assigned to the individual cells. The heart model was mounted in a homogeneous human torso model with a conductivity of σ_t. The dipole generated at each cell unit was calculated as

$$\vec{J}(r,t) = -\sigma_m \nabla \Phi_m(r,t) \tag{2.23}$$

where $\Phi_m(r,t)$ denotes the action potential at time t of the cell located at r, and σ_m the average myocardial conductivity. The propagation of the excitation wavefront was assumed to be as follows: initiating in the AV node, and propagating along the bundle branches through Purkinje fibres at a speed 5 times larger than that in the ordinary ventricular unit, then spreading into myocardial units and propagating step by step from activation units to the adjacent units at 3ms intervals. Furthermore,

the extracellular potential Φ_e satisfies Poisson's equation:

$$\nabla \cdot \sigma_t \nabla \Phi_e = \nabla \cdot \vec{J} \tag{2.24}$$

The potentials were calculated by the boundary element method in which Poisson's equation with homogeneous Neumann's boundary conditions on the torso surface was modified to Laplace's equation with inhomogeneous boundary conditions. The resulting ECG, VCG, and body surface potential maps (BSPM) were within the expected range of the clinical observation.

A similar concept was employed in the "SI" (spatial intracellular potential) model of Spach *et al.* [72]. It was assumed that a network of cells could be treated as one large cell so that the net membrane current could still be determined by the core model of Plonsey [30], that is, the membrane current could be approximated by the second spatial derivative of the intracellular potential Φ_i evaluated along the fibre axis z.

$$J_m(t,z) = \frac{\sigma_i a}{2} \frac{\partial^2 \Phi_i(t,z)}{\partial z^2} \tag{2.25}$$

The extracellular potentials could be calculated from the membrane current, based on Green's theorem [30]. The measured intracellular potentials were used to determine the extracellular potentials in their study. In separate experiments, this model successfully predicted the extracellular potentials surrounding a single Purkinje strand [72] and the normal epicardial ST-T potentials resulting from ectopic beats in dogs [73]. However, only a simplified ventricle geometry was used in the simulations.

2.5 Anisotropy

Myocardial cells are both anatomically and electrically anisotropic [74, 75]. Ventricular muscle is characterised by rotating fibre orientations with increasing epicardial to endocardial depth in the ventricular wall [76]. Anisotropic electrical properties of both the intracellular and extracellular domains are characterised by their electrical conductivity tensors (σ_i and σ_e). As pointed out by Roth [77], there is much

variability in the measured conductivity values. Firstly, whether intracellular or extracellular space has a higher conductivity has not yet been determined. The ratio of the measured extracellular to intracellular conductivities varied from 0.28 [75] to 1.2 [78]. Secondly, the ratio of the measured longitudinal to transverse conductivities in either space varied greatly. For instance, the ratio for the intracellular domain ranged from 5.77 [79] to 10.57 [80]. Despite this inconsistency, the longitudinal conductivity is surely much greater than the transverse conductivity. Therefore Φ_i and Φ_e depend not only on the value of the conductivity, but also on the direction relative to the fibre axis.

The uniform double layer model is not an accurate description of the myocardial activation because it does not take anisotropy into account [81, 79]. The bidomain model can take anisotropy into consideration. If σ is assumed to be anisotropic, equation (2.19) no longer possesses a simple solution. However, if the myocardial anisotropy (σ) is assumed to be constant, then Poisson's equation still holds, and the mathematics remains tractable. In this case, the source term which is associated with σ_i, will depend on whether the direction is parallel or transverse to the fibre axis. There are two simplified approaches to study the effects of anisotropy on the potential distribution.

2.5.1 Axial model

The first attempt to replace the uniform double layer by an anisotropic model called the axial model, was introduced by Corbin and Scher [82]. They suggested that the dipole sources during the cardiac depolarisation largely parallelled the local cell axis rather than being normal to the activation surface. The potentials were calculated for a hemispherical wavefront in an infinite homogeneous medium by numerical integration. They found that the axial theory predictions were much closer to the actual measurements in dogs than those of the uniform double layer, even though the axial theory alone did not exactly describe all the measured potentials. Roberts *et al.* [81] conducted epicardial recordings in dogs when canine epicardium was simulated, and found that the voltage across the depolarisation wave was approximately three

times as great in the longitudinal direction.

2.5.2 Oblique dipole layer

The assumption of purely axial orientation of cellular dipoles is an improvement over the uniform dipole theory [82]. However, as pointed out by Roberts *et al.* [81], the axial model probably predicted too strongly a dependence of the wavefront voltage on the fibre orientation. An oblique dipole model was suggested by Colli-Franzone *et al.* [83], which took both axial and transverse dipoles into account. The numerical simulations were carried out in an isotropic homogeneous medium with the shape of a cylinder (15cm in height and 23cm in diameter) as used in their experiments. The wavefront shape was assumed to be semi-ellipsoidal when the endocardium was paced. They found that the calculated potentials from the oblique dipole with longitudinal dipole moment m_l and transverse moment m_t matched the measurements of the paced dog hearts in the volume conductor when the ratio m_l/m_t was between 15 and 30. They also showed that the axial component of the potential field played a dominant role with respect to the normal component.

Roberts and Scher [79] solved equation (2.19) in the bidomain model analytically for a depolarisation in an infinite homogeneous medium with a simplified wavefront shape. The potentials were calculated by a surface integral where the wavefront was represented by a wavefront voltage, which was assumed to be a step function (ΔV=100mV). The extracellular potential in the wavefront was taken as

$$V_{ol} = \Delta V(\sigma_{il}/\sigma_l) \tag{2.26}$$

$$V_{ot} = \Delta V(\sigma_{it}/\sigma_t) \tag{2.27}$$

The potential fields of the stimulated waves on the epicardium could best be explained if the extracellular wavefront voltage was 74$\pm$7mV (mean $\pm$ SD) for a wave propagating parallel to the local muscle fibres, and 43$\pm$6mV for a wave propagating perpendicular to these fibres. That is, the extracellular voltage across a longitudinal wave was 1.75 times that of a transverse wave. They concluded that myocardial anisotropy greatly affects the propagation of depolarisation waves and the potential fields produced by depolarisation in the intact heart.

2.5.3 Full anisotropic model

Myocardial anisotropy affects not only the source but also the property of the myocardial part of the volume conductor (equation 2.19). The overall effects of anisotropy on the ECGs have been widely studied with this approach [84, 35]; however, the detailed analysis of the equation has been performed only on simplified two or three dimensional geometries.

A study carried out on 2D anisotropic tissue due to a circular-shaped wavefront using the bidomain model by Sepulveda and Wikswo [85], showed that simple depolarisation wavefronts produced complex current distribution as predicted by Plonsey and Barr [86].

The study of the effect of anisotropy by Colli-Franzone *et al.* [65] was carried out on a myocardial slab during paced beats using the bidomain model. The results were consistent with the predictions of the oblique dipole layer model [83]. It was found that the epicardial and endocardial potential maps provided information on the pacing site and depth, and on subsequent intramural propagation, by reflecting the clockwise or counterclockwise rotation of the deep positivity.

In Pollard and Burgess' study [35], a model of a 3D block was comprised of networks of microscopic elements arranged into rectangular parallelepipeds in which epicardial stimulation was applied. They found that the rotation of fibre axes accelerated epicardial activation distant from the stimulus site. The inhomogeneous conductivity caused regional acceleration and deceleration spread.

Wei *et al.* [87] solved equation (2.22) as used by Miller and Geselowitz [34] using the bidomain model, in which axially symmetric intracellular conductivity and the fibre rotation were taken into account, while the extracellular conductivity was assumed to be isotropic. Furthermore, the transmembrane potentials were used to approximate the intracellular potentials. The heart model was placed within a homogeneous, realistically shaped human torso model, and Poisson's equation still held and was tractable. The comparative simulations showed no significant difference in global excitation sequences of the heart and body surface ECG for the normal heart

between the isotropic and anisotropic myocardium.

It is difficult to fully evaluate the effects of myocardial anisotropy because the governing equation in the bidomain model is not tractable if the anisotropic conductivity is a function of position. Actually, measuring σ_i and σ throughout the heart is extremely difficult. Therefore some reasonable assumptions regarding myocardial anisotropy are necessary to study its effects. For instance, the fibre rotation was ignored in studies of the effect of anisotropy on activation wavefront in simplified geometry [86, 85]. The extracellular anisotropy was ignored in the study of Wei *et al.* [87] and the equivalent dipole sources were obtained assuming an isotropic bidomain model for the myocardium by Lorange and Gulrajani [88] to study the effect of anisotropy on the body surface ECG. Also, myocardial anisotropy was taken into account for the current source and for the volume conductor separately by Li [89].

Chapter 3

Literature review

3.1 Introduction

This chapter provides information on myocardial ischaemia, including its occurrence, the transmembrane potential of ischaemic cells, ischaemic boundaries, and its associated ST segment shift. It mainly covers mathematical models and the experimental and clinical observations of ST changes in ischaemia. Finally, the advantages and disadvantages of the models are discussed in terms of being able to explain the observations.

3.2 Myocardial ischaemia

Myocardial ischaemia occurs when coronary artery blood flow is insufficient to meet the myocardial metabolic requirements. This insufficiency of blood supply can result from either artery restrictions such as induced occlusion in experiments and coronary artery occlusion in patients, or greater demand from exercise testing in the presence of partial narrowing. Ischaemia affects myocardial cells by inducing ionic, metabolic, electrical and mechanical changes. The electrical changes are basically those of changed transmembrane potential, which affect injury current, ECG, recovery of excitability and electrical conduction. This review focuses only on the changes in

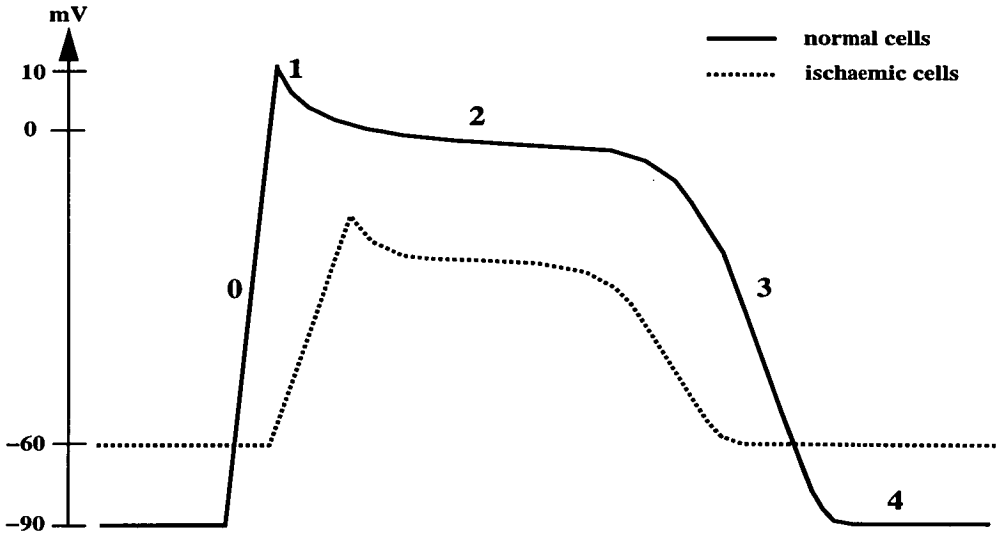

Figure 3.1: *Waveform of the action potential of normal cells (solid line) and ischaemic cells (dotted line). Normal cells have a resting potential of -90mV and ischaemic cells -60mV.*

the transmembrane potential, the injury current associated with ischaemia and ST segment shifts in ischaemia.

3.2.1 Transmembrane potential of ischaemic cells

It is well documented that ischaemia causes changes in the transmembrane potential of the affected cells [90, 91, 92, 8, 93]. The typical changes include a decrease of the resting membrane potential, a shorter duration of the action potential and a decrease of amplitude of the action potential. The times of onset and up-stroke of the action potential are also changed (Figure 3.1).

In 1960, Samson and Scher [90] observed that the plateau of the intracellular action potential was of a shorter duration after 4 minutes of coronary artery ligation in dogs; the intracellular potential revealed a decreased resting potential, as well as a shortened action potential after two minutes of ischaemia. Downar *et al.* [92] reported that, after 5 minutes of occluding the LAD in pigs, the action potential was reduced in both amplitude and duration, and the up-stroke velocity was also decreased. The ischaemic cells became unresponsive following 12-15 minutes of the LAD occlusion.

Other intracellular recordings [91] showed a substantial loss in the resting membrane potential, small changes in the duration and amplitude of phase 2 and in the slope of phase 3. Similar results were obtained in porcine hearts [8, 94]. Following the LAD occlusion in pigs, the first change was a decrease in the resting transmembrane potential; after a further 3 minutes, the action potentials were shortened and their amplitude reduced; finally, the ischaemic cells became totally unresponsive at a resting potential of about -60 to -65mV within 7-10 minutes of occlusion [8].

The degree of changes in the transmembrane potential varies with the time course of ischaemia. The transmembrane potential of ischaemic cells can vary from "near normal" to having a very small amplitude, depending on the location and duration of ischaemia [8].

3.2.2 ST segment shift

It is well known that ST segment shift is an important indicator of myocardial ischaemia and infarction and results from alterations of the transmembrane potential of ischaemic myocardial cells [90, 91, 92, 8, 93]. The ST segment shift results from the injury current in ischaemia. It has been suggested that the injury current occurs at the ischaemic boundary [31, 60, 8]. Because of the transmembrane potential difference between the ischaemic and non-ischaemic cells, local current will flow across the ischaemic border as long as the cells are well electrically coupled. The magnitude and direction of these currents vary throughout the cardiac cycle. Figure 3.2 shows the difference in transmembrane potentials between the normal and ischaemic cells, the cellular current direction and TQ/ST polarity during phase 4 and phase 2 of the action potential (AP). During phase 4, the difference in resting potential between ischaemic and normal cells produces the current which flows from ischaemic to normal cells through the intracellular compartments, giving rise to the current flowing from normal to ischaemic cells in the extracellular space [60, 95, 8, 93]. Electrical potential caused by this current is called TQ segment shift, thus phase 4 is also called the TQ interval. TQ segment depression is registered in the ischaemic area and TQ segment elevation in the normal area. During phase 2, the difference in the

action potential between normal and ischaemic cells produces a current source in the ischaemic side and a current sink in the normal side in the extracellular space. Electrical potential caused by this current during phase 2 is called the true ST segment shift. Thus ST elevation is registered in the ischaemic area and ST depression in the normal area. In a conventional AC coupled ECG recorder, TQ change and ST change can not be differentiated and the recorded ST change is a combination of both. Therefore both TQ depression and ST elevation are shown as ST elevation, while TQ elevation and ST depression are contributors to the recorded ST depression. The time course and the predominance of ST or TQ segment changes in ischaemia have not yet been settled [90, 91, 92, 8, 96], but this is beyond the scope of this review.

ST elevation and ST depression can appear depending on the ischaemic location and the recording position. For example, ST elevation is registered over the ischaemic region on the epicardium during transmural ischaemia [21]. Meanwhile ST depression appears over the non-ischaemic region on the epicardium. In the same study, however, ST elevation is registered over the ischaemic region on the endocardium while ST depression appears on the epicardium during subendocardial ischaemia.

3.2.3 Ischaemic region and boundary

To evaluate the injury current in ischaemia accurately, a precise knowledge of the ischaemic region is essential. The present study is based on the data obtained from a sheep model [21]. The anatomy of coronary arterial circulation of sheep is remarkably consistent. The arterial circulation of the ovine left ventricle is exclusively supplied by the left main coronary artery and its tributaries; the right coronary artery makes no contribution [97, 98, 21]. The LAD supplies the anterior wall, apex and the anterior two thirds of the septum while the LCX supplies the posterior septum, the inferior and lateral walls. In fact, Li [21] found that the LCX supplies 46% of the left ventricle, and the LAD 52%, so that both arteries can be assumed to supply approximately half of the left ventricle. When these arteries are narrowed, their supplied territories become ischaemic. In this thesis, ischaemia such as these

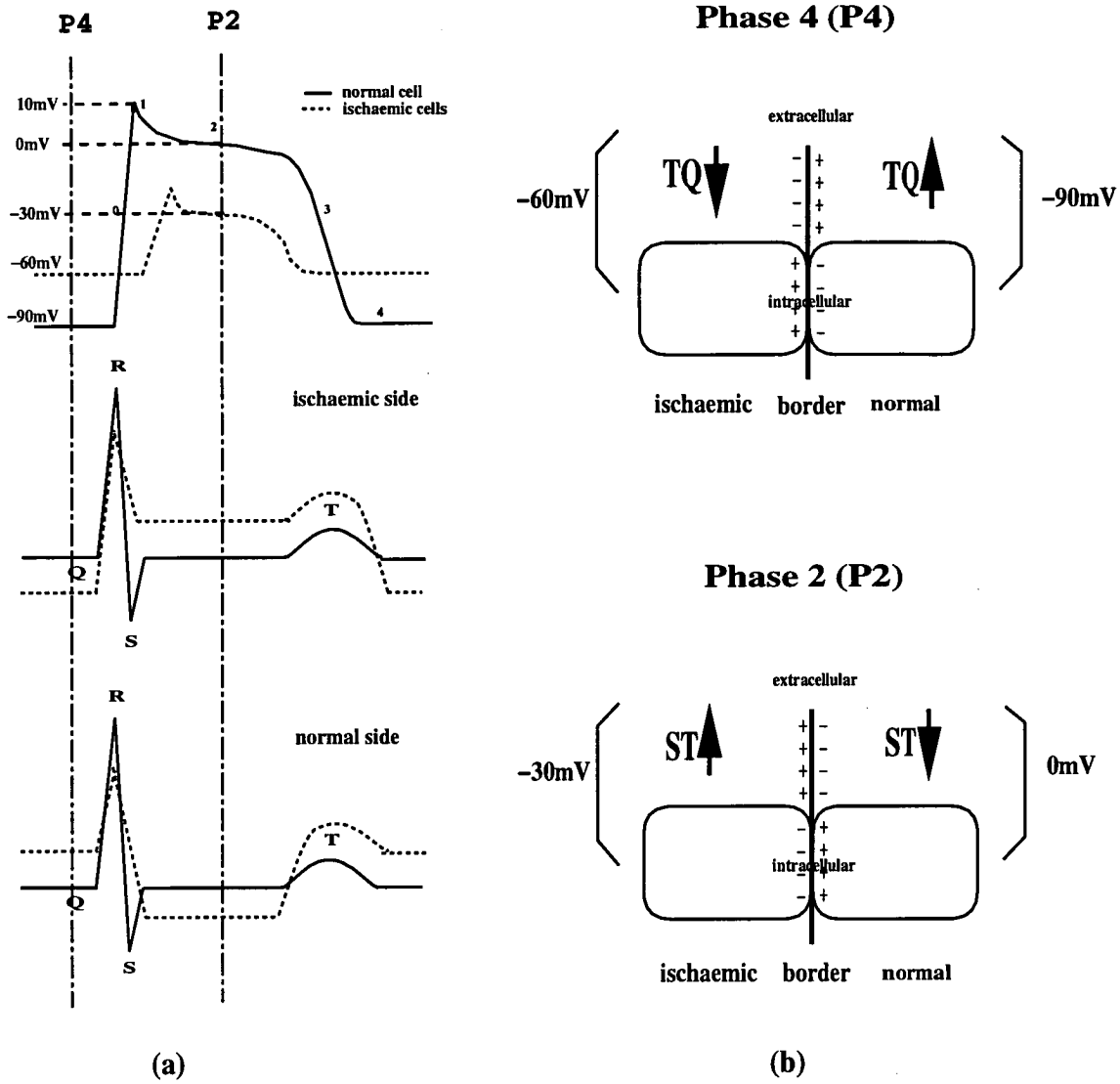

Figure 3.2: *Illustration of cellular current and TQ/ST changes produced in the ischaemic boundary. In diagram (a), the top figure shows the action potentials of normal cells (solid line) and ischaemic cells (dotted line), the middle shows normal ECG (solid line) and ischaemic ECG (dotted line) in the ischaemic side, and the bottom shows normal ECG (solid line) and ischaemic ECG (dotted line) in the normal side. Diagram (b) shows the polarity of TQ/ST changes during phase 4 (P4) and phase 2 (P2) of the AP. Sign* $\uparrow$ *indicates elevation and* $\downarrow$ *depression. Signs (+) and (-) indicate the source polarity. During the P4, the resting potential of normal cells is -90mV and ischaemic cells -60mV. During the P2, normal cells have an action potential of 0mV and ischaemic cells -30mV.*

are referred to as ischaemia of a large region. Both LAD and LCX have their own branches, and ligation of such a branch artery results in ischaemia of a small region. A study carried out in Dorset sheep [98] showed that the LAD had its first branch originating high on the anterior wall of the left ventricle, and that the second branch had a variable site of origin at the middle-LAD distributing over the lower anterior wall and apex. The LCX extended around to the posterior wall to give 2-3 marginal branches and a short posterior descending artery with septal branches.

The ischaemic boundary is another factor to influence the current sources derived from ischaemia. The existence and width of ischaemic gradients at the ischaemic boundaries are still debatable [99]. Many investigators have studied the myocardial blood flow [100, 101, 102], metabolic changes [103, 101] and electrophysiological changes [104, 105, 103] in samples from the lateral edges of the ischaemic regions. Some maintained that the transitional zone is a border zone of intermediate injury tissue [104, 106, 105]. But most agree that the transition from non-ischaemic to ischaemic tissues is sharp [100, 101, 102, 97].

Reimer and Jennings [100] suggested that the zone of intermediate reduction in blood flow between non-ischaemic and ischaemic regions in dogs occurs in a 1-2mm section because of interdigitation of ischaemic and normal cells. Studies of blood flow after acute coronary artery occlusion in dogs showed that the transition of an intermediate reduction in blood flow was limited to a narrow rim of myocardium of 3mm or less in width immediately inside the ischaemic region, and that the intermediate reduction in blood flow at the border resulted from an admixture of normal and ischaemic myocardium [102]. Euler and co-workers [97] observed that ligation of the LCX produced a sharp boundary between perfused and non-perfused tissues in the ovine heart. An electrophysiological, metabolic and histochemical study of the ischaemic boundary in the pig heart indicated that cells with nearly normal transmembrane potential were in close proximity to unresponsive cells with low resting potentials, suggesting that the ischaemic border was composed of interdigitating normal and ischaemic zones sharply demarcated from each other [103].

The zone between ischaemic and non-ischaemic regions in subendocardial ischaemia

is less well established. However, it is well known that the subendocardial segment is more frequently and more severely affected than the epicardial segment following coronary artery ligation [107]. Some studies of blood flow have shown that there is a gradual change in blood flow from the epicardium to the endocardium for partial thickness ischaemia [100, 108]. This suggests that there may be a border zone of intermediate injury between the ischaemic and normal regions in the transmural wall.

3.3 ST segment models during ischaemia

The ST segment is a part of the ECG. Like the QRS complex (Section 2.3.2), simulation of the ST segment potential includes two aspects: the cardiac current source and the volume conductor. Here four equivalent injury current generators and one cellular source description are discussed, including their potential distributions in various volume conductors.

3.3.1 Dipole theory

The dipole theory related to myocardial injury was introduced by Wilson and co-workers [31, 109, 110]. The electric field produced by an injured muscle fibre was approximately equivalent to that produced by a current dipole in an infinite media. The direction of the ST displacement produced by the injury in the endocardial and epicardial tissues depends primarily on the orientation of the injury relative to the exploring electrode. During the ST interval, the potential difference at the boundary of the injury was represented by a dipole so oriented that the injured muscle was positive while uninjured muscle adjacent to the boundary was negative. In epicardial injury, the epicardium and the precordium over the injured region face the positive side of the dipole. Unipolar leads from these sites should therefore register elevated ST segment, and the ventricular cavity and the opposing wall facing the negative side of the dipole should yield ST depression. In the event of subendocardial ischaemia, electrodes over the injury on the epicardium or body surface should register ST

depression while the cavity and opposing wall should yield ST elevation [111, 112]. For transmural ischaemia in the anterior wall, ST elevation appeared in the anterior, posterior and cavity leads.

The dipole theory can be used to approximate far field such as body surface potentials. Studies of body surface mapping in transmural ischaemia or infarction showed that ST elevation appeared in the ischaemic region while ST depression appeared in the opposite site [113, 114]. However, the maximum ST elevation on the epicardium does not necessarily occur over the centre of ischaemia [114]. Localised ST segment changes on the epicardium do not correspond to changes on the thoracic surface [114]. Although the dipole theory provides the basic information on ST changes on the body surface in transmural ischaemia, it does not work for ST depression in subendocardial ischaemia [4, 21].

3.3.2 Multiple dipoles

A multiple-dipole model was used by Thiry and co-workers [48, 115], with the ventricles being divided into 11 regions and each region being characterised by a dipole at the region's centre. The dipole had a fixed position and direction and a variable strength. They modelled acute ischaemia by reducing the amplitude of the action potential by 20% in one cell of a contiguous pair while keeping the other unchanged [115]. The data of the activation sequence were obtained from Durrer [49]. The corresponding 11 dipole moments were then calculated (Section 2.4.2). The standard 12-lead ECGs were calculated at the correct electrode locations by assuming that all 11 dipoles were coalesced at the centre of the heart, which was placed in an infinite homogeneous torso. Only endocardial and epicardial ischaemia were simulated and basic features of ST change were available in the model. When the subendocardial and epicardial ischaemia occurred in the same part of the ventricle, the ST segment shifts in these two cases were in opposite polarities. Although they claimed that the simulated results coincided with clinical observations of ST elevation over the injured areas, there was no validation for ST depression. Furthermore, they found that the amount of ST change was nearly the same for subendocardial and epicar-

dial ischaemia, although twice as much tissue volume was ischaemic in the epicardial case. The reduction in transmembrane potential amplitude was proportional to the volume of ischaemic tissue; the contiguity effect produced on the ischaemic boundary was an area effect. They concluded that the ST change was not a quantitative measure of the ischaemic volume but a measure of the cross-sectional area of such tissue normal to the direction of signal propagation. In this approach, however, other factors such as the realistic ischaemic boundary and the volume conductor were not taken into account.

As will be discussed in Section 3.3.5.2, Miller and Geselowitz [70] simulated ischaemia with 23 dipoles calculated from the bidomain model.

3.3.3 Multipole

Another alternative to the dipole model is to represent the current generator with a dipole having higher order moments. Mirvis *et al.* [113] determined the equivalent generator properties of acute transmural ischaemia inversely from the measured potentials on a sphere ($6.25cm$) of conductive solution in which an isolated rabbit heart was placed. The 32 ECG signals on the sphere surface were processed to quantify the potentials during ST segment attributable to a central dipole, a four-element multipole (dipole, quadrupole, octopole, hexadecapole) and a single moving dipole during ST segment. Fifteen minutes following the LAD ligation, 74%, 98% and 96% of summed square potential recorded 10 msec into the ST segment could be accounted for by a central dipole, a four-element multipole dipole and a single moving dipole model respectively. Furthermore, during the ST segment, the moment of the single moving dipole correlated directly with the area of the epicardial lesion (r=0.82). The surface potential maps uniformly demonstrated a single ST elevation maximum which was aligned with the ischaemic lesion, with an intensity proportional to the computed dipole moment and the epicardial size. Thus the four-element central multipole dipole and the single moving dipole models provide a quantitatively accurate description of the experimental data.

The solution of the inverse transformation is not unique; that is, one set of body

surface potentials can yield multiple source configurations. In the study of Mirvis *et al.* [113], no epicardial measurements were made to further validate their conclusion.

3.3.4 Solid angle theory

Since Wilson *et al.* [31] proposed that solid angle theory could be used to predict ST elevation during ischaemia, it has been widely used by Holland's group [60, 61, 116] to analyse ST changes recorded from precordial and epicardial locations during ischaemia. Solid angle theory states that the magnitude of ST-segment (Φ) recorded at a surface electrode is (Figure 3.3):

$$\Phi = (\Omega/4\pi) \cdot (\Delta\Phi_m) \cdot K \tag{3.1}$$

where Ω denotes the solid angle of the exploring point (P) subtended by the boundary of the ischaemic territory, $\Delta\Phi_m$ the difference in the transmembrane potential between the normal and ischaemic regions, and K a term correcting for differences in intracellular and extracellular conductivity and changes in gap-junction conductance. Thus ST change at a particular site is due to spatial factors such as the solid angle Ω and non-spatial factors such as the transmembrane potential difference ($\Delta\Phi_m$). During the TQ interval, Φ_{mN} = -90mV and Φ_{mI} = -60mV ($\Delta\Phi_m < 0$) while during the ST interval, Φ_{mN} = 0mV and Φ_{mI} = -30mV ($\Delta\Phi_m > 0$), the electrodes overlying the ischaemic area register TQ segment depression and true ST segment elevation.

In studies of Holland and Brooks [60, 116], the ventricles were represented by a spherical model with inner and outer wall radii of $2cm$ and $3cm$, and placed in an infinite medium with the uniform conductivity. The ischaemia had an assumed shape in the ventricles. They considered the total TQ-ST segment deflection and calculated epicardial ST potentials on the outer sphere and precordial ST potentials at locations $5cm$ above the epicardial surface. Under the assumption that myocardial ischaemic cells had a uniform transmembrane potential in the ischaemic region, the injury current was represented as a distributed dipole layer, which was further assumed to have a uniform potential difference at the boundary between the normal and ischaemic myocardium. They studied different ischaemic regions with various

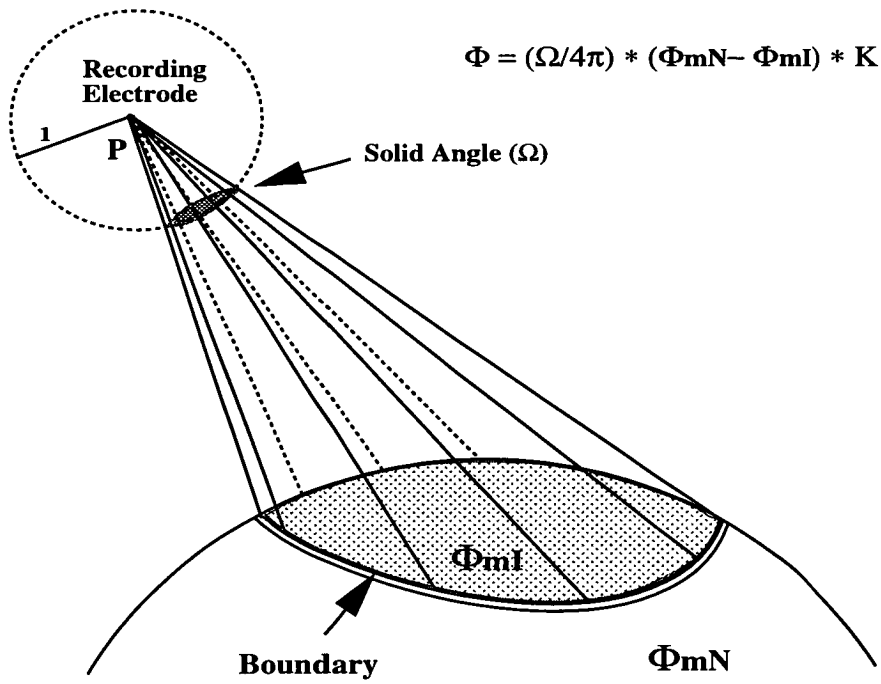

Figure 3.3: *Mathematical and pictorial illustration of solid angle theory. The solid angle Ω is defined as the area of spherical surface cut off a unit sphere (in broken line) by a cone formed by drawing lines from the recording electrode to every point at the boundary of interest. A current source, established by the difference of transmembrane potentials in normal cells (Φ_{mN}) and ischaemic cells (Φ_{mI}), is located at the ischaemic boundary. The shaded area indicates the ischaemic region. (From Holland and Brooks [59]).*

geometrical configurations, and their theoretical findings provided the first thorough examination of the model. Studies using the solid angle theory will be reviewed in the following sections.

3.3.4.1 ST elevation

The studies using solid angle theory by Holland's group [60, 116, 117] predicted that for epicardial and transmural ischaemia, the net TQ-ST potential recorded from a centrally located precordial and epicardial electrode was generally positive, with epicardial ST elevation greater than precordial ST elevation (Figure 3.4). With increased size of ischaemia, precordial ST elevation increased while epicardial ST elevation at the same site decreased in transmural ischaemia. A 22-electrode epicardial recording after ligation of the LAD in pigs [61] confirmed this prediction.

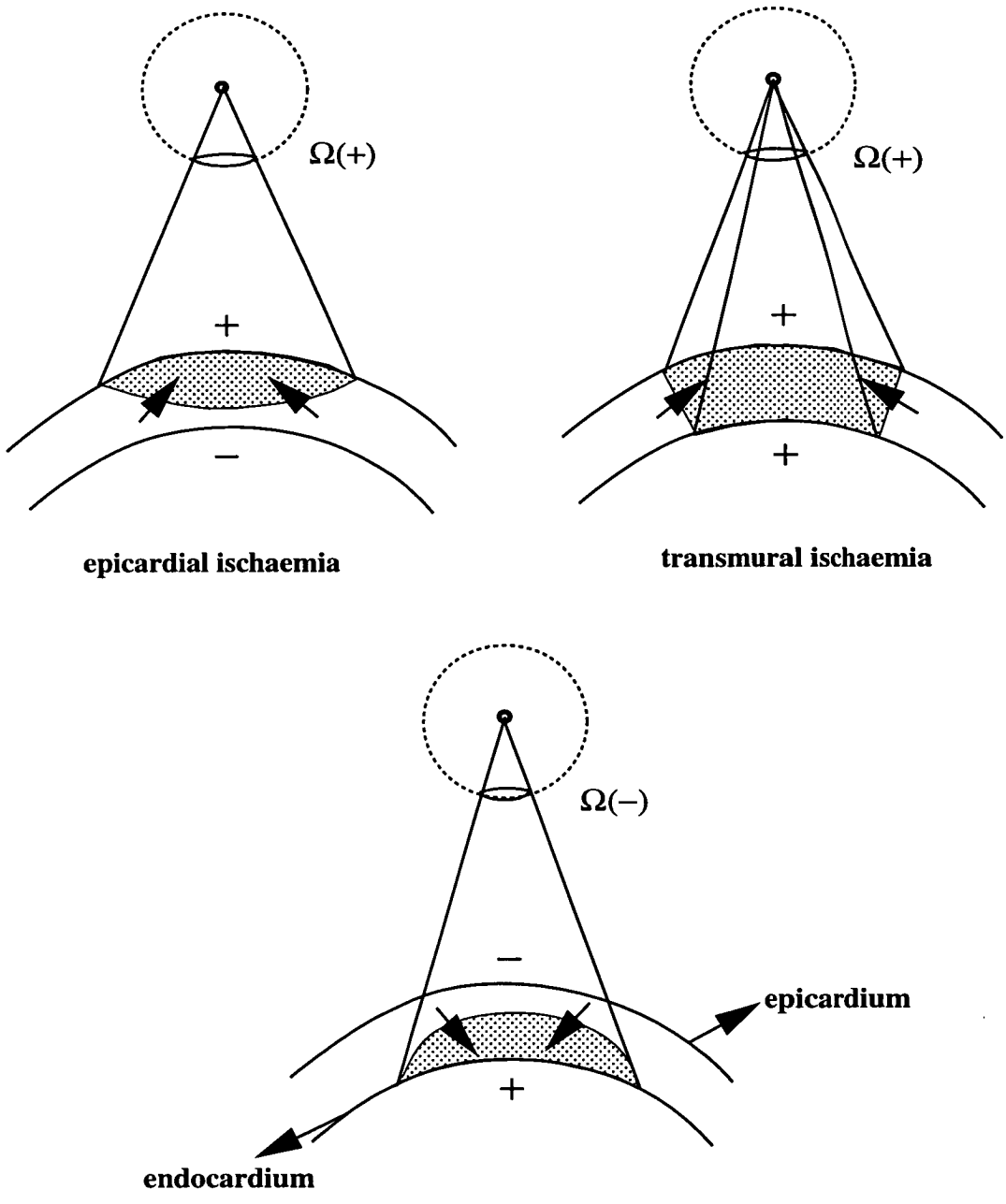

Figure 3.4: *Magnitude and polarity of the solid angle as a function of ischaemic shape. The arrows indicate the direction of intracellular current flow (positive to negative) at the boundary because of the potential gradient at the ischaemic boundary during phase 2 of the AP. The extracellular current would flow from the ischaemic cells to normal cells to complete the circuit. Signs of + and - indicate the polarity of TQ-ST segment deflection on the epicardium and endocardium in three different shapes of the ischaemic region. (From Holland and Arnsdorf [116]).*

Moreover the theory predicted that minimal epicardial ST elevation appeared at the centre, increasing towards the periphery of the ischaemic region, while maximal precordial ST elevation appeared over the centre of the ischaemic region, decreasing at more peripheral locations.

Richeson *et al.* [15] studied transmural ischaemia in open-chest pigs using solid angle theory to quantify the solid angle of an experimentally produced ischaemic zone and to relate it to the observed ST change. The heart was modelled by a sphere with an outer radius of $3cm$ and a uniform wall thickness of $1cm$. The ischaemic zone was assumed either to be cylindrical with its axis passing through the heart, or to be of the transmural shape (i.e. its margins were radially oriented). The ischaemia was generated in pigs by occluding the LAD or its branches. They showed that the maxima of ST depression and ST elevation occurred on either side of the injury boundary on the epicardium, but with smaller ST change in the ischaemic boundary and less reduction of the potentials at the centre, as predicted.

Maehara *et al.* [114] examined the relationship between ST change and the magnitude of solid angle in an isolated, perfused and isovolumically contracting canine heart within a homogeneous cylindrical volume conductor. During five minutes of the LCX occlusion, recording was made simultaneously with 246 electrodes (14 subendocardial, 112 epicardial, 120 precordial). The ischaemic boundary was obtained from postmortem angiography; the solid angle subtended by the ischaemic boundary was calculated for each electrode. A strong correlation was found between measured ST potential and calculated solid angle. However, the most pronounced difference between measured ST potential and calculated solid angle was around the ischaemic boundary on the epicardium.

The polarised volume model was proposed by Smith and associates [118, 119] based on observations [91] of a gradient in the transmembrane potential of ischaemic cells, which extended from the boundary to the centre of the ischaemic region. The source was represented by a volume of distributed dipoles in a heart model similar to that used by Holland and Brooks [60]. The total volume of ischaemia could be divided into an arbitrarily large number of volume elements. Each volume element had

a gradient transmembrane potential, thereby behaving as a small current dipole. This model explained the observation that the highest ST elevation occurred near the centre of the ischaemic region during the later stage of ischaemia (20 minutes after ligation). It also explained the increase in epicardial ST elevation everywhere when the ischaemic region was increased [118]. One suggestion was also put forward by Smith *et al.* [118, 119] to reconcile some of these conflicting viewpoints from the solid angle theory, that is, Holland and Brooks' hypothesis was applicable for early ischaemia. However, Richeson *et al.* [15] found a good correlation between the measured epicardial ST potentials and the calculated solid angles during late ischaemia (90 minutes after occlusion), although they suggested that even better correlations would have obtained if the dipole sources had been distributed in a rather wide ischaemic boundary. Nevertheless, there was strong evidence against the diffusive ischaemic boundary from the blood flow measurements [100, 101, 102].

3.3.4.2 ST depression

Holland and co-workers [60, 61], using solid angle theory, predicted that the epicardial ST depression occurred over the underlying injury area during subendocardial ischaemia (Figure 3.4); the ST potential was more negative when the size of ischaemia increased. However, their experiments in closed-chest pigs did not show these changes of ST depression. They suggested that the pig was more likely to develop epicardial ischaemia instead of subendocardial ischaemia.

Hyttinen [120] employed a detailed torso structure including thoracic inhomogeneity to simulate ST changes in subendocardial ischaemia on the body surface using the uniform double layer model. The border between normal and ischaemic regions was assumed to be mainly parallel to the epicardium, yielding a radial injury current. The whole torso was divided into about 90,000 nodes in a non-uniform grid. The source was assumed to have a constant potential difference at the ischaemic boundary. Laplace's equation (equation 3.2) for ST potential was solved by the finite difference method (FDM) with the source being represented by Dirichlet boundary

condition (equation 3.3) at the ischaemic boundary nodes.

$$\sigma \nabla^2 \Phi = 0 \tag{3.2}$$

$$\Phi|_B = C \tag{3.3}$$

where B represents the ischaemic boundary and C the given potential difference of the uniform dipole layer. In Hyttinen's study, a value of 65mV was used to represent the potential difference across the ischaemic border. The simulation showed that ST depression on the body surface could localise subendocardial ischaemia, but there was no clinical validation.

Holland *et al.* [61] further predicted that epicardial ST depression occurred over the non-ischaemic region just outside the ischaemic boundary in transmural ischaemia. This ST depression was observed in their experiments in pigs during early transmural ischaemia, and its amplitude increased after larger artery occlusion. The epicardial ST depression on the normal side of the ischaemic boundary was confirmed experimentally and theoretically (using solid angle theory) by Richeson *et al.* [15] and Maehara *et al.* [114]. However, they failed to show the predicted increasingly deep negativity as the ischaemic border was approached. Furthermore, the precordial ST depression was seen on the opposite side of the ischaemic region as predicted by solid angle theory.

3.3.5 Bidomain model

3.3.5.1 Tung's model

The bidomain model was introduced by Tung [62] to study the DC (direct current) changes during ischaemia. A sphere similar to that used by Holland and Brooks [60] was used to represent the ventricles, which in turn was placed in a semi-infinite volume conductor. In this way, the open chest preparation was modelled with the left free wall exposed to air. Poisson's equation was solved with the current source represented by the second gradient of the resting potential (equation 3.4):

$$\sigma \nabla^2 \Phi = -\sigma_i \nabla^2 \Phi_m \tag{3.4}$$

Where Φ_m is in phase 4 of the AP, corresponding with the TQ segment. The endocardial and epicardial TQ potentials were calculated when the ischaemic region was located in the subepicardium, subendocardium, transwall and intrawall with simplified ischaemic boundaries. Subendocardial and epicardial ischaemia were assumed to have only the transmural boundary, thus endocardial TQ depression and epicardial TQ elevation appeared over the ischaemic region in subendocardial ischaemia. The epicardial ischaemia had similar TQ changes with an inverted polarity.

In the model of transmural ischaemia, the ischaemic region was assumed to take 1/3 of the heart volume. Transmural ischaemia with an abrupt boundary yielded a decreasing TQ potential towards the centre of the zone. The epicardial potential distribution was biphasic over the surface with a reverse polarity at the border (TQ depression on the ischaemic side and TQ elevation on the normal side), while the endocardial potential distribution showed a monophasic change over the surface with TQ depression over the ischaemic region. When the ischaemic boundary was assumed to be diffusive in transmural ischaemia, the epicardial potentials were monophasic with an increasing amplitude towards the centre. Tung noted that epicardial potentials were much larger than endocardial potentials in the bidomain model, while solid angle theory predicted a similar amplitude for both epicardial and endocardial potentials in transmural ischaemia. He also pointed out that epicardial ST depression was a reciprocal change at the ischaemic zone. This reciprocal depression would disappear in either subepicardial or subendocardial ischaemia.

3.3.5.2 Miller and Geselowitz's model

Miller and Geselowitz [70] employed the heart and torso models and the techniques presented in their paper on the normal ECG simulation [34] (Section 2.4.5) to simulate ST potentials in myocardial ischaemia and infarction. The bidomain model was used to calculate intracellular dipole moment density at each model point, which was proportional to the negative spatial gradient of the intracellular potential distribution (equation 3.5). Extracellular potentials were calculated from the intracellular

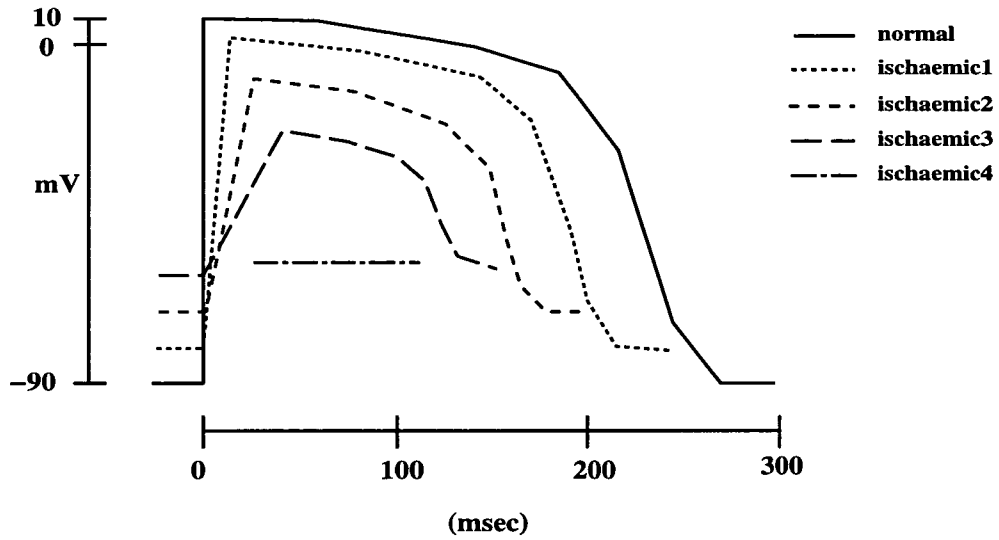

Figure 3.5: *Illustration of ischaemic action potentials with different severity as used by Miller and Geselowitz [69]. The number for ischaemic cells increases with increasing severity of ischaemia.*

dipole sources (equation 3.6).

$$\vec{J}_i = -\sigma_i \nabla \Phi_i \tag{3.5}$$

$$\nabla^2 \Phi_e = \frac{1}{\sigma_e} \nabla \cdot \vec{J}_i \tag{3.6}$$

where $\vec{J}_i$, Φ_i and Φ_e represent intracellular current density, intracellular potential and extracellular potential respectively. $\vec{J}_i$ could also be interpreted as the current dipole moment per unit volume in the extracellular space. By varying the resting potential and duration of the action potential to correspond to the changes observed during ischaemia and calculating the 23 dipoles, the potential distribution on the surface was then calculated from a set of 23 dipoles using the transfer coefficient previously obtained by Cuffin and Geselowitz [50]. The distribution of the severity of the injury within a particular injured region was modelled by dividing the injury into five segments running from the boundary to the centre of the injury. Increasing severity of ischaemia was simulated by progressively decreasing the magnitudes of the resting potential, the action potential and the maximum depolarisation potential, and by increasing the depolarisation rise-time (Figure 3.5). Miller and Geselowitz [70] stated that the calculated standard 12 lead ECGs in acute ischaemia and infarction were in good agreement with patient data reported in the literature.

Subendocardial ischaemia in an anterior location was also simulated. The decreased action potentials (from 0 to 20 mV less than normal) were assigned to the ischaemic region. The simulation showed that the ST depression was seen in leads I, aV_L and V_2-V_5, reflecting the baseline elevation in the same leads. Also the reduction in the duration and amplitude of action potential resulted in ST depression and inverted T waves in the same leads. The ST potential distribution on the body surface showed that ST depression appeared in leads over the injured region.

The ST potentials were calculated when the transmural ischaemic region was in the anterior, lateral and inferior walls of the left ventricle with assumed ischaemic shapes. There was a potential maximum (maximal ST elevation) on the portion of the torso facing the injury, and an opposing minimum (maximal ST depression) on the remote site. The exact placement of these maxima and minima was dependent on both the location of the injuries and their distance from the torso. ST potential distribution on the body surface from the anterior transmural ischaemia was found to be similar to that in the anterior subendocardial ischaemia, with the positions of the maximum and of the minimum reversed. Miller and Geselowitz also found that changes in the precise shape of the injury boundary could cause large changes in the surface ECG without significantly affecting the volume of the injured tissue.

3.3.5.3 Other simulations using the bidomain model

Dube *et al.* [121] simulated body surface potentials during percutaneous transluminal coronary angioplasty (PTCA) using a realistic geometry computer model. The torso model included regions of different conductivity to represent lungs, intraventricular blood masses and the skeletal muscle layer. An equivalent dipole source was determined from the spatio-temporal distribution of the transmembrane potential. The equivalent dipole density $\vec{m}$ at a model point was computed by assuming an isotropic bidomain model for the myocardium, and was given by

$$\vec{m} = -\frac{\sigma_i \sigma_e}{\sigma_i + \sigma_e} \nabla \Phi_m \tag{3.7}$$

The equivalent dipole density was then used to calculate the surface potentials on the torso model. Three assumed transmural ischaemic regions in the LAD, LCX

and right coronary artery (RCA) were simulated. The ischaemic zone was assumed to have mild, moderate and severe injuries, each with its own resting and action potentials. The calculated ST segment shift in each of these ischaemic regions was in the range of $\pm$(200-300)μV. They indicated that ST elevation overlaid the ischaemic region while ST depression over the non-ischaemic region was a reciprocal change of the primary ischaemic region. Even though the myocardial anisotropy was considered in the model, no comparison with a simulation of myocardial isotropy was made to draw conclusions about the effects of anisotropy on ST potentials.

3.4 Clinical and experimental observations

3.4.1 ST depression

3.4.1.1 ST depression in subendocardial ischaemia

It is well known that epicardial and precordial ST depressions are associated with subendocardial ischaemia. Six epicardial and six endocardial electrodes were placed over the affected region in LCX subendocardial ischaemia in dogs in the study of Guyton *et al.* [122]. The epicardial ST depression and endocardial ST elevation occurred with the average amplitude of epicardial ST depression much smaller than that of endocardial ST elevation.

Vincent *et al.* [123] produced subendocardial ischaemia by atrial pacing and partial occlusion of coronary artery in dogs. Progressive increase in the paced heart rate in the presence of 60% reduction in coronary flow produced a prominent TQ depression and a true ST elevation in the subendocardial recording with only minimal changes in the epicardial recording over the ischaemic region. They suggested that the magnitude of subendocardial injury currents produced in the heart could be too small to yield epicardial ST changes.

Li and co-workers [4] measured simultaneously epicardial (64 electrodes) and endocardial (40 electrodes) ST potentials in open-chest sheep during LAD or LCX subendocardial ischaemia. The ischaemia was produced by atrial pacing and par-

tial coronary ligation, and confirmed by fluorescent microspheres [108]. The results showed that the region of ST elevation on the endocardium correlated with the region of reduced blood flow while epicardial ST depression did not. However, the magnitudes of the maximal epicardial ST depression and maximal endocardial ST elevation correlated well with the average transmural blood flow ratio in the ischaemic region. The two regions of subendocardial ischaemia had a similar pattern of anterolateral epicardial ST depression while the endocardial ST elevation indicated the ischaemic region.

Mirvis [124] recorded body surface potentials (84 electrodes) during LAD, LCX, and RCA partial thickness ischaemia produced by constriction of a coronary artery in dogs. They found that the body surface ST depression had an overlapping area in the left lateral chest during these three episodes of regional subendocardial ischaemia. A further study [125] confirmed this ST depression location with partial LCX ligation. Mirvis *et al.* [125] reported that an abnormal ST depression developed when endo-epi flow ratio was reduced to 0.45. Although the magnitude of ST depression showed a significant correlation with the transmural flow ratio (r=0.87), there was no correlation between the position of ST depression and the ischaemic region. The maximal ST depression clearly appeared over the left lateral chest with an amplitude of about 1mV after LCX ligation.

Exercise-induced ST segment depression was studied by Cohen *et al.* [96] with direct-current magnetocardiogram. In a well-documented patient with typical coronary artery disease, ST depression was detected on the anterior location of the chest after exercise testing. They concluded that exercise-induced ST depression was mostly due to an injury current during the TQ interval.

A clinical study of the 12-lead ECGs during exercise stress testing with angiographically documented one-vessel disease [126] showed that ST depression developed in 54 of the 56 patients who had a positive stress test. There was no correlation between the diseased coronary artery and the leads in which ST depression occurred. Similar results were reported by Dunn *et al* [1]. Mark and co-workers [2] studied 452 consecutive patients with one-vessel disease (LAD, LCX and RCA) who underwent

treadmill testing, showing that the ST depression occurred most commonly in leads V_5 or V_6 regardless of which coronary artery was involved.

Body surface mapping with 87 leads [3, 127, 128] was performed after treadmill exercise in patients with single-vessel disease which could be located in the LAD, or RCA, or LCX supplied region. The results showed that the sites of maximal ST depression (40ms after J point) were located in the limited area of the left anterior chest in all patients. However, Kubota *et al.* [128] reported that the changes in patterns of isopotential maps after exercise testing from the ST segment to the T wave were dependent on the obstructed coronary artery. Moreover, ST-T isointegral maps, defined as the algebraic sum of all potentials from the J point and T wave for each lead [127], were useful for diagnosing the ischaemic region evaluated by exercise testing. That is, the negative ST-T integral area was found to correlate with the ischaemic region.

Kilpatrick *et al.* [5] examined the computed epicardial ST maps of patients with ST depression who had no evidence of ST elevation on 12-lead electrocardiogram. The technique of inverse transformation to produce epicardial ST maps from the body surface maps has been described elsewhere [129, 130]. Epicardial current density distributions showed a region of current flow out of the heart and over the great vessels in 88 out of 93 patients. This suggested a selective current path from the ischaemic endocardium that travelled out of the heart through the great vessels. If the current from endocardial ST elevation was flowing out of the great vessels back to the epicardium, then most of the epicardium could appear negative relative to the superior aspect of the heart. The low resistance in the great vessels would explain why ST depression can not indicate coronary artery disease. In open-chest sheep, however, subendocardial ischaemia produced by partial ligation of either LAD or LCX and confirmed by fluorescent microspheres, showed a similar pattern of ST depression on the epicardium regardless of the artery involved [21]. Insulating the heart surface with plastic only increased the amplitude of epicardial ST depression and did not change its distribution pattern. Li [21], therefore, suggested that epicardial ST depression in subendocardial ischaemia was due to the current flowing inside the heart rather than the current flowing through the great vessels. In ad-

dition, Green *et al.* [131] provided no evidence in support of this special current path suggested by Kilpatrick *et al.* [5]. They found that the amplitude of epicardial potentials from isolated dog hearts was markedly higher when the heart was surrounded by an insulating medium, but potential patterns were less affected by the surrounding medium [131].

3.4.1.2 ST depression in transmural ischaemia

Epicardial ST depression at the normal tissue adjacent to the ischaemic boundary in transmural ischaemia was shown by Wolferth and co-workers [14] in 1945 and by Katcher *et al.* [132] in 1960. Studies with epicardial recording in baboons [7] and pigs [61, 15] following coronary artery ligation confirmed these earlier findings in dogs. However, studies of Kleber *et al.* [8] and Li [21] showed that there was little or no epicardial ST depression on the non-ischaemic region with small regions of transmural ischaemia. Moreover, Li and co-workers [9] found that there was a strong dipole of ST changes over the left lateral region of the epicardium with ST depression on the non-ischaemic area and ST elevation on the ischaemic area during either LAD or LCX total ligation in a sheep model. Interestingly, a similar pattern of ST changes but with a lower amplitude appeared on the endocardium, namely ST elevation on the ischaemic region and ST depression on the non-ischaemic region.

In earlier dog studies, the ECG leads overlying the non-ischaemic myocardium, opposite to the region affected by total ligation of a single vessel, invariably demonstrated ST depression during coronary occlusion [112, 133]. The body surface mapping in animal experiments with the isolated heart in a bounded isotropic volume conductor showed ST elevation over the ischaemic region and ST depression over the opposite side of the body surface at 5-15 minutes after occlusion of a single coronary artery [113, 114]. Both the maximum and minimum of ST segment shift increased in strength with the ischaemic size. Crawford *et al.* [134] measured 6-limb lead ECG in baboons after LAD ligation and observed reciprocal ST depression at sites distant from the injured area.

Precordial ST depression has been frequently reported in patients with acute my-

ocardial infarction [16, 135, 17, 136]. The mechanisms responsible remain controversial [20]. Two mechanisms are generally discussed. Firstly, the anterior ST depression may reflect reciprocal change of the inferior ST elevation in inferior LAD infarction [16, 124, 17, 136]. Patients with acute inferior myocardial infarction had a similar degree of segmental dysfunction in the infarcted wall, while no abnormalities in segment wall motion in the remote wall were seen, regardless of the presence or absence of ST depression on the remote wall [137, 138]. Studies in patients during PTCA [139, 17, 140] demonstrated that the regions showing precordial ST depression had no indication of being ischaemic on the basis of the study on regional left ventricular wall motion [17]. Precordial ST depression in inferior infarction may also reflect more extensive inferior myocardial infarction which might have posterolateral or inferiorseptal extension of the infarction [16, 134, 135, 136]. Other workers suggested that the ST depression correlated well with the magnitude of ST elevation [138, 140]. The other possible mechanism lies in the fact that the ST depression could be produced by an additional ischaemia from a second artery occlusion [18, 19]. The additional remote ischaemia might have resulted from a second critically narrowed vessel caused by the increased oxygen demands in the non-infarcted myocardium. Kilpatrick *et al.* [129, 130] performed an inverse transformation to produce the epicardial ST maps on patients with acute inferior myocardial infarction. They found that there was a strong dipole of ST changes from the inferior to the lateral surface on the epicardium, which showed a significant correlation with the mortality rate [141]. The dipole patterns were thought to be evidence of a second active current source such as subendocardial ischaemia. However, no confirmation of subendocardial ischaemia such as blood flow measurement was made and the patients who had this pattern did not necessarily have any coronary disease other than the single occluded artery.

3.4.2 ST elevation

3.4.2.1 ST elevation in subendocardial ischaemia

ST elevation is seen on the endocardium over the ischaemic region in subendocardial ischaemia [122, 123, 4]. Studies with several endocardial electrodes placed over the ischaemic region in dogs [122, 123] indicated TQ depression [123] and ST elevation [122] on the endocardium in subendocardial ischaemia. Endocardial ST mapping during subendocardial ischaemia in sheep showed that maximal ST elevation occurred in the centre of the ischaemic area, decreasing towards the boundary [4]. These studies showed that the endocardial ST elevation had a higher amplitude than the epicardial ST depression. In LCX subendocardial ischaemia in dogs, for example, an average endocardial ST elevation of six sites over the ischaemic area was in the order of 2.5mV, while the average ST depression of the corresponding six sites on the epicardium was -0.7mV [122]. Vincent *et al.* [123] demonstrated that TQ depression was present in endocardial leads, but there were no TQ segment or true ST segment changes in the epicardial leads during partial ligation of either the LAD or the LCX. In addition, both LAD and LCX subendocardial ischaemia in sheep showed that the maximal epicardial ST depression ranged from -6mV to -10mV, while the maximal ST elevation on the endocardium ranged from 10mV to 15mV [21].

ST elevation together with ST depression also appeared on the body surface in subendocardial ischaemia induced by atrial pacing in dogs with coronary stenosis at various locations [124, 125].

3.4.2.2 ST elevation in transmural ischaemia

ST elevation is a marker of transmural ischaemia. There is some discrepancy about the relationship between epicardial or body surface ST elevation over the ischaemic region and the ischaemic size. Studies in dogs [104, 142] showed that epicardial ST elevation increased when the area of ischaemia was enlarged. High resolution (54-72 electrodes over the ischaemic region) epicardial ST mapping [118] during ligation of a

diagonal branch of the LAD showed that after 60 minutes of pre-existing ischaemia, epicardial ST elevation increased with an increase in the size of an ischaemic region, and decreased with a reduction in the ischaemic size. By contrast, in the same study by Smith *et al.* [118], they found that a decrease in ischaemic size resulted in an increase in ST elevation on the epicardium during early ischaemia (less than 20 minutes of ischaemia), and vice versa. Holland and co-workers [61] demonstrated that within the first two minutes after LAD ligation, an increase in the size of an ischaemic region in the pig heart resulted in a decrease in epicardial ST elevation. In some instances, when the coronary artery was occluded more proximally, no epicardial ST elevations were recorded at the ischaemic centre [61]. Cohen and Kirk made similar findings in dogs [10]. The epicardial ST elevation in the centre might be minimised or abolished if a focal intra-ventricular block developed and the QRS duration was extended [143]. However, focal conduction block was seldom pronounced in the early stages of myocardial ischaemia [90], and Maehara *et al.* [114] found a similar epicardial pattern in dogs after 5 minutes of LCX ligation without widening QRS duration.

There is a general agreement about body surface ST elevation over the ischaemic region. Muller *et al.* [143] found an extremely close and consistent relationship between changes in epicardial and precordial average ST changes regardless of the size of ischaemia during LAD ligation. They noted that precordial ECG mapping was useful for evaluating changes in myocardial ischaemic injury, while the sites of epicardial ST elevation were not reliable indices of ischaemic injury. The precordial ST segment mapping in pigs confirmed that ST elevation was a direct reflection of the extent of myocardial injury [144]. Furthermore, epicardial ST elevation decreased while precordial ST elevation increased as the area of ischaemia became larger [60]. Maehara *et al.* [114] stated that both the peak precordial potential and the area of ST elevation tended to increase with the size of ischaemia during LCX ligation in dogs.

Controversy also arises when considering the epicardial ST elevation distribution over an ischaemic region. For a branch ligation [133, 104, 145, 118], ST elevation decreased towards the ischaemic boundary, with the lowest ST elevation near the

ischaemic boundary. It was shown that constant epicardial ST elevation appeared over the ischaemic region with distal LAD or LCX ligation [7, 8, 9]. However, the maximum ST elevation was recorded on the boundary [95, 61, 15, 114, 9] and lowest ST elevation at the centre of the ischaemic region [61, 15, 114] during the occlusion of a major coronary artery. An epicardial ST mapping with 64 electrodes following LAD or LCX ligation in sheep [21] showed that a strong dipole of ST changes appeared on the left lateral region, with the amplitude decreasing towards the centre. This typical ST potential distribution for transmural ischaemia of large regions corresponded well to the calculated epicardial maps of patients with acute infarction who had a bad prognosis, as reported by Kilpatrick *et al.* [141].

Studies were carried out to correlate epicardial ST elevation with the severity and the size of the ischaemic region predicted by blood flow [11, 12, 13, 9]. Smith *et al.* [11] studied the relationship between the regional myocardial blood flow (RMBF) and epicardial ST segment elevation in open-chest dogs with LAD ligation and found no simple quantitative relationship between epicardial ST elevation and myocardial blood flow following acute coronary artery occlusion. Epicardial ST changes over the developing infarction after proximal LAD ligation correlated poorly with either the RMBF or the degree of tissue enzyme depletion [12]. By occluding the proximal LAD in dogs, significant ST elevation did not occur at many sites with reduced flow and infarction [13]. Despite a good correlation of the RMBF with the severity of myocardial infarction, epicardial ST elevation correlated poorly with either RMBF or the severity of infarction in the same sites. Li [21] found that the greatest epicardial ST elevation occurred in regions with the lowest flow during large acute infarction in either LAD or LCX territory.

3.5 Discussion

This chapter has reviewed relevant mathematical models, and experimental and clinical studies of ST segment changes in ischaemia. There are advantages and disadvantages of these models in terms of being able to explain the observed ST changes.

The dipole model represents the heart's electrical activity by a current dipole which is fixed in position but varies in magnitude. It assumes that the distance from recording electrodes to the heart is large in comparison with the involved size of electrical sources in the heart and that the volume conductor is infinite, homogeneous and isotropic. Body surface potentials can be approximated by the dipole theory, but not the endocardial or epicardial potentials, as shown in the body surface mapping [113, 124, 114]. Furthermore, the cardiac inhomogeneity and myocardial anisotropy can not be easily taken into account with this model.

Although the model of multiple dipoles more accurately represents the electrical cardiac current than the single dipole model, it has the same limitations. That is, it can only approximate the far field in a homogeneous volume conductor.

Solid angle theory provides a specific physiological interpretation of the ECG [60, 61, 15, 114], and is valid at the electrodes far from the heart. As pointed out by Maehara *et al.* [114], the greatest difference between the prediction from solid angle model and the measurements exists at the ischaemic boundary on the epicardium where the electrode is too close to the source. In Holland and Brook's studies [60], the ischaemic region had an assumed unrealistic shape, particularly during subendocardial ischaemia. For both theoretical and practical reasons, solid angle theory does not provide a complete mathematical representation of the electrical activity. Solid angle analysis is of limited value because the thorax is neither a homogeneous nor an infinite volume conductor. The inhomogeneity and irregular shape of the thorax, irregular shape of the ischaemic boundary make mathematical calculation extremely complex [117]. Besides, it is nearly impossible to include the myocardial anisotropy in the solid angle theory.

The bidomain model turns out to be a good model to represent the current source in the heart [62, 70, 121]. The cardiac current can be precisely computed by the spatial gradient of the transmembrane potential. Miller and Geselowitz's model [70] provides excellent results when compared with observations, not only qualitatively but quantitatively as well. However, it is not clear how the intracellular potentials can be calculated from the known activation times and data on action

potential. Neither epicardial nor endocardial data are available to compare with those from animal studies. Moreover, the model did not address the poor localisation of endocardial ischaemia by ST depression. Dube *et al.* [121] studied only the transmural ischaemia using the bidomain model. Even though Tung [62] used the bidomain model to represent the myocardium, many unrealistic assumptions such as the configuration of ischaemic boundaries, and isotropic, semi-infinite volume conductor were made, which drew conclusions similar to those of solid angle theory. The myocardial anisotropy can be easily included in the bidomain model. However, to precisely solve the governing equations in a bounded medium, it is necessary to use numerical methods which normally involves more complicated mathematical computation and requires high performance computers.

As discussed in this review, no modelling studies have yet explained all the observed ST changes in ischaemia. In particular, no modelling study has been made to simulate the endocardial, epicardial and body surface ST changes simultaneously to fully establish 3D ST potential fields in ischaemia. A model, including realistic volume conductor, realistic ischaemic boundary and bidomain myocardial representation, needs to be developed to identify the injury and to explain experimental and clinical ST observations in ischaemia.

Chapter 4

Methods

4.1 Introduction

This chapter presents a description of the models employed, the governing equation in the bidomain model and its numerical solution by the finite element method.

4.2 Model description

Three models are used in the simulation: a simplified three dimensional (3D) block model representing an unfolded heart, a realistic isolated heart model and a realistic torso model. For the 3D block model, numerical computation is easy to realise. The isolated heart model bears resemblance to open-chest animal experiments while the torso model is used to simulate closed-chest experiments or clinical situations.

4.2.1 3D block model

The 3D block model (Figure 4.1) is used to simulate an unfolded heart. According to studies in sheep [98, 21], the left coronary artery provides all of the blood supply to the left ventricle and only a small rim of both the anterior and posterior right ventricle. Thus the right and left ventricles have separate circulations supplied by

separate coronary vessels with minimal overlap. The LAD supplies the anterior wall of the left ventricle and the anterior two thirds of the septum, while the LCX artery supplies the posterior and lateral walls of the left ventricle, and the posterior septum. Therefore the heart can be unfolded from either the posterior descending artery (PDA) or the LAD positions (thick solid line). Cutting through the LAD results in the LCX supplied territory sitting in the centre of the block, while cutting through the PDA gives rise to the LAD supplied territory also being located in the centre of the block. In this way, the potentials resulting from the injury current could be evaluated with minimal boundary effects.

According to Li's measurements of an unfolded sheep heart [21], the unwrapped left ventricle measures 16cm x 10cm x 1cm. In this study, a 3D block model is used to represent the heart and is constructed on the basis of these measurements (Figure 4.1). The x and z axes are assumed to be parallel to the circumflex and transmural directions respectively, and the y axis runs from the base to the apex of the heart. The origin of the axes of x, y and z is located at the centre of the base plane of the block, and the 3D block has a dimensional range of -8 to 8cm, -5 to 5cm and 0 to 4cm respectively. The endocardium is represented by the plane of z=1cm, and the epicardium by the planes of z=2.0cm for $x \geq 0$ and of z=4.0cm for $x \leq 0$. The left ventricular cavity (LVC) is represented by the block between z=0 and z=1cm. The left ventricle is represented by the volume between z=1cm and z=2cm, with $x \geq 0$ for the left ventricular wall (LVW) and $x \leq 0$ for the septum (SPT). The blood in the right ventricle (RV) is represented by a block with a sectional area of 7.2cm x 1.6cm, surrounded by a wall 0.4cm thick and located on the top of the SPT block.

4.2.2 Isolated heart model

The geometry of the heart of a normal female human is constructed from a series of 11 magnetic resonance imaging (MRI) scans at 1cm spacing. The three dimensional surface meshes representing the heart structure with the digitised data were kindly provided by Dr. Gale [146]. The model includes myocardium, venous and arterial blood cavities and partial major vessels (Figure 4.2). Quadrilateral elements are

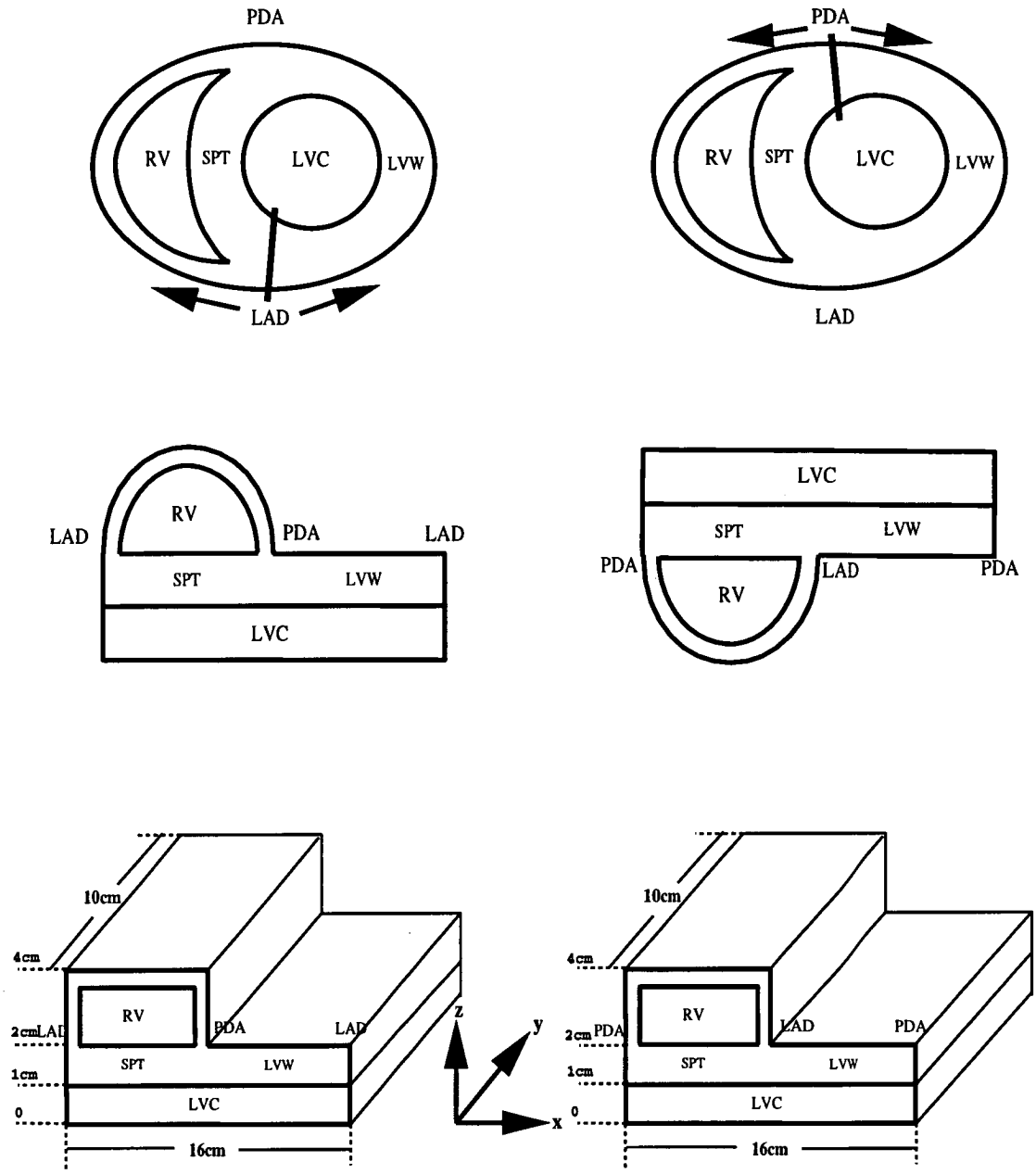

Figure 4.1: *Illustration of the development of the 3D block model for the heart. Top left: A cross section of a heart. The thick solid line at the LAD indicates the location where the myocardium is cut through. The arrows indicate the directions of unwrapping following the cutting. Middle left: The first geometric simplification of the unwrapped section. Bottom left: The block model of the unfolded heart. The three plots on the right show a similar treatments to the PDA location.*

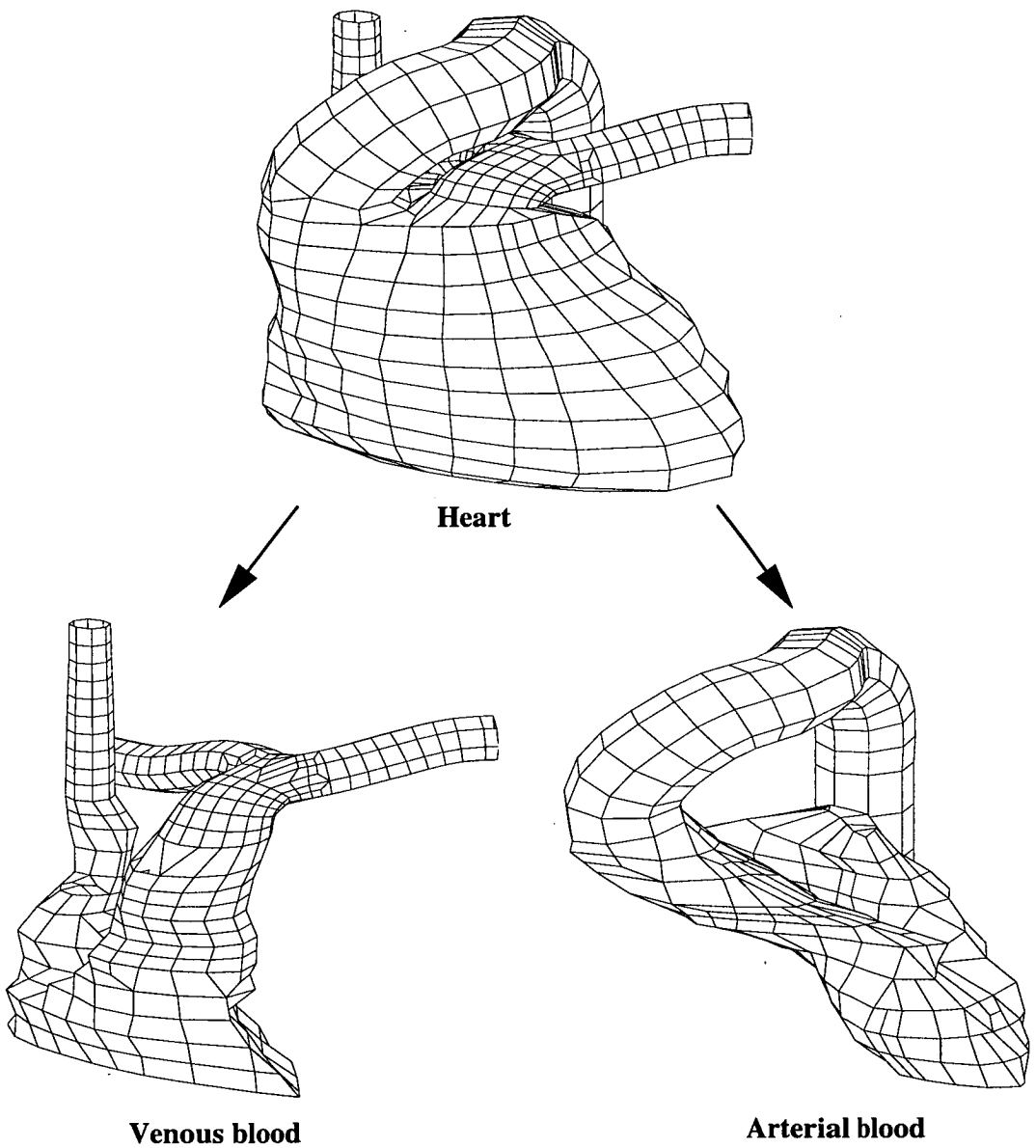

Figure 4.2: *Surface structures of the isolated heart and its internal cavities.*

used to define the surface. The heart surface has 917 nodes and 907 quadrilateral elements. The surface of the venous blood volume is constructed with 760 nodes and 720 elements, and the surface of the arterial blood volume with 505 nodes and 503 elements.

4.2.3 Torso model

The geometry of a male human torso was constructed from a series of 25 computerised tomography (CT) scans at 1cm spacing and 20 MRI slices through the heart also at 1cm spacing[146]. The surface meshes are used to represent the different regions in the torso. In addition to the heart structure described above, there are lungs, spine, sternum, and four ribs on the left side. Although it is not ideal to take scans from different people, the torso and heart are compatible and only a minor modification to the shape of the lungs is needed when the heart is placed in the torso. The digitised surface meshes for different regions in the torso are shown in Figure 4.3 and the numbers of the nodes and the elements in the surfaces are listed in Table 4.1.

	Left lung	Right lung	Spine	Sternum	Torso
Nodes	621	535	362	706	622
Elements	619	533	360	696	620

Table 4.1: *Nodes and elements of regional surfaces in the torso.*

4.3 Governing equations

4.3.1 Poisson's equation

The bidomain model is used to represent the myocardium in this study, in which intracellular and extracellular potentials are governed by the following equations. The detailed derivation of these equations is found in Section 2.4.5.

$$\nabla \cdot \sigma \nabla \Phi_e = -\nabla \cdot \sigma_i \nabla \Phi_m \tag{4.1}$$

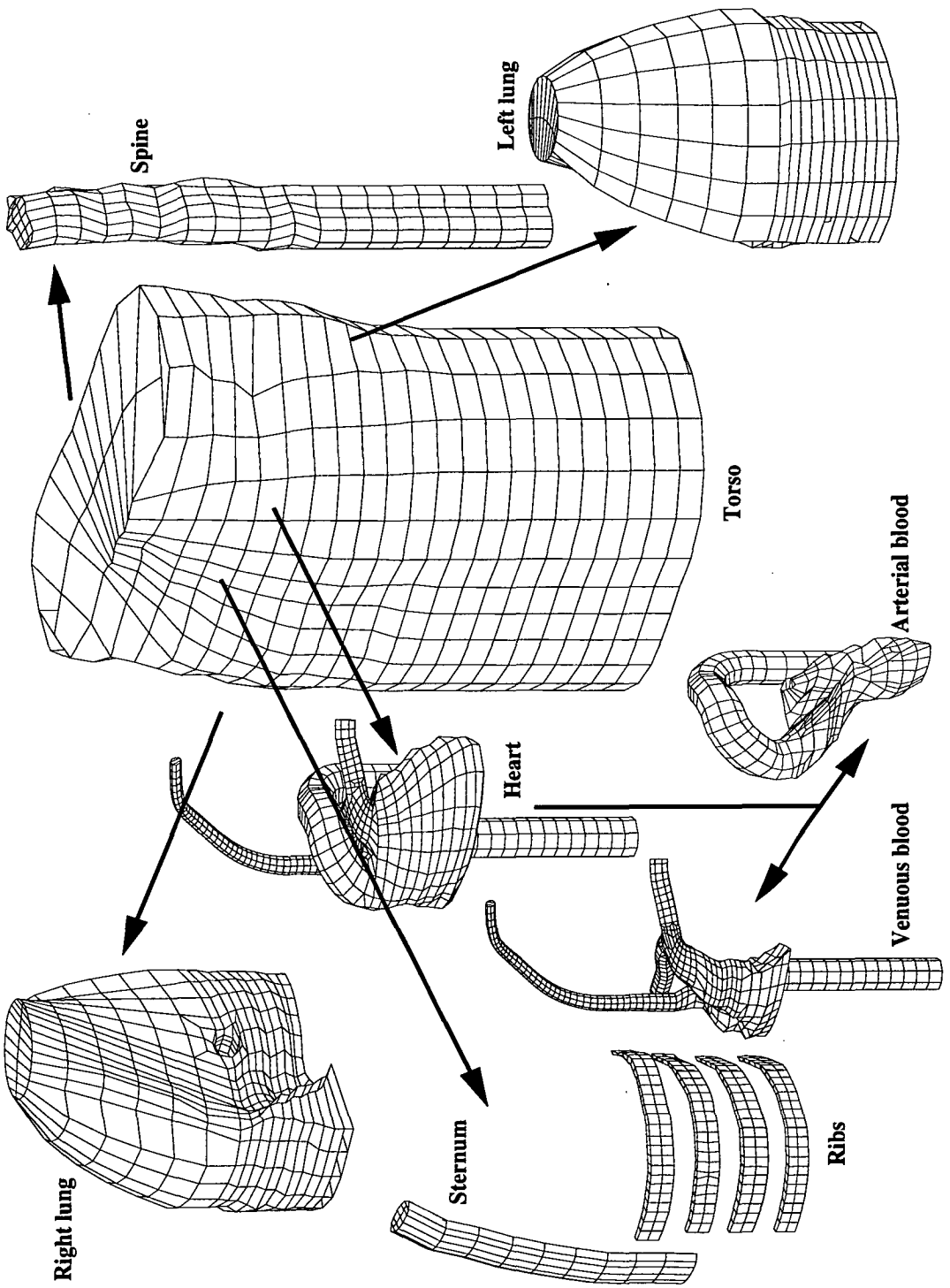

Figure 4.3: *Surface meshes of different regions in the torso.*

$$\nabla \cdot \sigma \nabla \Phi_i = \nabla \cdot \sigma_e \nabla \Phi_m \tag{4.2}$$

where σ_i, σ_e and σ denote intracellular, extracellular and bulk myocardial conductivities; and Φ_i, Φ_e and Φ_m intracellular, extracellular and transmembrane potentials. As discussed in the previous chapter, ST segment shift of the ECG has two contributors. One is the TQ baseline shift which results from the resting potential difference between the normal and ischaemic cells. The other is the true ST segment shift which is caused by the difference in the action potential during the plateau between the normal and ischaemic cells. In this study, only the true ST segment is considered. To be able to compare simulation results with experimental measurements, only Poisson's equation for the extracellular potential (equation 4.1) is solved.

Both the intracellular conductivity σ_i and the transmembrane potential Φ_m are functions of position. Their values are known from the experimental measurements. Thus, the source intensity is a known variable for the Poisson's equation.

In the model volume, the source is within the myocardium, and the current can only flow within the volume and no current can flow out of the enclosed surface of the volume, so that the Neumann boundary conditions (equation 4.3) on the epicardial surface of the myocardial volume are applied to solve the equation.

$$\left.\frac{\partial \Phi_e}{\partial n}\right|_S = 0 \tag{4.3}$$

where n denotes the normal orientation of the surface.

Apart from the above boundary condition there are also transmission conditions at the boundary between regions with different electrical conductivities [147]. The surface source (i_s) produced at the boundary between regions 1 and 2 can be expressed by

$$i_s = \sigma_1 \left.\frac{\partial \Phi}{\partial n}\right|_1 - \sigma_2 \left.\frac{\partial \Phi}{\partial n}\right|_2 \tag{4.4}$$

where n is the normal direction of the interface surface.

According to the uniqueness theorem, the potential solution is unique within a constant if it satisfies Poisson's equation and has known Neumann boundary conditions on the closed surface. Thus, an inner point needs to be set to a given value to solve the equation uniquely.

4.3.2 Laplace's equation

To be able to compare the simulated results of the bidomain model with that from solid angle theory, Laplace's equation is solved with the cardiac source being represented by Dirichlet boundary conditions (Dirichlet B. C.). In this way, the source at the ischaemic boundary, represented by a constant potential difference as used in solid angle theory [60], can be simulated as

$$\nabla \cdot \sigma \nabla \Phi_e = 0 \tag{4.5}$$

$$\Phi_e|_{B_1} = V_g, \quad \Phi_e|_{B_2} = V_g + C \tag{4.6}$$

where B_1 and B_2 represent the normal and ischaemic sides of the ischaemic boundary respectively, V_g any given value and C a constant potential. A value of 65mV was used to represent the potential difference between the ischaemic and healthy myocardium in a simulation of subendocardial ischaemia [120] while 20mV was used by Holland and Arnsdorf [117].

4.3.3 Transmembrane potential distribution

From the studies of cellular transmembrane potentials during ischaemia [92, 8], the plateau of Φ_m of ischaemic cells during artery ligation was reduced. The extent of such reduction depends on the duration of ligation and is directly associated with the reduction of blood flow in the region. A value of -40mV was measured for ischaemic cells in phase 3 after 5 minutes of LAD clamping in pigs while normal cells remained at -10mV [8]. No attempt was made to measure ischaemic transmembrane potentials in subendocardial ischaemia.

Li *et al.* [108] developed a model of subendocardial and transmural ischaemia using coronary artery ligation and atrial pacing in the anaesthetised sheep. Using fluorescent microspheres, the RMBF of the involved region was measured before and during ischaemia [148]. They showed that epicardial ST depression occurred when the RMBF in the endocardium (the inner one third of the myocardial wall) was reduced to 30-50% of the normal value during subendocardial ischaemia. In full thickness ischaemia, OM occlusion reduced the flow to the ischaemic region to

39% of the normal value. For complete ligation of a major coronary artery, the RMBF of the ischaemic region was reduced to 10-20% of the normal. There was a uniform flow reduction to each third of the ventricular wall in complete ligations. Therefore, the severity of ischaemia was assumed to be uniform in the ischaemic region. The RMBF could represent the severity of ischaemia, but no data are available on RMBF and transmembrane potentials during artery ligation. Although the blood flow reduction was different during different artery ligations, the difference between the transmembrane potential of the ischaemic cells during subendocardial ischaemia and that during transmural ischaemia was ignored in the present study. That is, the same value of the transmembrane potential of ischaemic tissue was used in simulations of both subendocardial and transmural ischaemia.

According to studies of blood flow in ischaemia [100, 148], there was a sharp interface (1-2mm) in the lateral ischaemic boundary and a gradual transition in the transmural boundary between ischaemic and non-ischaemic regions in subendocardial ischaemia. In the present study, however, the boundary difference between the transmural and lateral boundaries was ignored to simplify the computation. The width of the boundary zone was assumed to be 2mm in both transmural and lateral boundaries in the simulations.

Based on the measurements by Kleber *et al.* [8], the transmembrane potential of ischaemic cells was reduced to -40mV and that of normal cells remained at -10mV in phase 3 (late repolarisation). In this study, it was assumed that the ischaemic cells had Φ_m = -30mV while the normal cells were at 0mV during phase 2 of the action potential. The Φ_m was uniform in both the ischaemic and normal regions. In the boundary width of 2mm, Φ_m was assumed to change linearly from -30mV in the ischaemic region to 0mV in the normal region.

4.3.4 Electrical conductivities

4.3.4.1 Myocardial conductivity

Cardiac tissue exhibits anisotropic conductivity in both intracellular and extracellular domains [86]. From equation (4.1), intracellular conductivity σ_i affects the source intensity directly and the potential distribution indirectly, while the bulk myocardial conductivity σ affects the potential distribution as it reflects the conductivity of a part of the volume conductor. These two types of effects of the myocardial anisotropy on ST changes were investigated separately. The values of the anisotropic myocardial conductivity from Clerc [75][1] were used in the simulation (Table 4.2). The fibre rotation was ignored in the study. The axes of muscle fibres were assumed to be parallel to the x axis and perpendicular to the y and z axes. The anisotropic conductivity was assumed to be axially symmetric, that is, $\sigma_y = \sigma_z$. The longitudinal direction was assumed to be parallel to the fibre axes and denoted as l; the transversal direction was assumed to be transverse to the fibre axes and denoted as t.

σ_{il}	σ_{it}	σ_{el}	σ_{et}
0.174	0.0193	0.0625	0.0236

Table 4.2: *Anisotropic myocardial conductivity (Siemens per meter, S/m).*

To study the effects of anisotropy on the source and volume conductor, four different combinations of the intracellular and bulk conductivities[2] were examined (Table 4.3). In this study, the isotropic conductivities were assumed to be the same as the longitudinal conductivity, i.e. $(\sigma)_{iso} = \sigma_l$, $(\sigma_i)_{iso} = \sigma_{il}$.

[1]Measured data expressed by Clerc [75] as a specific resistivity in the restricted intracellular or extracellular space. It was converted to the values listed above by using the ratio (intracellular space)/(extracellular) = 0.7/0.3, as was used by Clerc.

[2]The values of σ_l and σ_t were calculated by $\sigma_l = \sigma_{il} + \sigma_{el}, \sigma_t = \sigma_{it} + \sigma_{et}$

Iso σ_i,Iso σ	Iso σ_i, Ani σ	Ani σ_i, Iso σ	Ani σ_i, Ani σ
σ_i=0.174	σ_i=0.174	σ_{il}=0.174,σ_{it}=0.0193	σ_{il}=0.174,σ_{it}=0.0193
σ=0.236	σ_l=0.236,σ_t=0.0429	σ=0.236	σ_l=0.236,σ_t=0.0429

Table 4.3: *Four combinations of intracellular and bulk myocardial conductivities (S/m). Iso and Ani represent isotropic and anisotropic conductivities respectively.*

4.3.4.2 Tissue Conductivities

Different regions in the torso are characterised by different electrical conductivities. The values of the conductivities were taken from Rush *et al.* [74] (Table 4.4). They were all assumed to be isotropic.

Lung	Blood	Bone	Thoracic tissue
0.05	0.67	0.00	0.23

Table 4.4: *Conductivity values of different regions in the torso (S/m)*

4.4 Numerical solution

A numerical method, the finite element method (FEM), was used to solve the governing equation. The objective of the FEM is to reduce the continuum problem to a discrete problem described by a system of algebraic equations. The finite element procedure begins with the division of the continuum region of interest into a number of simply shaped regions called elements (identified as mesh generation). Within each element, the unknown variables are interpolated by functions of compatible order in terms of values to be determined at a set of nodal points. Substitution of the unknown variables represented by the nodal values into the governing equation and boundary conditions at certain nodes yield a set of equations with residuals resulting from the approximated interpolations. By applying the Galerkin form of the method of weighted residuals to reduce these residuals to zero, the equations are converted into matrix equations. Solution of the matrix equations for a finite number of unknown nodal values is the numerical solution of the governing equation

in the continuum domain. The details of the FEM theory have not been reproduced here as they are described in detail elsewhere [149].

4.4.1 FIDAP implementation

A commercial package based on FEM, known as Fluid Dynamics Analysis Package (FIDAP[3]), was used in this study. The electrostatic problem in the present study can be treated as a problem of heat transfer by conduction (no convection or radiation involved). Thus, equation (4.1) can be treated as the equation of thermal energy conservation when the fluid is incompressible and homogeneous, and the flow is a single phase, laminar and Newtonian in a steady state. The electrical potential in equation (4.1) will be equivalent to the temperature and the electrical conductivity to the thermal conductivity in FIDAP.

4.4.1.1 Mesh generation

The region was meshed into different elements for different model geometries.

- For the 3D block model, the model volume was divided uniformly into 60,000 2mm×2mm×2mm cubic elements (8-node linear elements). There were 20,000 elements in the LVC, 10,000 elements in the RV cavity and 30,000 elements in the myocardium.
- For the isolated heart model, the model volume was divided uniformly into 60,661 2mm×2mm×2mm cubic elements with 70,653 nodes. The heart muscle was meshed into 32,517 elements; the venous blood volume into 15,497 elements; and the arterial blood volume into 12,647 elements.
- For the torso model, the model volume was meshed non-uniformly. A fine mesh with 2mm×2mm×2mm 8-node linear elements was used in the heart region, while regions outside the heart were meshed with non-uniform 8-node brick elements. The elements became larger as they retreated from the heart and

[3]Fluid Dynamics International, Inc., 500 Davis Street, Suite 600, IL 60201, USA

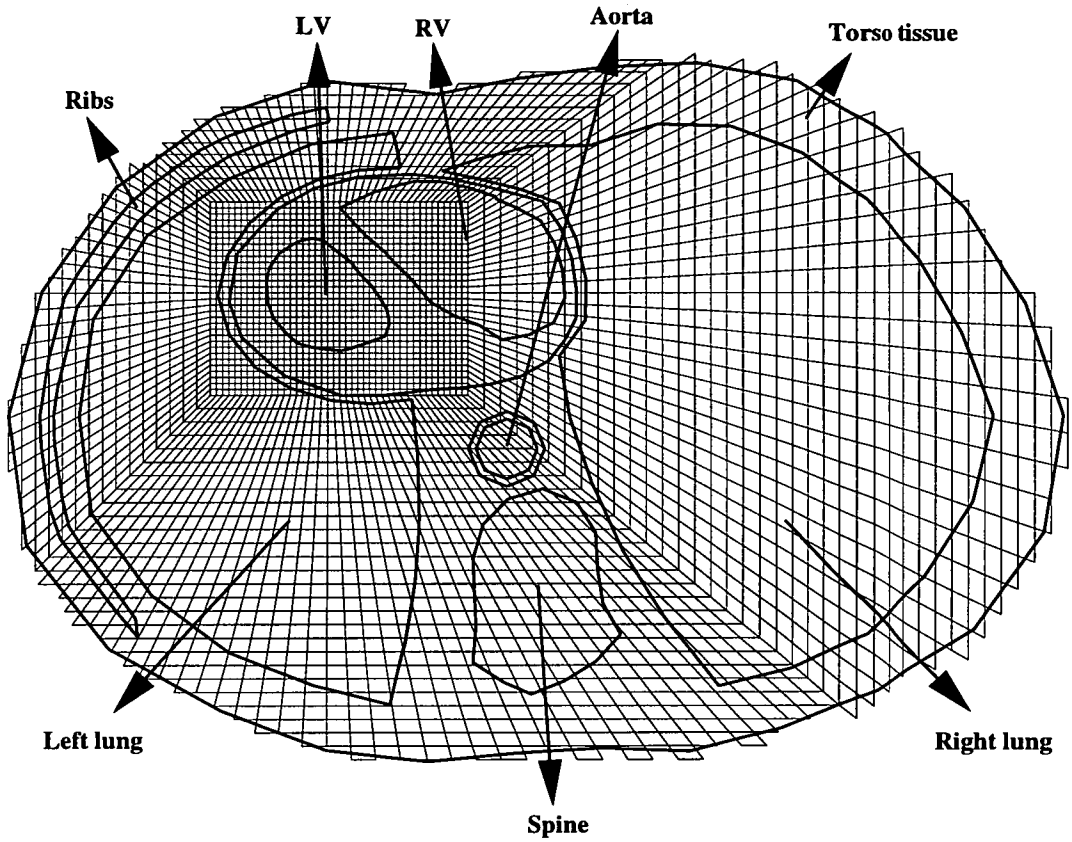

Figure 4.4: *Illustration of the non-uniform meshes in the torso, as shown on a cross-section of the torso.*

approached the torso surface, as shown in Figure 4.4. The mesh generation was done by a mesh generator (FIMESH) in FIDAP. The torso model was divided into 274,424 elements with 292,654 nodes.

After the ischaemic boundary was defined, some 8-node elements at the boundary were split into two 6-node wedge elements to smooth the boundary (Figure 4.5).

4.4.1.2 Element grouping

After the mesh was generated for the model volume, each element was assigned to the proper group which in turn was identified by the conductivity. The centre of the element was used to determine which group the element belonged to according to the surface definition of the regions. Because 8-node brick elements were used, the boundaries between regions would not be smooth. However, it was assumed to be acceptable because of the small size of the elements. After the elements were

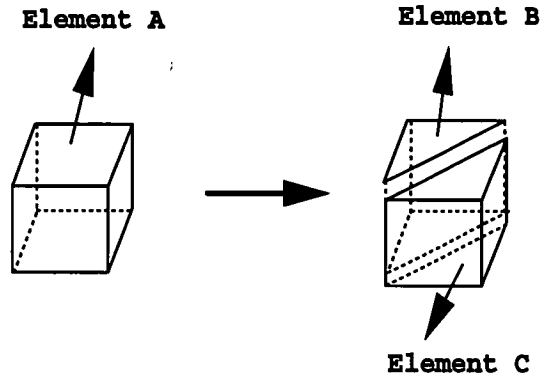

Figure 4.5: *Illustration of the method used to smooth the boundary by splitting an 8-node element (A) into two 6-node wedge elements (B & C).*

grouped, the conductivity value for each group was assigned. The second source in the regional boundaries was automatically handled by the FIDAP package.

As shown in equation (4.1), the bulk myocardial conductivity affects the potential distribution as it reflects the conductive property of a part of the volume conductor. To examine the effects of the anisotropy, an anisotropic conductivity was assigned to the myocardial group.

4.4.1.3 Source calculation

The source term $(\nabla \cdot \sigma_i \nabla \Phi_m)$, derived from the spatial distribution of transmembrane potential Φ_m, depends on the shape and location of the ischaemic region. When σ_i is constant and the fibre's major directions are chosen to be parallel to the Cartesian coordinate system, the source is reduced to:

$$\sigma_i = \begin{pmatrix} \sigma_{ixx} & 0 & 0 \\ 0 & \sigma_{iyy} & 0 \\ 0 & 0 & \sigma_{izz} \end{pmatrix} \tag{4.7}$$

$$\nabla \cdot \sigma_i \nabla \Phi_m = \sigma_{ixx} \frac{\partial^2 \Phi_m}{\partial x^2} + \sigma_{iyy} \frac{\partial^2 \Phi_m}{\partial y^2} + \sigma_{izz} \frac{\partial^2 \Phi_m}{\partial z^2} \tag{4.8}$$

where the heart muscle fibre is assumed to be along the x axis, and its two transversal directions along the y and z axes. Thus the ischaemic boundary perpendicular to the fibre direction (longitudinal boundary) would have a much intensive source than the boundary parallel to the fibre direction (transmural boundary).

Furthermore, when the σ_i was assumed to be isotropic, i.e. $\sigma_{ixx} = \sigma_{iyy} = \sigma_{izz} = \sigma_i$, the source term can be expressed by:

$$\nabla \cdot \sigma_i \nabla \Phi_m = \sigma_i \nabla^2 \Phi_m \tag{4.9}$$

The derivative of Φ_m can be calculated numerically. The continuous formulation can be transformed to a discrete formulation by replacing derivatives using finite difference approximations. After discretisation of a continuous 3D domain with uniform spacing, the Laplacian of Φ_m ($\nabla^2\Phi_m$) at a point with coordinates x_0,y_0,z_0, can be approximated by [150]:

$$\begin{aligned}\nabla^2\Phi_m(x_0,y_0,z_0) = \frac{1}{h^2}[&\Phi_m(x_0+h,y_0,z_0) + \Phi_m(x_0-h,y_0,z_0) + \\ &\Phi_m(x_0,y_0+h,z_0) + \Phi_m(x_0,y_0-h,z_0) + \Phi_m(x_0,y_0,z_0+h) + \\ &\Phi_m(x_0,y_0,z_0-h) - 6\Phi_m(x_0,y_0,z_0)]\end{aligned} \tag{4.10}$$

where h is the uniform spacing of the discretisation. In one-dimension, the equation is reduced to

$$\nabla^2\Phi_m(x_0) = \frac{1}{h^2}[\Phi_m(x_0+h) + \Phi_m(x_0-h) - 2\Phi_m(x_0)] \tag{4.11}$$

When the formula (4.11) is applied to the ischaemic boundary, the source in the normal side is positive and the source in the ischaemic side is negative (Figure 4.6):

$$\nabla^2\Phi_m(x_0)\Big|_+ = \frac{1}{2h^2}[\Phi_{mN} - \Phi_{mI}], \quad \nabla^2\Phi_m(x_0)\Big|_- = \frac{1}{2h^2}[\Phi_{mI} - \Phi_{mN}] \tag{4.12}$$

where x_0 is the ischaemic boundary. Figure 4.6 shows the transmembrane potential distribution and the Laplacian of Φ_m in one-dimension. Clearly, the source density is proportional to the difference in transmembrane potentials between the normal and ischaemic tissues (equation 4.12). This indicates that the density of injury current increases with the severity of ischaemia. Also, because the source intensity is inversely proportional to the square of the ischaemic boundary width ($2h$), a narrower boundary produces a more intensive current source.

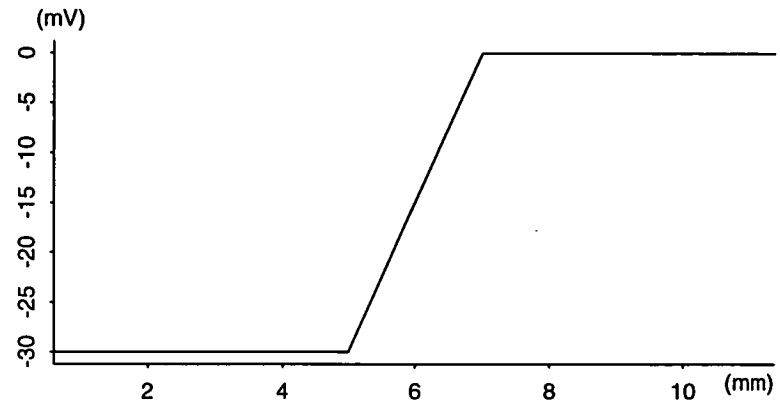

(a) The transmembrane potential distribution

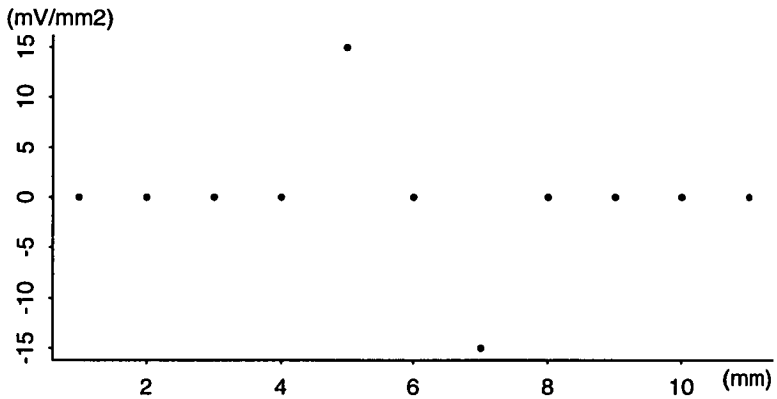

(b) The Laplacian of transmembrane potential

Figure 4.6: *Transmembrane potential and the Laplacian of the transmembrane potential at the ischaemic boundary in one-dimension. The ischaemic region ($x < 5mm$) has Φ_m=-30mV, and the normal region ($x > 7mm$) has Φ_m=0mV during the ST segment. The ischaemic boundary, the transition zone, is from x=5mm to x=7mm. $h = 1mm$.* $\nabla^2\Phi_m(x = 5) = 15mV/mm^2$, $\nabla^2\Phi_m(x = 7) = -15mV/mm^2$.

When σ_i is assumed to be isotropic and constant (σ_i=0.174 S/m), $\sigma_i\nabla^2\Phi_m$ is in the order of $\pm 2.6\mu A/mm^3$, which is in the same order as those calculated from the measured epicardial ST potentials by Kleber *et al.* [8] and by Janse *et al.* [151]. Kleber *et al.* [8] found that during the first 5 minutes after LAD ligation in pigs, the estimated maximal current sources at the ischaemic side of the border had a density in the order of 1.0 $\mu A/mm^3$ during the ST segment. Similarly, the maximal current density ($2\mu A/mm^3$) was produced at the ischaemic border when normal cells had repolarised and ischaemic cells had not (phase 3) during LAD ligation in pigs [151]. To comply with the data of Kleber *et al.* [8], a density of 1.0 $\mu A/mm^3$

was adopted to represent the intensity of the cardiac source during ischaemia in the present study.

According to the divergence theorem, when no current flows out of the enclosed surface of a volume, the net source in the volume must be zero. When the source is assumed to be distributed uniformly at the ischaemic boundary, the positive source occupies less space than does the negative source in the case of subendocardial ischaemia and transmural ischaemia of a small region. Therefore, the positive source must be more intensive than the negative source. For transmural ischaemia of a large region, both ischaemic and normal regions occupy the same space, so that the positive and negative source densities are equal.

Source densities are approximated by defining the ischaemic boundary based on the ischaemic region, and grouping a layer (one element in width) of elements just next to the boundary on the ischaemic side as the positive source group, and a layer on the normal side as the negative source group. Assuming that there are M elements in the positive group and N elements in the negative group; if the positive source is given a density of V_+, the density for the negative source will be: $V_- = V_+ * M/N$.

4.4.1.4 Numerical solver

The source densities were assigned to the relevant elements. An arbitrary point inside the region was set to a given value. A numerical solver and its convergence criterion needed to be chosen to solve the linear system of equations. In all simulations the segregated solver was used, in which conjugated gradient based iterative solvers were used to solve the linear system of equations and the convergence criterion was set to 1.0E-5. The execution time could vary from several hours to three days depending on the problem size.

It should be noted that the implementation was performed on Silicon Graphics Iris Indigo XZ 4000[4], with 96 megabyte of random access memory.

[4]Silicon Graphics, Inc., Mountain View, California, USA.

4.5 Post processing

After the equation was successfully solved, the potentials at all nodes were obtained. To simulate the Wilson's terminal, the average potential on the heart surface (isolated heart model), or on the torso surface (torso model), served as the reference potential. All the data were displayed against the reference. The surface data were extracted by representing the points on the surface with potentials of the closest nodes in the model region. In the 3D block model, the potentials on the surfaces can be exactly represented by those of the nodes on the surface. For the isolated heart model, the epicardial surface is represented by the closest nodes in the model region with a maximal error of 2.14mm while the torso surface is represented by the closest nodes with a maximal error of 8.81mm.

The S-PLUS[5] package running under the UNIX operating system and a technical computing package MATLAB[6] were used to construct the graphical displays.

[5]Statistical Sciences, Inc., Seattle, Washington, USA.

[6]The MathWorks, Inc., Natick, MA, USA.

Chapter 5

Simulation of subendocardial ischaemia

5.1 Introduction

ST depression is a marker of acute ischaemia in the subendocardium, although its distribution on either the epicardium or the body surface does not indicate the ischaemic location [1, 128, 4]. Moreover, in animal studies, ischaemia with different ischaemic locations show a similar pattern of ST depression on the epicardium [4] or have an overlap of ST depression over the left lateral area of the chest [124]. In addition, exercise-induced ST depression occurs most commonly in leads V_5 and V_6 with 12-lead ECG [1, 2], and maximal ST depression appears in a limited area of the left upper chest by body surface mapping on patients regardless of which coronary artery is involved [3, 128]. However, the existing physical models predict that distribution of ST depression on the epicardium or the body surface localises the ischaemic region [60, 62, 70, 120]. Recently Kilpatrick *et al.* [5] have suggested that ST depression in endocardial ischaemia is due to current flowing from a region of ischaemic endocardium through the great vessels and back onto the epicardium.

This chapter presents results from simulation of subendocardial ischaemia to explain the observed ST depression. The simulation was carried out in three different model geometries: the 3D block, the isolated heart and the torso including all its major

organs. Subendocardial ischaemia from two different arterial territories (LAD and LCX) were simulated, based on such spatial information as ischaemic location and volume, as determined by measuring blood flow using fluorescent microspheres in sheep [21]. For the 3D block model, both Poisson's equation (the bidomain model) and Laplace's equation (solid angle theory) were solved for comparison. The importance of the intracavitary blood was tested by reducing its conductivity, and the contribution of the narrow lateral boundary in subendocardial ischaemia was examined. The current path suggested by Kilpatrick *et al.* [5] was tested by the isolated heart model. For the torso model, ST depression on the body surface was examined. Finally, the relationship between the epicardial and the body surface ST potentials was examined in the realistic torso model.

5.2 Simulations

5.2.1 3D block model

Because only the inner part of the myocardium is ischaemic in subendocardial ischaemia, the injury boundary in the ischaemia has not only a transmural boundary parallel to the endocardium but also lateral boundaries perpendicular to the endocardium. With partial LAD or LCX ligation, half of the left ventricle becomes ischaemic [21], thus both ischaemic regions share the same lateral ischaemic boundaries which are located in the central septum on one side and the lateral region of the left ventricular wall on the other. As shown in Figure 5.1, for the ischaemic region in the LAD territory, the heart is cut along the PDA and opened flat; for the LCX territory ischaemia, the heart is cut along the LAD and opened flat. These cutting areas are chosen so that the source is far away from the cutting boundary, thus minimising boundary effects. LAD and LCX subendocardial ischaemia could be simulated by the same model configuration.

As discussed previously, subendocardial ischaemic regions in either the LAD or LCX territory share their lateral boundaries in the septum and the left lateral region through the base to the apex. In the 3D block model, the ischaemic region was

assumed to extend to the inner 2/5 of the transmural wall, with a rectangular shape (8cm×0.4cm) (Figure 5.1). To avoid the boundary effect, the ischaemic region was assumed to be located in the centre and to extend 7cm along the y axis. The ischaemic region had a volume of 22.4 cm^3. The sources at the boundaries at y=-3.5cm and y=3.5cm were ignored. Only the ischaemic boundaries at x=±4.0cm (lateral) and at z=1.4cm (transmural) were considered.

5.2.1.1 Bidomain model

In this section, myocardial electrical conductivity was assumed to be isotropic with values:

$$\sigma_i = 0.174 S/m, \quad \sigma = 0.244 S/m \tag{5.1}$$

Before the governing equation in the bidomain model (equation 4.1) was solved by the FEM method, the density of current source due to ischaemia in the following situations was calculated.

ST potential in subendocardial ischaemia The ischaemic region occupied the inner 2/5 of the heart wall with a volume of $22.4 cm^3$. The positive source occupied a volume of 1470 elements on the ischaemic side of the boundary, while the negative source had 1610 elements on the normal side of the boundary. Therefore the positive source was assumed to have a density of 1.0 $\mu A/mm^3$ and the density of negative source -0.913 $\mu A/mm^3$.

Contribution of narrow lateral boundaries From equation (4.12), the density of current source at the ischaemic boundary is inversely proportional to the square of the boundary width (h). As discussed in Chapter 3, there are sharp lateral boundaries and a gradual transmural boundary in subendocardial ischaemia. If the width of the lateral boundary was $\frac{1}{\sqrt{2}}$ times that of the transmural boundary for example, the density of the current source at the lateral boundaries was twice that at the transmural boundary. When the transmural sources were in the range

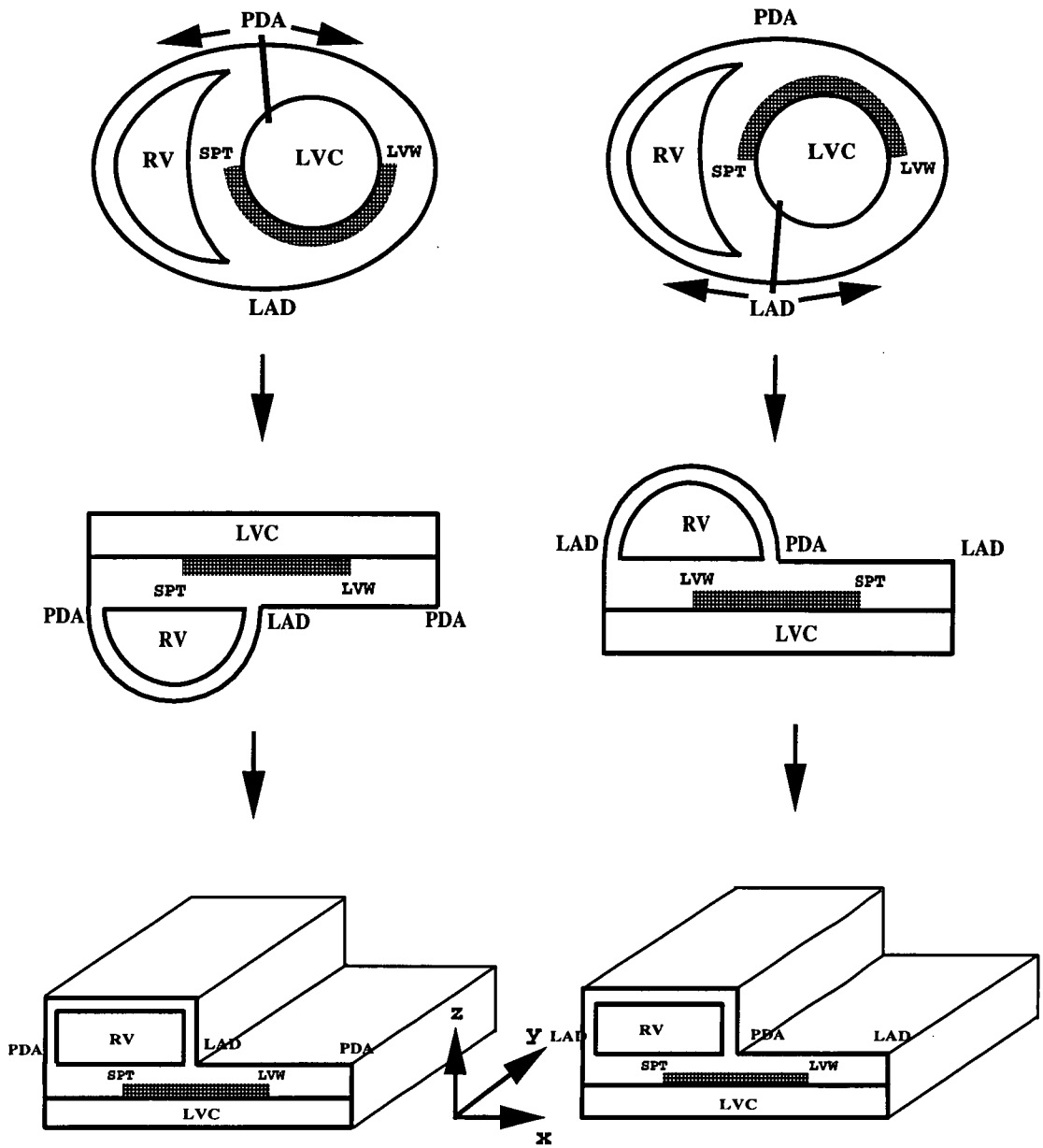

(a) LAD subendocardial ischaemia **(b) LCX subendocardial ischaemia**

Figure 5.1: *3D block model for subendocardial ischaemia. Top plots represent a cross-section of the heart with the ischaemic area shown hatched, and the middle plots represent the unfolded heart in a cross-section. Bottom plots represent the actual 3D model geometries. Diagram (a) illustrates the conversion of the heart structure to a 3D block for LAD subendocardial ischaemia and diagram (b) for the LCX subendocardial ischaemia.*

of $\pm 1\mu A/mm^3$ and the lateral boundaries $\pm 2\mu A/mm^3$, subendocardial ischaemia with such ischaemic configuration was simulated.

Transition to transmural ischaemia When the endocardial ischaemic region is extended to the epicardium, the injury region becomes larger and the transmural boundary closer to the epicardium. To simulate a stage of the transition from subendocardial ischaemia to full thickness ischaemia, the subendocardial ischaemic region was increased from the inner 2/5 of the transmural wall to 3/5. Thus, the ischaemic region had a volume of $33.6cm^3$. The corresponding positive source had a density of $1\mu A/mm^3$ and the negative source $-0.917\mu A/mm^3$.

Effects of intracavitary blood To test the effect of the intracavitary blood masses, the blood conductivity was reduced to nearly 1/3 of the actual value (from 0.67 to $0.244S/m$), and the ischaemic configuration was the same as that in the simulation of subendocardial ischaemia in the inner 2/5 of the heart wall.

5.2.1.2 Laplace's equation

To compare the solution obtained by using a constant potential difference to represent the cardiac current source with that of the bidomain model , Laplace's equation was solved, with the source represented by Dirichlet boundary condition. The details of solving Laplace's equation are found in Section 4.3.2. A potential difference of 20mV was used at the ischaemic boundary in the subendocardial ischaemia of the inner 2/5 of the myocardial wall. Similarly, the average potential on the epicardium was used as the reference in data presentation.

5.2.2 Isolated heart model

Myocardial conductivity was assumed to be isotropic to simplify computation, and to be the same values as in equation (5.1). The ischaemic region located in either the LAD or the LCX territory was simulated. Like the 3D block model, the endocardial

ischaemic region occupied the inner 2/5 of the ventricular wall and extended to half of the left ventricular myocardium, which was supplied by either the LAD or the LCX. The positive source had a density of $1.0\mu A/mm^3$ and the negative source $-0.7\mu A/mm^3$.

5.2.3 Torso model

The same ischaemic configuration as that in the isolated heart model (Section 5.2.2) was used in the torso simulation for the LAD and LCX subendocardial ischaemia. Similarly, the myocardial conductivity was assumed to be isotropic.

5.3 FIDAP solution

After the source densities were assigned to the corresponding elements (for Poisson's equation) or potential values (Dirichlet B. C.) to the corresponding nodes (for Laplace's equation), the governing equation was solved by the finite element method package FIDAP. The details for solving the equation were described in Section 4.4. Displays of simulated data were described in Section 4.5.

5.4 Results

5.4.1 3D block model

5.4.1.1 ST potential from the bidomain model

As shown in Figure 5.2, on the epicardium, ST depression mainly appeared over the left free wall (x > 0), with a maximal ST depression of about -10.15mV at the ischaemic boundary (x=4.0cm). On the endocardium, ST elevation appeared over the ischaemic region with a maximal ST elevation of 16.09mV at the centre of the ischaemic region (x=0, y=0) (Figure 5.3). On the cross section of the left ventricle (y=0), ST depression mainly occurred in the non-ischaemic area of the

lateral region, while ST elevation occurred at the ischaemic endocardium. The maximal ST depression and ST elevation on the cross section were -12.65mV and 17.08mV respectively.

For the 3D block model, when the ischaemic region was either in the LAD or the LCX territory, epicardial ST depression mainly occurred over the lateral region of the left ventricle, while ST elevation covered the ischaemic region on the endocardium. However, ST potential patterns would differ slightly between the two ischaemic regions in the same heart. Since ST depression on the epicardium was not symmetric about the ischaemic boundary (Figure 5.2), epicardial ST depression on the left free wall was slightly different during LAD and LCX subendocardial ischaemia. Endocardial ST elevation was not symmetric about the centre of the ischaemic region, so ischaemia in the LAD and LCX territories had a slightly different ST elevation pattern on the endocardium. This asymmetry of epicardial ST depression was partly due to the asymmetry of the geometry, that is one side has the right ventricle and the other has not, and partly due to the blood which surrounds only a part of the ischaemic boundary.

5.4.1.2 Contribution of narrow lateral boundary

The simulated results of the reduced lateral boundary are shown in Figure 5.4; a comparison with those of an equal width for the transmural and the lateral boundaries is shown in Figure 5.5. The ST potential pattern did not change significantly, and epicardial and endocardial ST potentials were increased generally. The greatest change was that the maximal ST depression on the epicardium at the lateral boundary increased by 16% from -10.15 to -11.74mV.

5.4.1.3 Transition to transmural ischaemia

When the ischaemic region was transmurally 2mm closer to the epicardium (inner 3/5 of the heart wall), the ST potential pattern remained unchanged but its amplitude changed (Figures 5.6 & 5.7). On the epicardium, the maximal ST depression changed from -10.15 to -13.42mV, while ST elevation decreased from 16.09

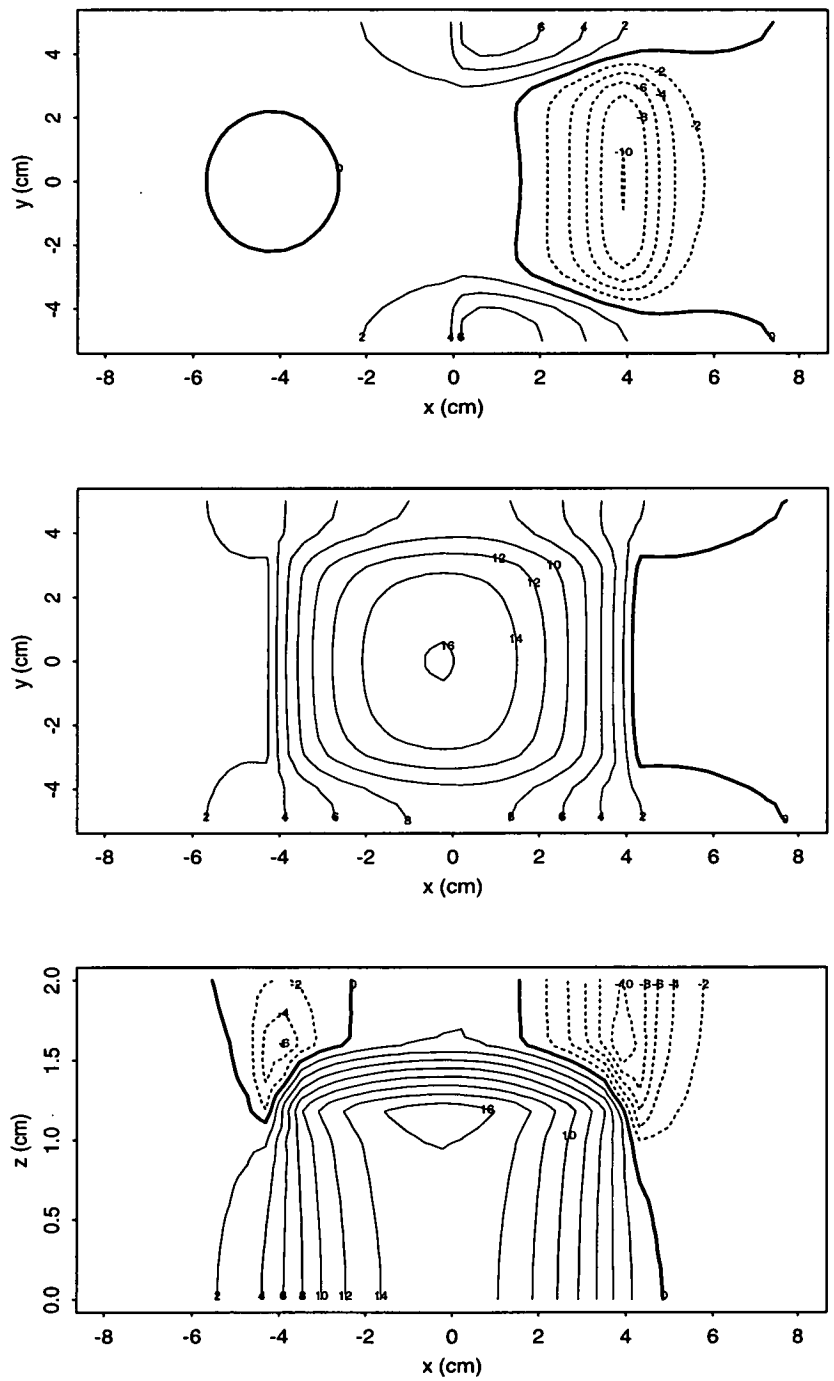

Figure 5.2: *Contour plots of ST potential on the epicardium (top), the endocardium (middle) and a cross section (y=0) of the heart (bottom) during subendocardial ischaemia (inner 2/5 of the heart wall) in the 3D block model. The thick solid lines represent the zero potentials, the thin solid lines ST elevation and the dashed lines ST depression respectively. The contour interval is 2mV.*

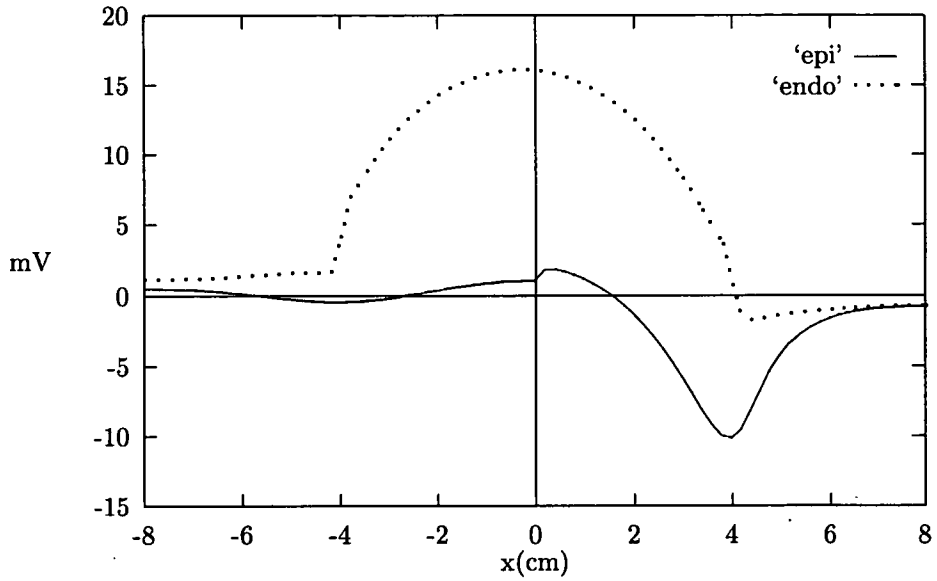

Figure 5.3: *ST potential along x axis across the ischaemic region on the epicardium (solid line) and the endocardium (dotted line) when the inner 2/5 of the myocardium is ischaemic.*

to 15.30mV. On a cross-section of the left ventricle, the extremes of ST potential were -14.71mV and 17.17mV, as compared with -12.65mV and 17.08mV in subendocardial ischaemia in the inner 2/5 of the heart wall (Section 5.4.1.1).

5.4.1.4 Effects of blood mass

With the same ischaemic configuration, the comparison between the simulation with the blood conductivity of 0.67S/m and that with 0.244S/m is shown in Figure 5.8. The lower conductivity of the intracavitary blood increased maximal endocardial ST elevations by 6-8mV and maximal epicardial ST depression by 2-4mV. Although ST potential distributions were not changed significantly, an area of ST elevation appeared over the centre of the ischaemic region on the epicardium (Figure 5.9).

5.4.1.5 Solution of Laplace's equation

In solid angle theory, the injury current source was represented by a constant potential difference. As shown in Figure 5.10, ST depression (-2 to -4mV) appeared over the ischaemic region on the epicardium, even though there was a slight difference in amplitude between the left side ($x < 0$) and the right side ($x > 0$). On the

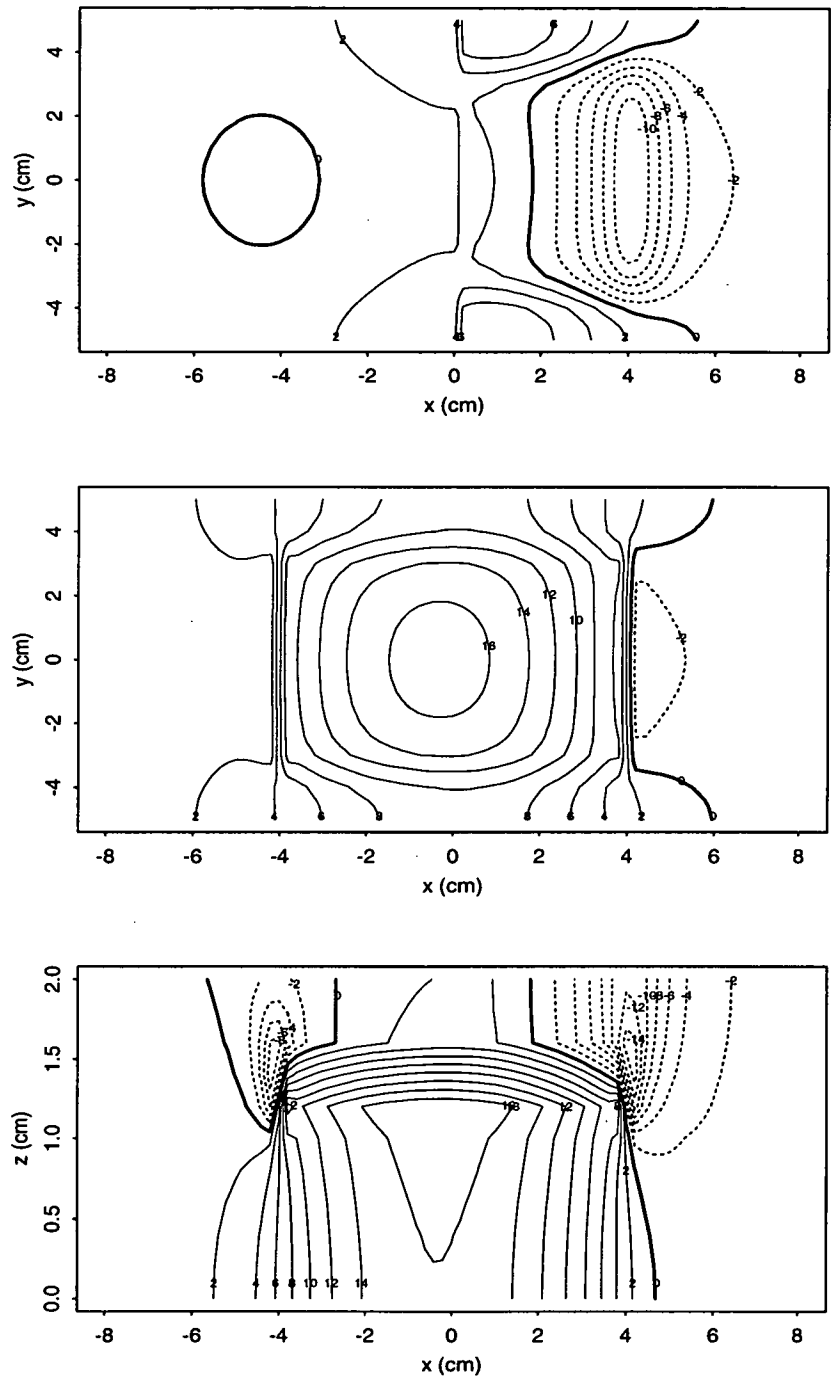

Figure 5.4: *Contour plots of ST potential on the epicardium (top), the endocardium (middle) and a cross section (y=0) of the heart (bottom) during subendocardial ischaemia with a reduced lateral boundary width (0.707 times the transmural boundary width). The thick solid lines represent the zero potentials, the thin solid lines ST elevation and the dashed lines ST depression. The contour interval is 2mV.*

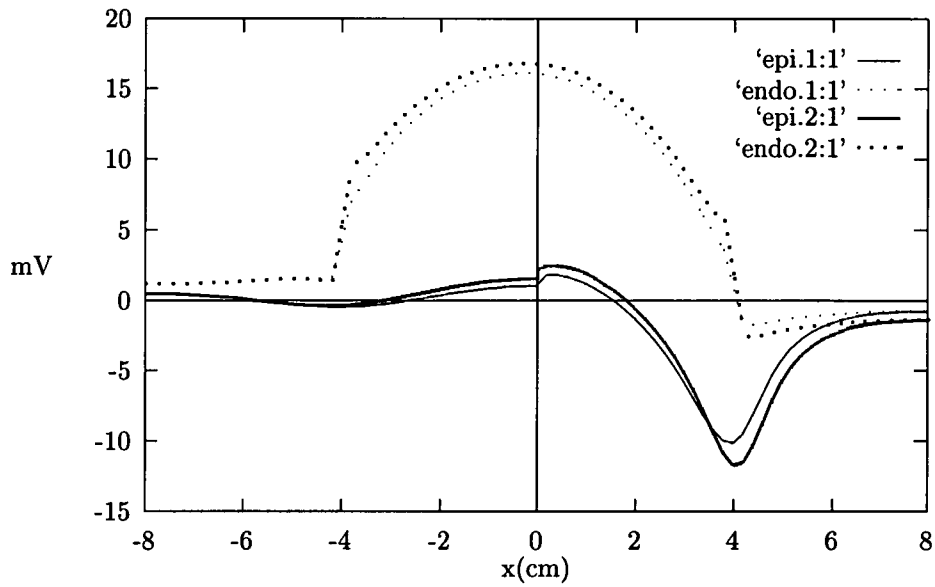

Figure 5.5: *Comparison of ST potential between ischaemia with the same boundary widths (thin traces) and that with reduced lateral boundary widths (0.707 times transmural width, thick traces). The thin solid trace represents epicardial ST (epi.1:1) and the thin dotted trace endocardial ST (endo.1:1) potentials along the x axis crossing the ischaemic region when the transmural and lateral boundaries are of the same width. The thick solid trace represents ST potential on the epicardium (epi.2:1) and the thick dotted trace on the endocardium (endo.2:1) when the lateral boundary width is 0.707 times that of the transmural boundary.*

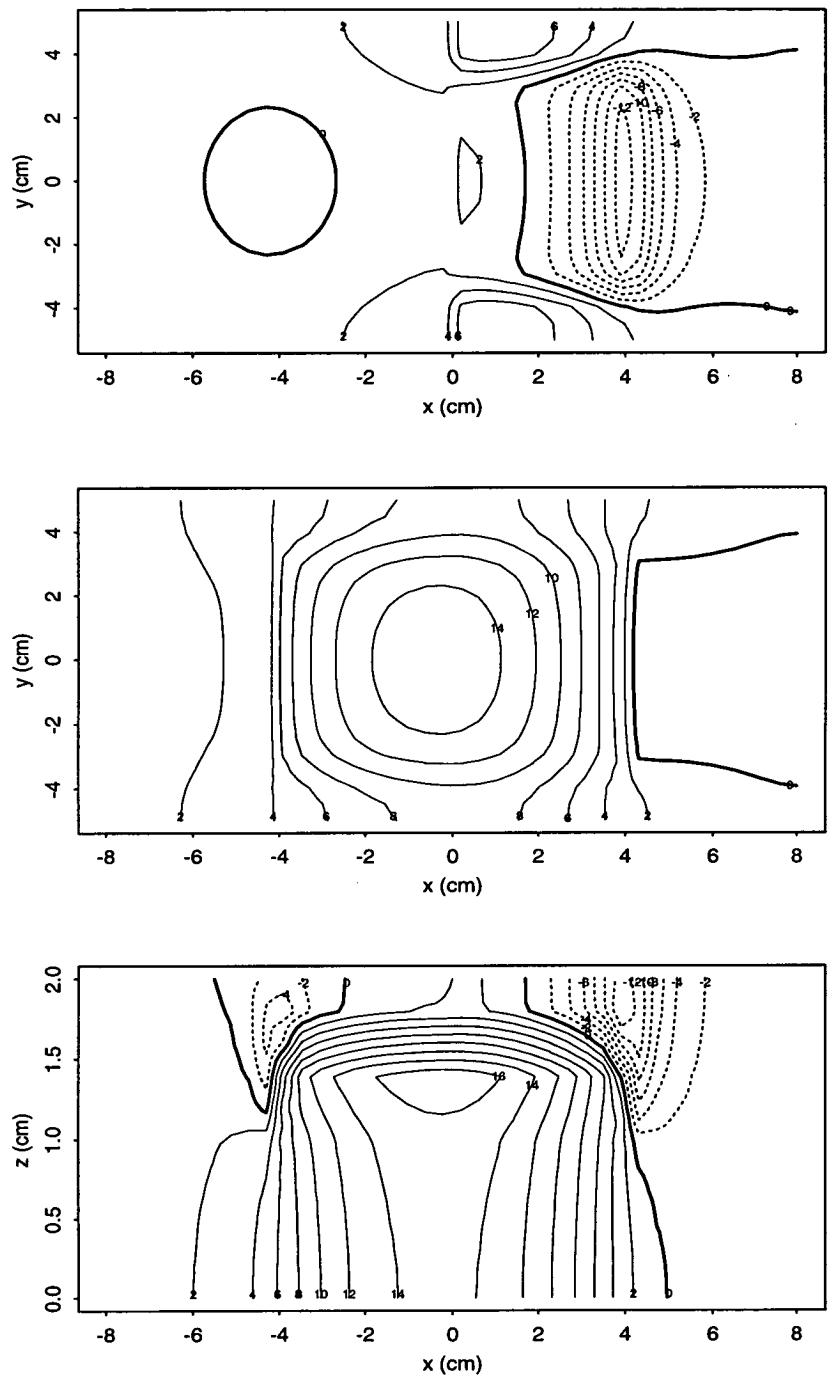

Figure 5.6: *Contour plots of ST potential on the epicardium (top), the endocardium (middle) and a cross section (y=0) of the heart (bottom) during a transition to transmural ischaemia (inner 3/5 of the heart wall). The thick solid lines represent the zero potentials, thin solid lines ST elevation and dashed lines ST depression. The contour interval is 2mV.*

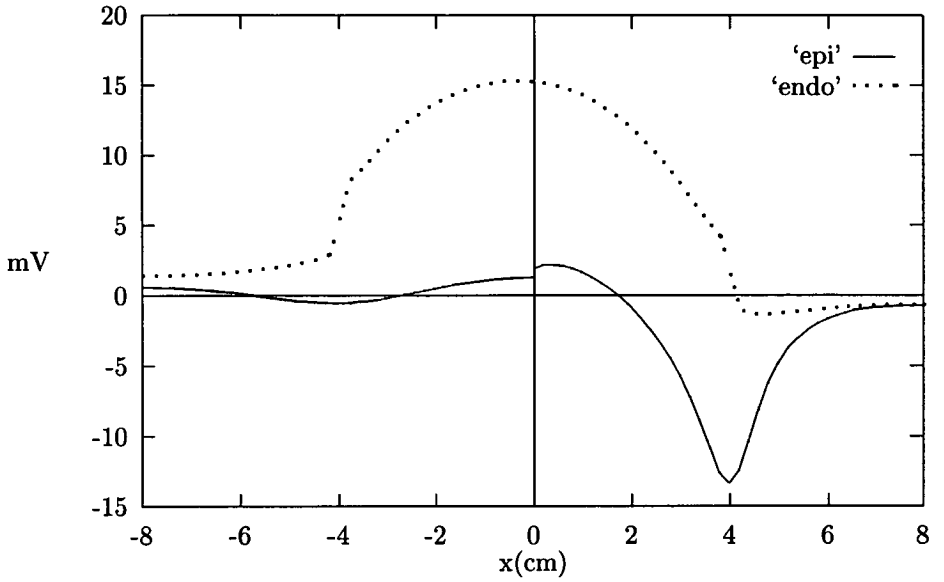

Figure 5.7: *ST potential along the x axis crossing the ischaemic region on the epicardium (solid line) and the endocardium (dotted line) during the transition to transmural ischaemia (inner 3/5 of the heart wall).*

endocardium, ST elevation (12 to 14mV) occurred over the ischaemic region with a sharp potential change of 20mV from -4.25 to 15.75mV on the ischaemic boundaries (Figure 5.11).

These results suggest that epicardial ST depression indicates the location of underlying subendocardial ischaemia, with posterior ST depression on the left ventricle greater than that on the right ventricle during LCX subendocardial ischaemia. In LAD subendocardial ischaemia, anterior epicardial ST depression indicates the LAD ischaemic region even though its amplitude was slightly higher on the left than the right side. Although endocardial ST elevation mainly appears over the ischaemic region, ST depression occurs on the normal side of the ischaemic boundary on the endocardium.

5.4.2 Isolated heart model

ST potential distributions in both LAD and LCX subendocardial ischaemia are shown in Figure 5.12. On the epicardium, ST depression mainly appeared over the left lateral free wall and ST elevation over the ischaemic region on the endocardium.

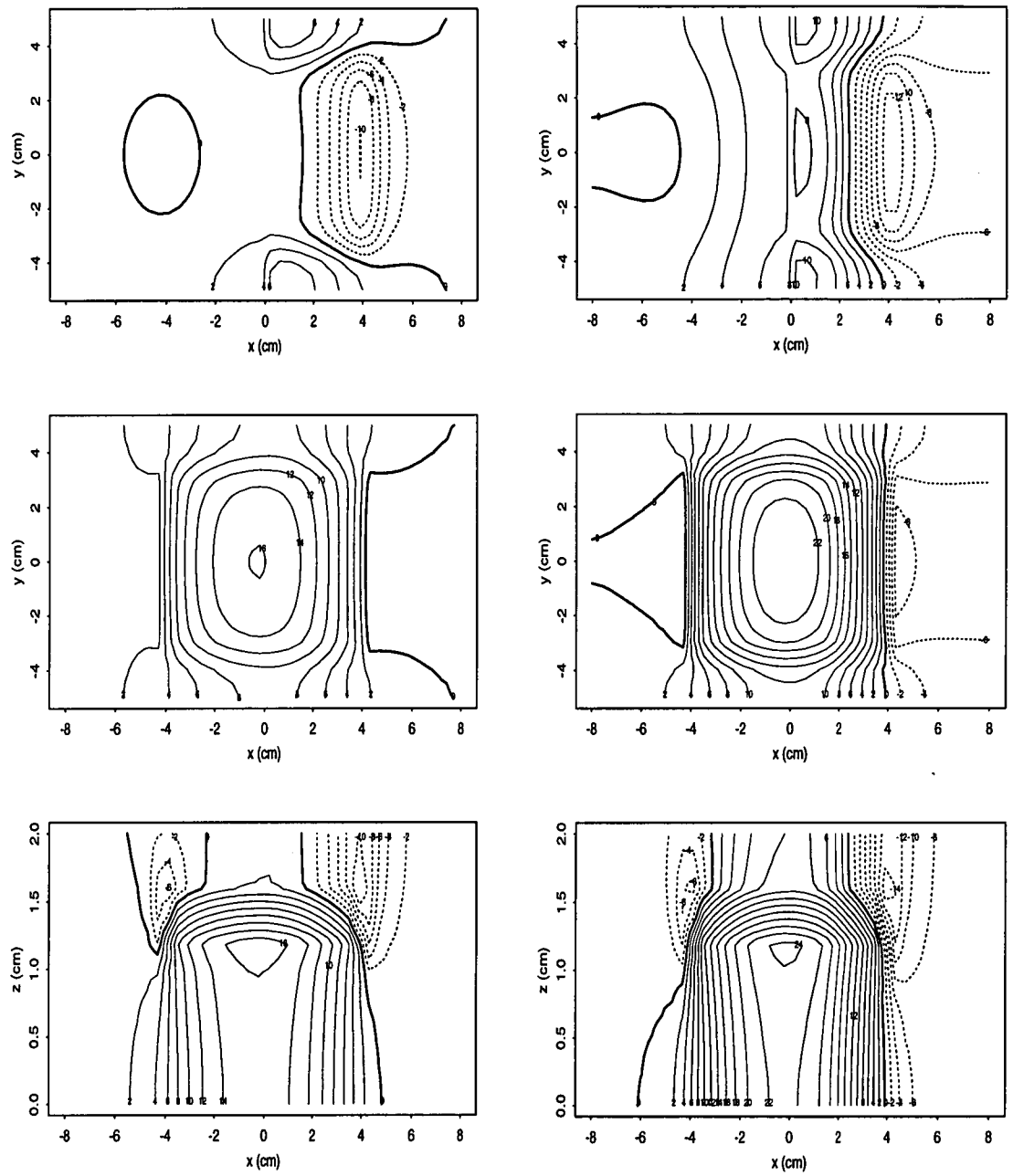

Figure 5.8: *Contour plots of ST potential when* $\sigma_{blood} = 0.67 S/m$ *(panel a) and* $\sigma_{blood} = 0.244 S/m$ *during subendocardial ischaemia (inner 2/5 of the heart wall). From top to bottom, the plots represent the potentials on the epicardium, the endocardium and a cross section (y=0) of the heart. The thick solid lines represent the zero potentials, thin solid lines ST elevation and dashed lines ST depression. The contour interval is 2mV.*

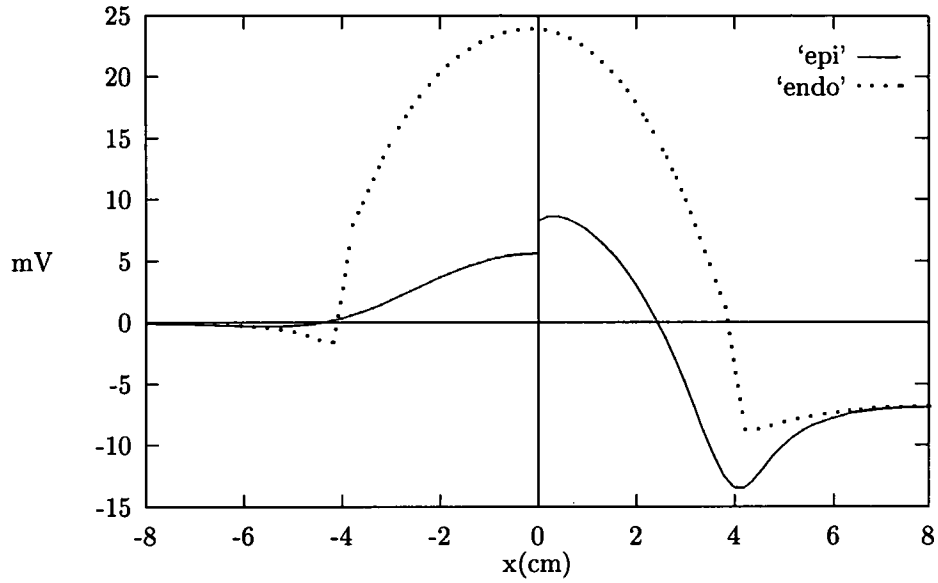

Figure 5.9: *ST potential along x axis across the ischaemic region on the epicardium (solid line) and the endocardium (dotted line) during subendocardial ischaemia (inner 2/5 of the heart wall) when the blood has a lower conductivity.*

A maximum ST depression of -5 to -7mV occurred on the epicardium and a maximum ST elevation of 10-12mV on the endocardium. Positive ST potential mainly occurred in the ischaemic endocardium and left ventricular cavity, while ST depression appeared at the normal region in both the lateral regions. The ST depression in the septum did not extend to the epicardium, and that from the lateral boundary at the left free wall was clearly expanded towards the epicardium. The maxima of ST potential on the cross-section were 12.83mV and -5.47mV in the LAD ligation, and 10.75mV and -6.44mV in the LCX ligation. The contour plots and the direction of current density of ST potential on a cross-section of the heart are shown in Figure 5.13.

5.4.3 Torso model

The results from the torso simulation are shown in Figure 5.14. In either LAD or LCX subendocardial ischaemia, epicardial ST potentials were distributed similarly to that in the isolated heart (Figure 5.12) but with a much lower amplitude. The maxima of epicardial ST depression were -3.8mV in LAD ischaemia and -3.5mV

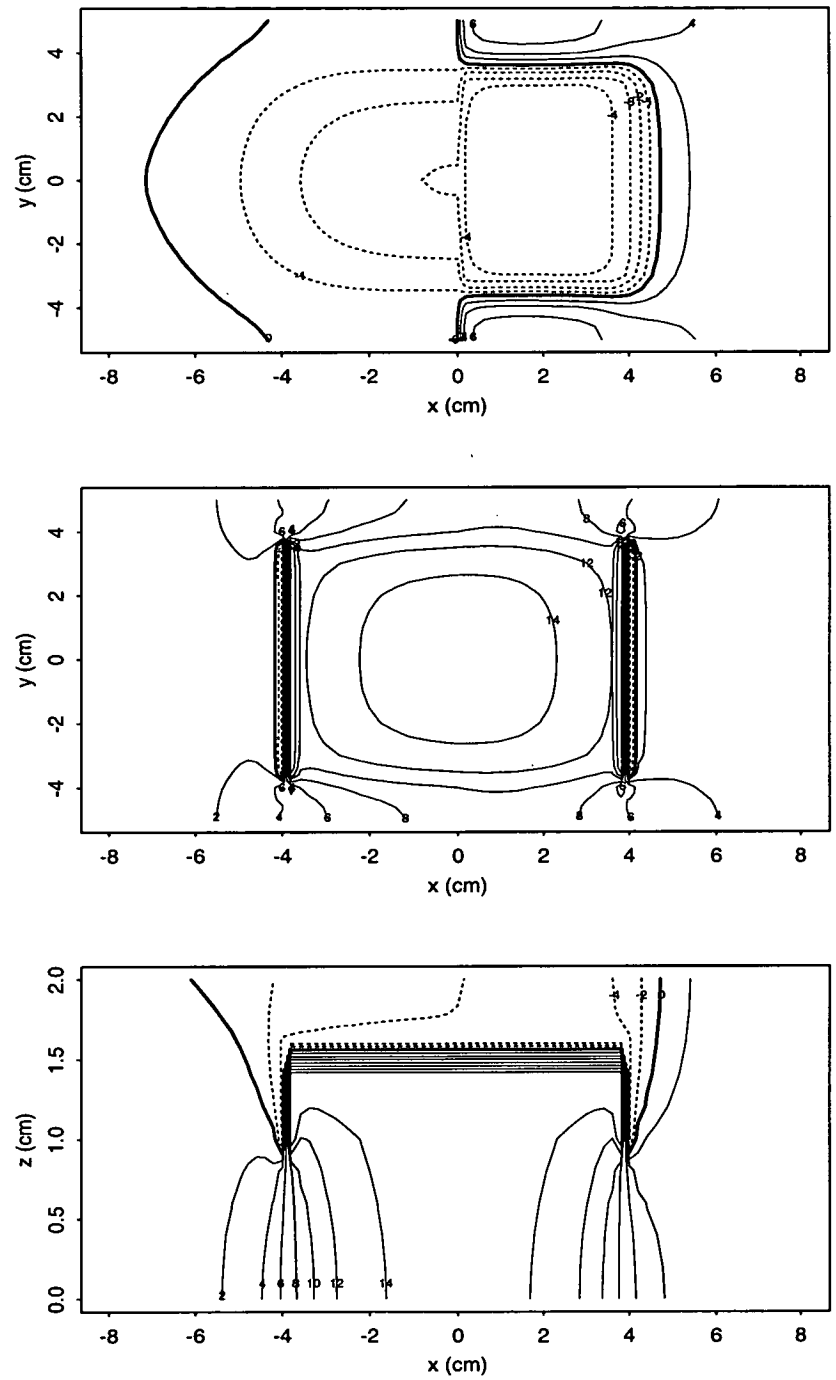

Figure 5.10: *Contour plots of ST potential from Laplace's equation during subendocardial ischaemia. The top panel represents the potentials on the epicardium, the middle panel the potentials on the endocardium and the bottom panel those on a cross section (y=0) of the heart. The thick solid lines represent the zero potentials, the thin solid lines ST elevation and the dashed lines ST depression. The contour interval is 2mV.*

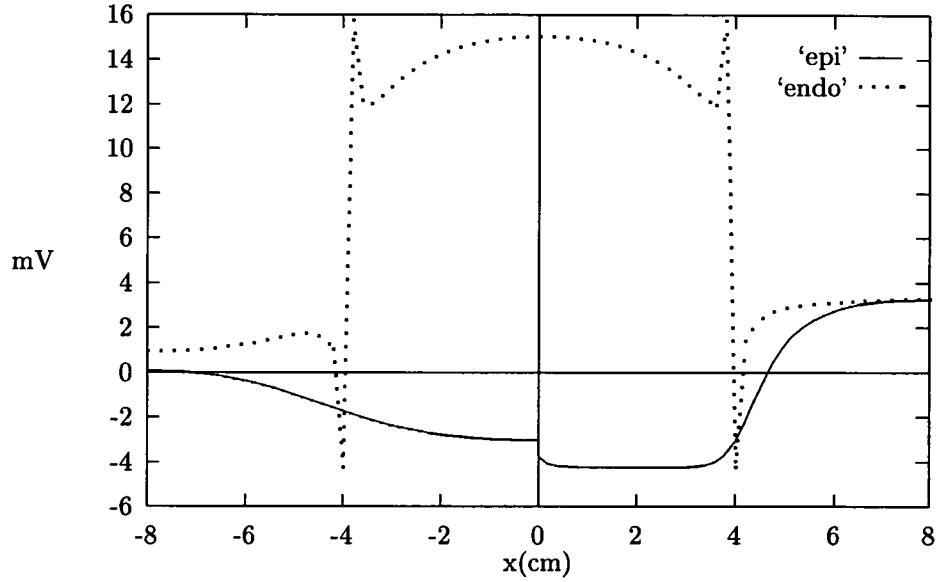

Figure 5.11: *ST potential from Laplace's equation on a line (y=0, z=1) across the ischaemic region on the endocardium (dotted line), and on a line (y=0, z=2) across the ischaemic region on the epicardium (solid line).*

in LCX ischaemia. For LAD ischaemia, ST depression on the body surface was seen over the left lateral region. Also, ST depression on the torso surface in LCX ischaemia had a larger area of ST depression over the left lateral region. In either ischaemia, an area of ST elevation appeared over the right anterior chest. The maximum of ST potential on the body surface was -219μV for ST depression and 98μV for ST elevation in LAD ischaemia, and -104μV for ST depression and 208μV for ST elevation in LCX ischaemia.

5.5 Discussion

5.5.1 Epicardial ST depression does not localise subendocardial ischaemia while endocardial ST elevation does

The main finding of the simulation is that epicardial ST depression does not indicate the location of subendocardial ischaemia while endocardial ST elevation does. During anterior and posterior subendocardial ischaemia, epicardial ST depression mainly occurred over the lateral region of the left ventricle (Figures 5.12 & 5.14).

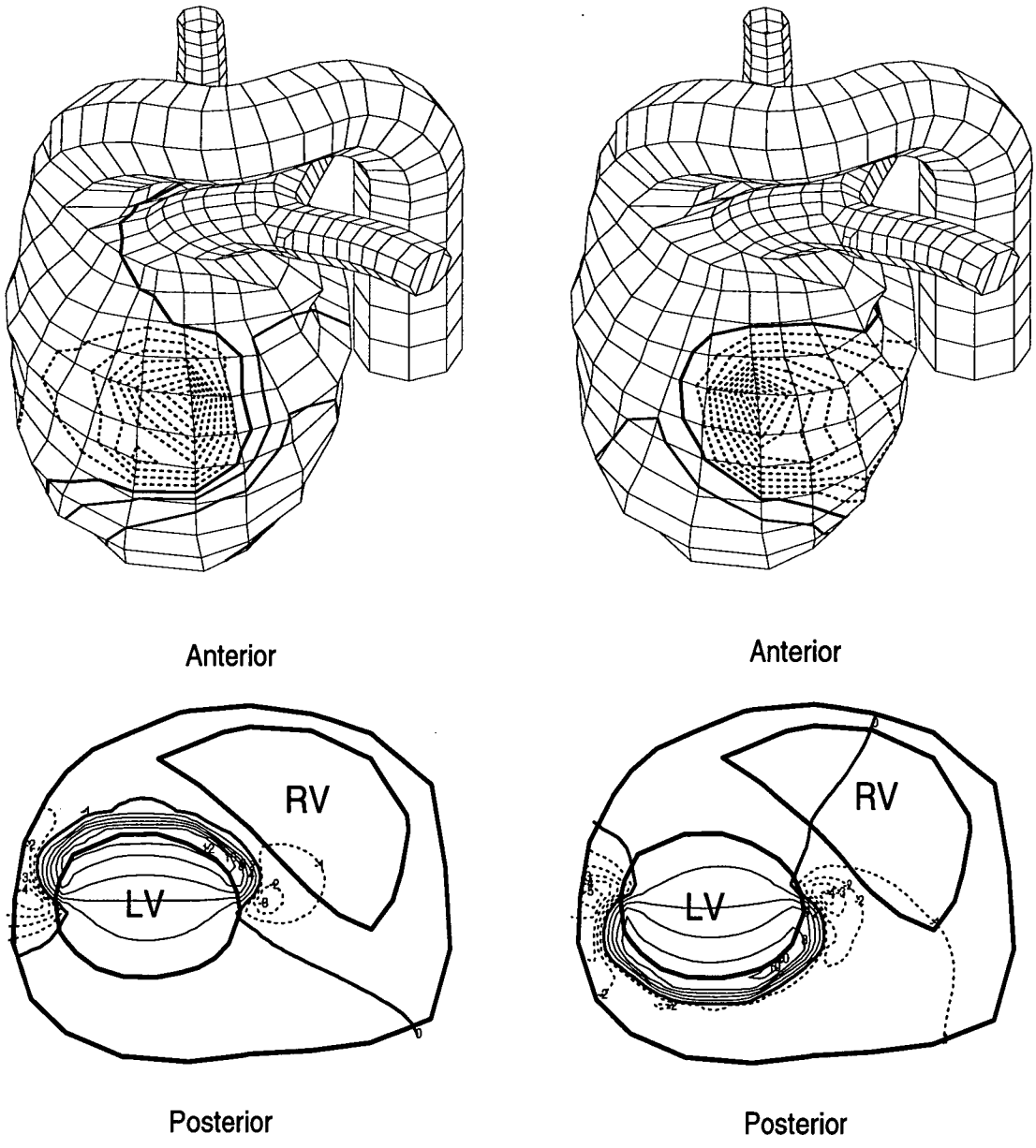

(a) LAD subendocardial ischaemia **(b) LCX subendocardial ischaemia**

Figure 5.12: *Contour plots of ST potential on the epicardium (top plots) and a cross section of the heart (bottom plots) during LAD (column a) and LCX (column b) subendocardial ischaemia from the isolated heart model. The thickest solid lines represent the outlines of the left ventricle (LV) and right ventricle (RV) in the bottom plots. The less thick solid, the thin solid and the dashed lines represent zero, ST elevation and ST depression respectively. The contour interval is 0.5mV for the top and 1mV for the bottom plots.*

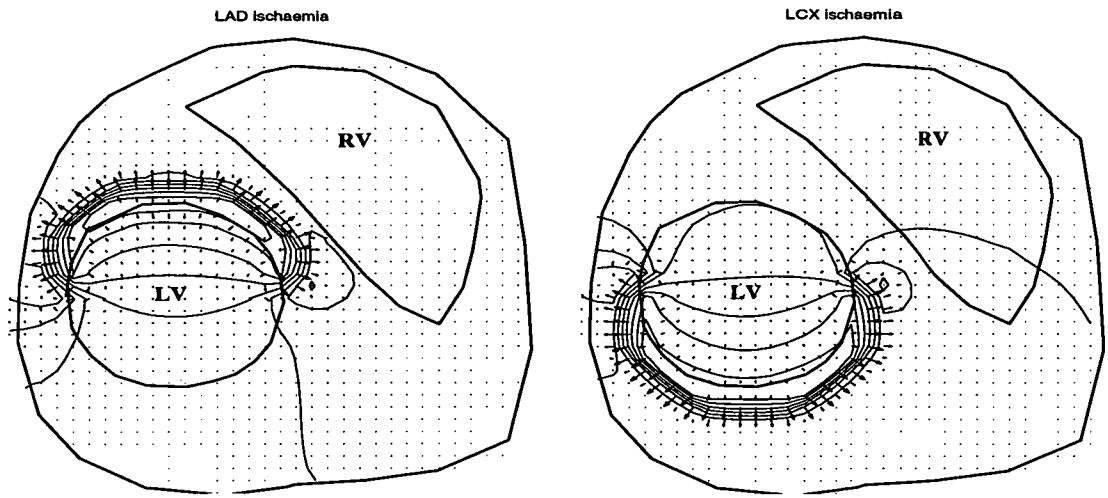

Figure 5.13: *Contour plots (thin lines) and current density plots of ST potential on a cross section of the heart in the isolated heart model. The thick solid lines represent the outline of the left ventricle (LV) and right ventricle (RV). Arrows indicate the direction of current flow.*

These results were in good agreement with epicardial and endocardial ST maps in open-chest sheep by Li [21], where ST depression occurred over the whole surface of the left ventricle, with a maximum change at the anterolateral wall in either LAD or LCX partial ligation, and the patterns of epicardial ST potential were similar in both ligations. Furthermore, endocardial ST elevation occurred in the ischaemic region in both subendocardial ischaemia. However, this simulation showed that epicardial ST depression occurred in a relatively smaller area on the left ventricular wall than that measured by Li [21]. The wider area of epicardial ST depression may be explained by including myocardial anisotropy in the simulation; the effect of myocardial anisotropy on ST potentials will be discussed in Chapter 7.

The simulated ST potentials also have an amplitude similar to that of Li's measurements [21]. The maximal epicardial ST depression ranged from -10 to -12mV in the 3D block model, and form -6 to -7mV in the isolated heart model. In the 3D block model, some current paths are blocked because no current can flow out of the 3D volume. For instance, current can flow freely in the left cavity of the heart while the current path is somehow blocked in the left cavity in the 3D block model (no current can flow out of the surface of z=0). This blockage of current path explains

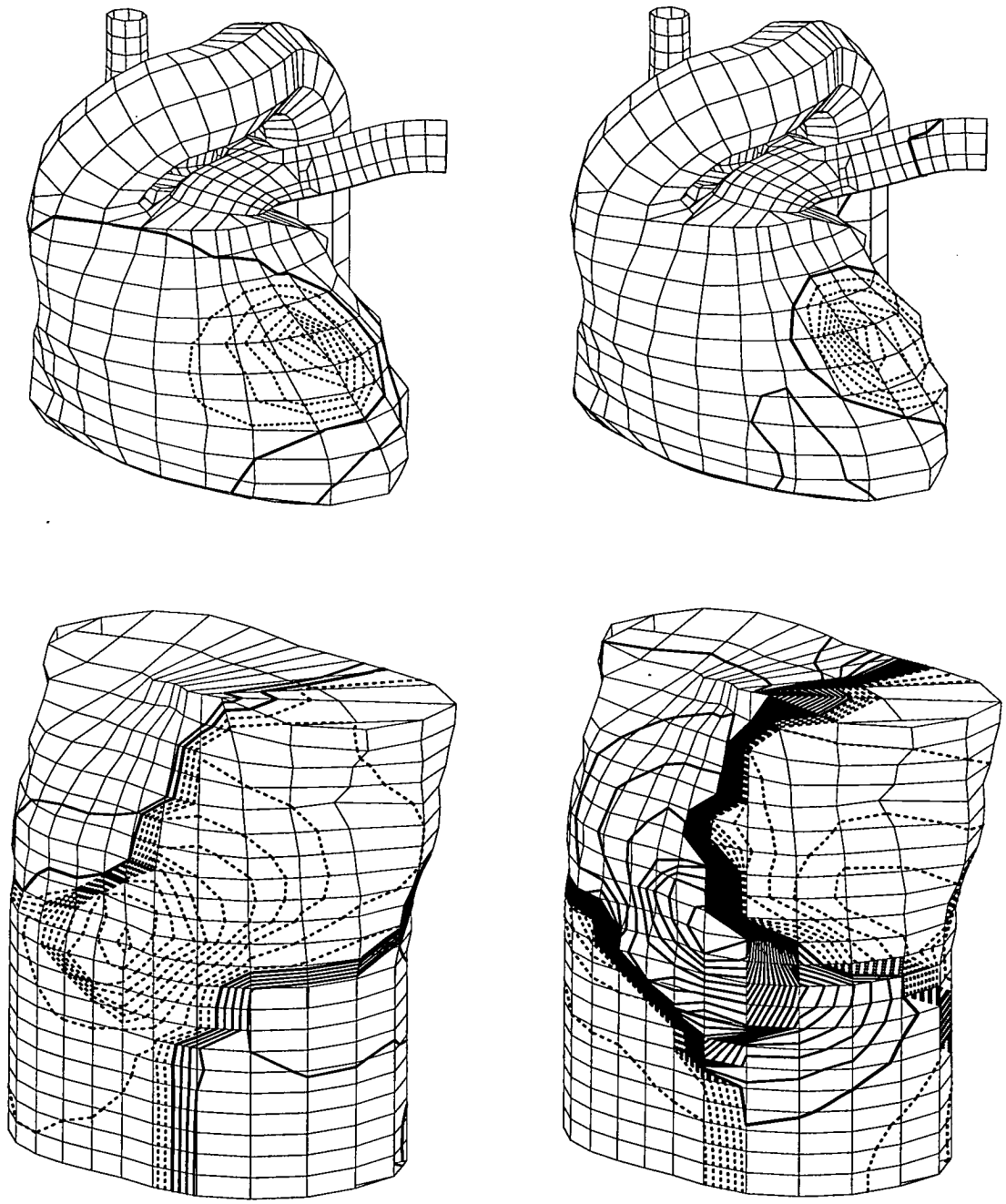

(a) LAD subendocardial ischaemia **(b) LCX subendocardial ischaemia**

Figure 5.14: *Contour plots of ST potential on the epicardium (top plots) and the torso surface (bottom plots) during LAD (a) and LCX (b) subendocardial ischaemia in the torso model. The contour interval is 0.5mV for the top and 20μV for the bottom plots.*

why the amplitude of epicardial ST depression is higher in the 3D block model than that in the isolated heart model. The amplitude of simulated ST depression in the isolated heart model was very close to the measured maximal ST depression on the epicardium (-4 to -10mV) in open-chest sheep [21]. The simulated endocardial ST elevation ranged from 0 to 16mV in the 3D block model and from 0 to 12mV in the isolated heart model, which can also be explained by the blockage of current paths. The simulated maximal ST elevation on the endocardium was also in the same order of magnitude as Li's measurements in sheep which ranged from 10 to 15mV [21]. As shown in Figure 5.14, the spatial distribution of the epicardial ST depression is slightly different in LAD and LCX ischaemia, although the ST depression mainly appears over the left lateral region. This spatial gradient may be able to differentiate the two ischaemia.

Therefore this model successfully simulates subendocardial ischaemia both qualitatively and quantitatively; produces results consistent with experimental observations; and predicts that the location of subendocardial ischaemia can not be indicated by epicardial ST depression but by endocardial ST elevation. In addition, the spatial gradient of epicardial ST depression may help to locate the ischaemic region.

5.5.2 Current source

The current source during subendocardial ischaemia is a type of current dipole layer, with an unequal intensity. For the bidomain model (equation 4.1), the current source due to ischaemia is derived from the second spatial gradient of transmembrane potentials when intracellular conductivity is constant ($\sigma_i \nabla^2 \Phi_m$). In the normal heart, there is no spatial gradient of transmembrane potential during phase 2 of the AP because all ventricular myocardial cells are activated, thus there is no ST segment shift. During ischaemia, the transmembrane potential of ischaemic cells changes, producing non-zero current sources at the ischaemic boundary during phase 2. As shown in Figure 4.6, the positive source is produced at the ischaemic side of the ischaemic boundary and the negative source at the normal side. When the ischaemic border zone was assumed to be 2mm in width and the amplitude of the

action potential was reduced to -30mV, these source densities were in the same order of magnitude, i.e. $\mu A/mm^3$, as those calculated from the Laplacian of the measured potentials during transmural ischaemia in pigs [8]. In the present study, the source was approximated to be uniformly distributed at the boundary, with the density of positive source of $1\mu A/mm^3$ and that of negative source $-0.7\mu A/mm^3$, which reproduced the ST distribution pattern in a sheep model [21].

The density of current source and its associated ST potential increase with the severity of ischaemia. As the severity of ischaemia increases, the amplitude of the action potential in phase 2 reduces, which in turn produces a large difference in transmembrane potentials between normal and ischaemic cells. As shown in equation (4.12), the source density is directly associated with this potential difference. Therefore severe ischaemia produces an intensive current source. ST potential also increases linearly with an increase of the source density, thus the amplitude of ST potential reflects the severity of ischaemia, although epicardial ST depression does not indicate an ischaemic region. Mirvis [124] found that in addition to ameroid constriction of the coronary artery, pacing to heart rates of 230-250 beats/min in dogs increased the intensity of positive and negative surface extremes of ST potential without altering their spatial features.

5.5.3 Ischaemic boundaries

The current source at the lateral boundaries is more intensive than that at the transmural boundary. As shown clearly in the governing equation (equation 4.1), the source density is directly associated with the spatial changes of the transmembrane potentials. In the numerical approximation (equation 4.11), the source density is inversely proportional to the square of the width of the transition zone between the normal and ischaemic cells. There is strong evidence that the lateral boundary is narrower than the transmural boundary, which suggests that the source density at the lateral boundary is larger than that at the transmural boundary.

Studies of blood flow after coronary artery ligation [100, 21] showed that subendocardial ischaemia has both transmural and lateral boundaries; the flow changes

gradually in the transmural direction and sharply in the lateral direction. This sharp change across the lateral ischaemic boundary was validated by the study of transmembrane potentials in dogs after LAD ligation [151]. The ischaemic boundary extended over a distance of 2-3mm or less in transmural ischaemia [100, 102, 97], which may be regarded as the width of the lateral boundary in subendocardial ischaemia. Even though the transmural boundary is a gradual transition from the endocardium to the epicardium [21], the spatial resolution is not high enough to evaluate the boundary width. Therefore it is difficult to evaluate quantitatively the difference in the density of current sources originating at the transmural and the lateral boundary. Intensive lateral current source increases the negativity of ST depression on the epicardium, particularly the maximal ST depression on the left lateral region (Figure 5.5).

Other researchers accounted for the transmural ischaemic boundary but ignored the lateral boundary in their simulations of subendocardial ischaemia [62, 120]. Consequently, they concluded that the distribution of epicardial ST depression indicated the location of underlying subendocardial ischaemia. Therefore the lateral boundary is an important contributor for epicardial ST depression in subendocardial ischaemia.

5.5.4 Current path

The current density is defined as

$$\vec{J} = -\sigma \nabla \Phi \tag{5.2}$$

where σ and Φ represent the conductivity and the electric potential, respectively. This implies that $\nabla\Phi$, as a vector, has the direction of the greatest rate of change of Φ. Therefore the direction of $\vec{J}$ goes from high to low potentials and its lines are perpendicular to the isopotential surfaces when σ is isotropic.

At the transmural boundary, current flows mainly across the boundary, while at the lateral boundary, current flows not only by crossing the boundary but also by going through the surrounding media (Figure 5.13). This current flows from the ischaemic

side of the lateral boundary to the normal region where both transmural and lateral boundaries meet, producing epicardial ST depression on the lateral region. The lateral source in the septum is not seen because it is surrounded by highly conductive blood. A large amount of current goes through the cavity blood, leaving the potential difference across the lateral ischaemic boundary on the endocardium very small. Thus ST potential on the endocardium shows a monophasic distribution (Figure 5.3).

The current path suggested by Kilpatrick *et al.* [5] is not confirmed in the simulation. In the isolated heart model, the current going through the great vessels and the torso tissue back to the heart surface does not exist. The simulation showed that epicardial ST depression was mainly due to the current flowing inside the heart. Even when other regions in the torso were included, the distribution of epicardial ST depression remained unchanged (Figure 5.14), therefore the great vessels may not affect the current path significantly.

5.5.5 ST potential on the body surface

There is an overlap of ST depression at the left anterior chest, and ST elevation appears on the right upper chest regardless of which vessel is involved in single-vessel subendocardial ischaemia. Studies of ST depression in subendocardial ischaemia in dogs showed characteristic patterns for single-vessel lesions, but there was a considerable overlap over the left anterior chest [124]. The body surface mapping study of Kubota *et al.* [3, 128] also showed a similar overlap of ST depression on patients with single vessel disease after treadmill exercise, but with its maximum most often occurring in the left anterior chest leads and ST elevation on the right upper anterior chest. Exercise-induced ST depression appeared most commonly in leads V_5 and V_6 on patients with single-vessel diseases [1, 2]. Although the present study showed an overlap of ST depression over the left lateral chest and ST elevation over the right anterior chest (Figure 5.14), the maximal ST depression did not appear over the left lateral area. This discrepancy could be explained by the fact that two important factors were ignored in the simulations, i.e. the width of the lateral

boundary is narrower than that of the transmural boundary, and the myocardium is anisotropic. Both factors cause the lateral source to be more intensive than the transmural source, which may produce a maximal ST depression at the left lateral chest facing the lateral boundary in either LAD or LCX subendocardial ischaemia, when the field from the lateral source in the septum is shunted by its surrounding blood. This would explain the poor localisation of subendocardial ischaemia by ST depression. However, this suggestion needs to be tested by a simulation including these two factors. The effect of myocardial anisotropy will be studied in the 3D block model in Chapter 7.

5.5.6 Transition to full thickness ischaemia

Epicardial ST depression increases when subendocardial ischaemia is in transition to transmural ischaemia. When the subendocardial ischaemic region was extended to the epicardium, i.e. the transmural boundary moved closer to the epicardium, epicardial ST depression increased but remained in the same position (Figures 5.6 & 5.7). Li [21] produced a transition of subendocardial ischaemia to transmural ischaemia by increasing the percent stenosis of a coronary artery at 10-15 minutes of subendocardial ischaemia in sheep, and found that ST depression increased gradually as the ischaemia progressed until epicardial ST elevation occurred.

As discussed in Section 5.5.2, epicardial ST depression increases with the severity of ischaemia. Therefore it is difficult to differentiate whether ischaemia becomes more severe or the transmural boundary moves closer to the epicardium with an increase of epicardial ST depression. However, endocardial ST elevation may distinguish these two changes, because an increased severity of ischaemia produced a higher endocardial ST elevation, while subendocardial ischaemia, with the transmural boundary closer to the epicardium, reduced the ST elevation.

5.5.7 Solid angle theory

Use of a constant potential difference to represent the injury source at the ischaemic boundary is not a valid approximation for the near field (endocardial or epicardial potentials). Solid angle theory predicts an epicardial ST depression appearing over the ischaemic region (Figures 5.10 & 5.11) which differs from that predicted by the bidomain model. Holland and Brooks [60] predicted that the net TQ-ST potential recorded from a centrally located epicardial electrode in subendocardial ischaemia was negative; the central epicardial ST depression would increase with an increase in size of ischaemia. Hyttinen [120] employed a detailed torso structure and similar injury current sources to simulate body surface ST potential, showing that ST depression could localise subendocardial ischaemia. Furthermore, a sharp potential change on the endocardium also appeared at the boundary as predicted by the solid angle theory (Figure 5.11), and ST depression occurred on the normal side of the ischaemic boundary. However, no such biphasic endocardial ST changes have ever been documented. As discussed in Section 5.5.1, the bidomain model predicts a monophasic distribution of endocardial ST changes at the ischaemic boundaries which matched well with the endocardial ST maps [21].

In solid angle theory, the boundary width does not affect the source intensity. The potential difference (the source representation) at the ischaemic boundary was assumed to be the difference in transmembrane potential between normal and ischaemic cells. It only slightly changed the epicardial distribution in the vicinity of the boundary [61]. Thus, the narrow lateral ischaemic boundary would not make any contribution to the observed pattern of epicardial ST depression in subendocardial ischaemia. However, the bidomain model predicts that a narrower ischaemic boundary produces an more intensive current source. Consequently, the current source at the lateral boundary is more intensive than that at the transmural boundary, which contributes to epicardial ST depression on the left lateral area.

Solid angle theory can not represent the cardiac current accurately but the bidomain model can. In electrostatics, solid angle formula is used to calculate the far field produced by a uniform dipole layer in an infinite homogeneous media. It was

first introduced by Wilson [31] to predict ST elevation on the body surface during ischaemia, and used by Holland's group [60, 61] to study TQ-ST changes on the epicardium and the precordium. However, the endocardium, epicardium and even anterior chest can not be regarded as far points compared with the size of cardiac sources, and the torso is not a homogeneous volume conductor. As shown in Figures 5.3 & 5.11, potentials at the locations of current sources were affected by their surrounding media. Even though the source intensity was proportional to the difference in transmembrane potentials between ischaemic and normal cells, the electric potential difference across the ischaemic boundary produced by this current source was not proportional to this difference in transmembrane potentials at all. Tung [62] made a thorough comparison of the bidomain model with solid angle theory in modelling ischaemia, and concluded that the bidomain model (using Poisson's equation) was more appropriate for most experiments of this nature.

5.5.8 Blood effect

The intracavitary blood within the heart is an important current path. The effect of intracavitary blood on the field from cardiac sources, the Brody effect [152], was first studied by Brody based on an idealised spherical cavity surrounded by heart muscle that extended indefinitely. In general, the field generated by radial dipoles is enhanced by the blood cavity, while the field from tangential dipoles is reduced [152]. Brody effects produce an increase of electromotive forces (EMF) oriented radially and a decrease of EMFs oriented tangentially, and have been confirmed by simulation of realistic inhomogeneous torso [153]. In the present study, when blood conductivity was reduces to 1/3 of its actual value, the whole heart became homogeneous and the amplitude of ST potential increased (Figure 5.8). This suggests that the lower blood conductivity increases the intensity of current source, i.e. the real blood reduces the source intensity. Although both radial and tangential EMFs were present, no attempts were made to test blood effects on them separately. As a whole, the blood reduces the current source in subendocardial ischaemia, which suggests that the lateral (tangential) component is more predominant than the transmural (radial) component based on the Brody effect. In addition, the ST distribution patterns

slightly changed, particularly those on the endocardium which became biphasic at the ischaemic boundary (Figure 5.8). The less conductive media reduces the amount of current flowing through the cavities, producing a large potential gradient which in turn changes the potential pattern. Therefore the cavitary blood provides a significant path for current flowing from the positive to the negative sources.

5.5.9 Effect of torso tissues

Torso tissues reduce the amplitude of the epicardial potential but do not change its distribution pattern. The effect of tissues outside the heart on ECG potentials was examined in dogs by Green *et al.* [131]. They found that the amplitude of ECG potentials from an isolated heart was markedly higher when the heart was surrounded by an insulating medium, but the location of positive and negative regions was less affected by surrounding media during QRS. Li [21] demonstrated the same effect in subendocardial ischaemia in sheep. In the present study, with the same ischaemic configuration, the epicardial ST potential shows a similar distribution pattern in both the isolated heart and the torso (Figures 5.12 & 5.14). However, the amplitude of ST potential is much higher in the isolated heart than in the torso. The amplitude on the epicardium is reduced to 50% when the torso tissue is included. In the isolated heart, the current flows only within the heart, while in the torso, a certain amount of current can flow out of the heart through tissues outside the heart. This out-flow current reduces the current density in the heart, which in turn reduces the ST potential gradient inside the heart. Therefore the amplitude of the epicardial potential decreases in the torso model.

5.5.10 Clinical implications

ST depression reflects the size of the ischaemic region in a given artery supplied territory at constant ischaemic severity, and vice versa. However, it is very difficult to differentiate these two situations clinically unless endocardial ST potential is measured. The amplitude of endocardial ST elevation increases with the severity

of ischaemia and reduces when the transmural boundary is close to the epicardium. Although localisable by endocardial ST elevation, subendocardial ischaemia can be localised by neither epicardial nor body surface ST depression. Therefore it would be necessary to examine the contribution of an inverse transformation from the body surface to the endocardium to locate the ischaemic region.

5.5.11 Conclusion

The current source produced at the lateral ischaemic boundary plays the dominant role in epicardial ST depression distribution in subendocardial ischaemia. In either LAD or LCX subendocardial ischaemia, epicardial ST depression is centred near the left lateral area where their supplied territories share their boundary. The current density in the septum is not seen because it is surrounded by highly conductive intracavitary blood.

5.5.12 Evaluation of the source approximation

The source was approximated as a uniformly distributed double layer with an unequal intensity for an isotropic myocardial conductivity. This may overestimate the density of the negative source and underestimate that of the positive source at the regions where the transmural and lateral boundary meet, based on equation (4.10). This approximation was used to compare with the approximation used by Holland's group [60, 61], i.e. a constant difference in the current source density versus a constant potential difference across the ischaemic boundary. However, this approximation may be closer to the real source because it reproduces the measured ST potential distribution. Furthermore, this approximation should not affect the conclusion of this study because the importance of the lateral boundary is also reflected by the narrow boundary and myocardial anisotropy.

5.5.13 Limitations

First, the effects of the narrow lateral boundary and the anisotropy were not evaluated in the isolated heart and the torso models. Because myocardial anisotropy is a function of position, inclusion of the anisotropy in a 3D realistic model would involve individual anisotropy to be addressed for each element which was not practical with our current resources. In addition, only subendocardial ischaemia of large regions was considered in this study. No measured data were available for subendocardial ischaemia of small regions.

Chapter 6

Simulation of transmural ischaemia

6.1 Introduction

Transmural ischaemia produces ST segment elevation over the ischaemic region which may be associated with ST depression outside the infarcted region. There is some controversy regarding the precise distribution of epicardial ST elevation over the ischaemic region. Ligation of a relatively small artery produces nearly uniform ST elevation over the ischaemic region on the epicardium [7, 8] while ligation of a large artery produces epicardial ST elevation on the epicardium which increases towards the ischaemic boundary [114, 9, 21]. Also the relationship between the amplitude of ST elevation and the size of the ischaemic region remains unresolved [118, 104, 61]. Some studies show that ST elevation over the ischaemic region decreases with an increase in size of the ischaemic region [10, 61, 114], while others suggest exactly the opposite [104, 118].

The origin of ST depression in transmural ischaemia also remains unresolved. ST depression in acute transmural ischaemia is observed at the normal side of the ischaemic boundary on the epicardium [14, 7, 15]. A dipole pattern of ST depression and ST elevation on the epicardium is found in either LAD or LCX transmural ischaemia in sheep [9]. Precordial ST depression in patients with acute myocardial

infarction [20] is suggested to be either a reciprocal change of ST elevation [16, 136], or a resultant of an additional subendocardial ischaemia [19, 140].

However, no single model has addressed all these problems in transmural ischaemia. Solid angle theory has been used to analyse ST elevation over the ischaemic region both on the epicardium and the body surface [60, 116]; Miller and Geselowitz [70] used the bidomain model to study only ST changes on the body surface. Dube *et al.* [121] employed a detailed torso structure and simulated ST changes on the body surface in different ischaemic regions, concluding that ST depression on the body surface was a reciprocal change of ST elevation. No endocardial or epicardial ST potentials were calculated in the model. Even though myocardial anisotropy was included in the simulation, no conclusion could be drawn as to the effects of myocardial anisotropy on ST potential distributions.

This chapter presents results from simulation of transmural ischaemia to study the origin of both ST elevation and ST depression in transmural ischaemia. Ischaemia of different sizes and at different locations were simulated in the three model geometries: the 3D block, the isolated heart and the torso models. First, changes in ST potential with the size of ischaemia, including its amplitude and distribution pattern, were evaluated for small and large regions of transmural ischaemia in the 3D block model. Then, for both sizes of transmural ischaemia, the simulation was also carried out in both the isolated heart and the torso models to elucidate the relationship between ST changes on the epicardium and on the body surface.

6.2 Transmural ischaemia of a small region

A small region of transmural ischaemia results from complete narrowing of a small branch of a major coronary artery such as the diagonal branch of the LAD and the obtuse marginal (OM) branch of the LCX. The OM branch supplies the lateral region of the left free wall [98, 9], and has been used experimentally to produce small infarcts in sheep which were documented by blood flow measurements [9]. In this study, transmural ischaemia in the OM territory was chosen on the basis of Li's

measurements [9].

6.2.1 3D block model

The 3D block model of OM transmural ischaemia is shown in Figure 6.1. The ischaemic region is located around the centre of the left ventricular free wall (x=4, y=0). The ischaemic boundary has an octagon shape through the left ventricular wall (Figure 6.2). To evaluate the relationship between ST changes and transmural ischaemic size, four different sizes of ischaemia were simulated, with an area of $1.28cm^2$ (OM 1.28), $3.52cm^2$ (OM 3.52), $8.64cm^2$ (OM 8.64) and $19.68cm^2$ (OM 19.68) respectively. Because the left ventricle was assumed to be 1cm thick, their ischaemic volumes were $1.28cm^3$, $3.52cm^3$, $8.64cm^3$ and $19.68cm^3$ respectively. The centres of all ischaemic regions were located at the centre of the LVW. Comparison was made only when both σ_i and σ were isotropic. After the ischaemic boundary was properly defined according to the ischaemic region, the source densities were calculated and assigned to the relevant elements (Table 6.1).

	Area (cm^2)	Positive source ($\mu A/mm^3$)	Negative source ($\mu A/mm^3$)
OM 1.28	1.28	1.0	-0.750
OM 3.52	3.52	1.0	-0.842
OM 8.64	8.64	1.0	-0.895
OM 19.68	19.68	1.0	-0.930

Table 6.1: *Source densities for different sizes of OM ischaemia in the 3D block model*

6.2.2 Isolated heart model

Two different small sizes of transmural ischaemia were simulated in the realistic heart model: one had an area of $1.28cm^2$ (OM 1.28) and the other $2.40cm^2$ (OM 2.40); their volumes were $1.28cm^3$ and $2.40cm^3$ respectively. The ischaemic boundary had the same shape as that used in the 3D block model, i.e. an octagon shape. The source densities are shown in Table 6.2. Also the myocardial conductivity was assumed to be isotropic.

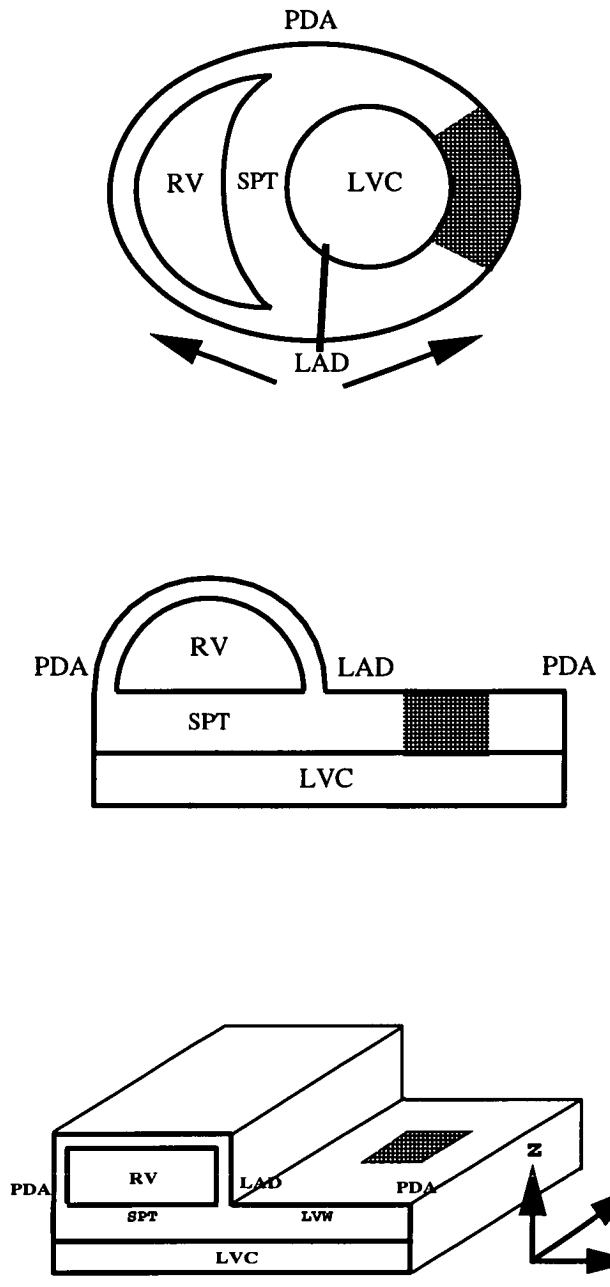

Figure 6.1: *Illustration of the development of the 3D block model for the isolated heart with OM transmural ischaemia (shaded area). Top: Diagram showing a cross section of the heart with the thick line indicating the cutting line and the arrows indicating the directions of unwrapping. Middle: Diagram showing the unwrapped heart structure. Bottom: The geometry of the 3D block model. The details of this simplifying procedure is found in Section 4.2.1.*

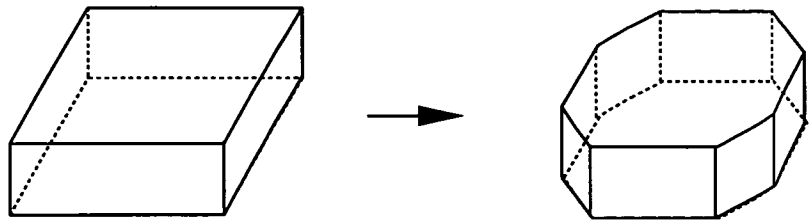

(a) Square **(b) Octagon**

Figure 6.2: *Illustration of converting a square boundary (a) to an octagon boundary (b).*

	Area (cm^2)	Positive source ($\mu A/mm^3$)	Negative source ($\mu A/mm^3$)
OM 1.28	1.28	1.0	-0.750
OM 2.40	2.40	1.0	-0.8125

Table 6.2: *Source densities for two different sizes of OM ischaemia in the isolated heart model*

6.2.3 Torso model

To examine the body surface ST potential, the simulation was carried out in a torso model with the same ischaemic configurations as used in the isolated heart model. Thus the two OM ischaemic areas of $1.28cm^2$ and $2.40cm^2$, and their source densities (Table 6.2) were used for these two ischaemia. Also σ_i and σ were assumed to be isotropic.

6.3 Transmural ischaemia of a large region

Large full thickness ischaemia results from occlusion of large coronary arteries such as the LAD and LCX. For ovine mammals, the left coronary artery provides the blood supply for the left ventricle [97, 98, 9]. The territory of the LAD artery mainly includes the anterior of the left ventricle and the anterior part of the septum. The LCX artery supplies the posterior regions of the left ventricle and the septum. Furthermore, Euler *et al.* [97] observed that the LAD perfused 42% of the left ventricular mass in the ovine heart, and Li [21] found that the LCX territory weighed

46% and the LAD territory weighed 52% of the left ventricle. Therefore it was assumed in the present study that the territory of either the LAD or LCX occupied half of the left ventricle. For ischaemia in either the LAD or LCX territory, the ischaemic and non-ischaemic regions occupy the same volume in the left ventricle, thus the intensities of both the positive and negative source are equal.

6.3.1 3D block model

In this section, both LAD and LCX transmural ischaemia were simulated. The model geometry for LAD transmural ischaemia is shown in Figure 6.3.a and that for LCX transmural ischaemia in Figure 6.3.b. Both regions of ischaemia share the boundaries at the central septum (x=-4.0) and the lateral region of the LVW (x=4.0). Similarly, both could be simulated by the same model with an opposite polarity for the current source.

For ischaemia of a large region where the ischaemic and non-ischaemic regions occupy the same volume in the left ventricle, the ischaemic region should extend from y=-5 to y=5. However, this would cause the sources at y=±5 to face the volume boundary where no current could flow out. In reality, however, only the sources on the epicardium face the volume boundary, and no sources in the transmural wall face the volume surface. Therefore in the simulation of transmural ischaemia of a large region, an ischaemic region was assumed to extend from y=-3.0 to y=3.0 and only the ischaemic boundaries at x=-4.0 and x=4.0 were considered for the source calculations. The ischaemic boundaries at y=-3.0 and y=3.0 were ignored, otherwise they would cause an inequality in the intensity of positive and negative sources. The source density of $\pm 1.0 \mu A/mm^3$ was used in the simulation.

6.3.2 Isolated heart model

In this section, the myocardial conductivity was assumed to be isotropic to simplify computation. Transmural ischaemia located in the territory of either the LAD or the LCX was simulated. Both territories share their boundaries at the septum on

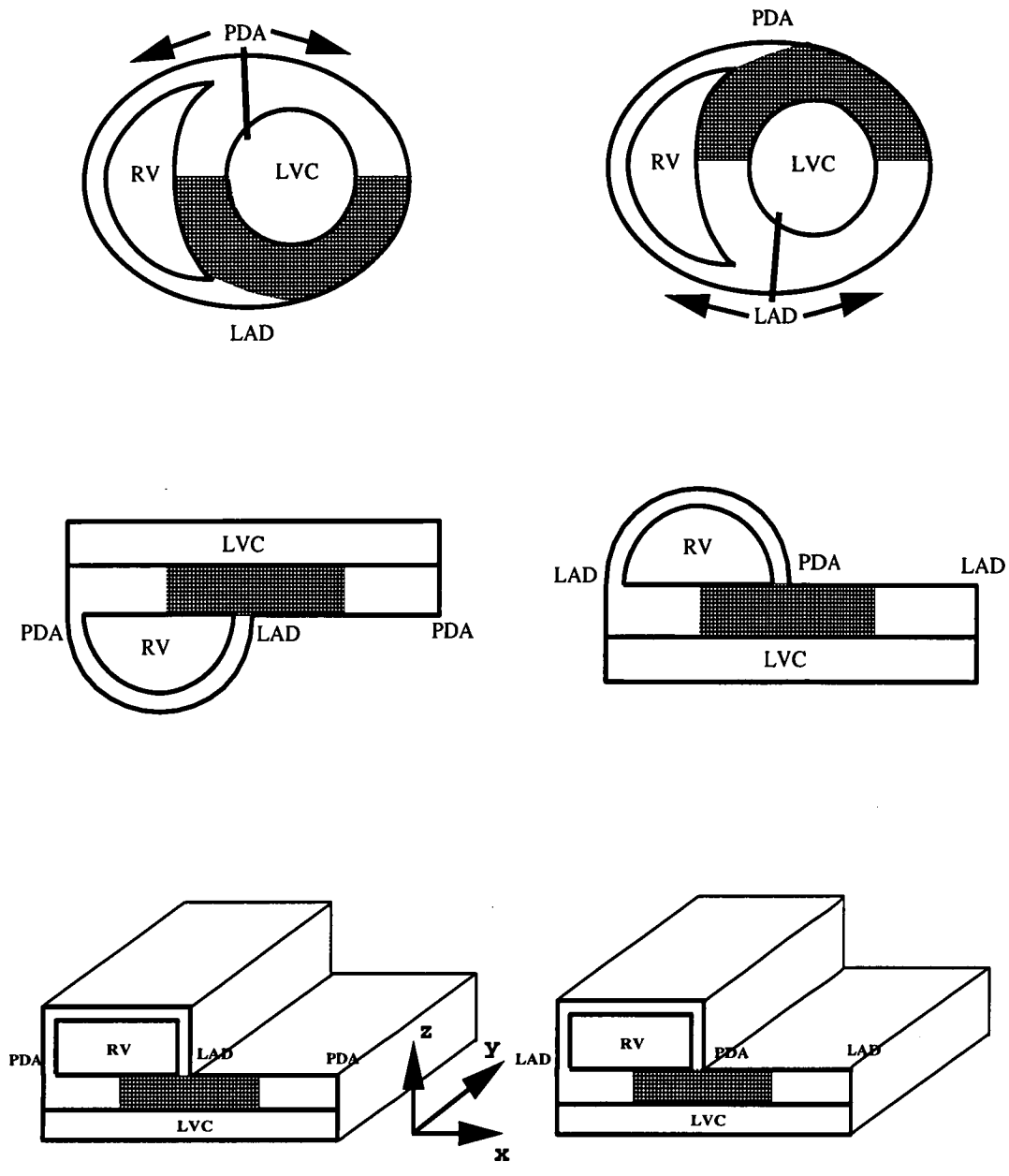

(a) LAD transmural ischaemia **(b) LCX transmural ischaemia**

Figure 6.3: *Illustration of the development of the 3D block model for transmural ischaemia of a large region. Diagram (a) represents the conversion of the heart with LAD transmural ischaemia to the 3D block model; when the heart is cut along the PDA (thick line) and opened flat following the directions indicated by the arrows, the heart is turned into the first simplified model (middle) and the actual 3D model (bottom) is obtained when the first simplified model is turned upside down. Similarly, diagram (b) represents the conversion of the heart with LCX transmural ischaemia (top) into a 3D block model (bottom). The details of the block dimensions are described in Section 4.2.1.*

one side and the lateral region of the left ventricular free wall on the other. In either ischaemia, the ischaemic region and non-ischaemic region occupy the same volume, so the current densities for the source and the sink are the same. A source density of $\pm 1.0 \mu A/mm^3$ was used in this simulation.

6.3.3 Torso model

Simulation was performed in a torso model in which the ischaemic configurations for LAD and LCX transmural ischaemia were identical to those of the isolated heart model. ST potentials in the whole torso region were calculated. Myocardial anisotropy was ignored in this section.

6.4 FIDAP solution

After the source densities were assigned to the corresponding elements (for Poisson's equation), the governing equation was solved by the finite element method package FIDAP. Details of solving the equation were described in Section 4.4. Displays of the simulated data were described in Section 4.5.

6.5 Results

6.5.1 Transmural ischaemia of a small region

6.5.1.1 3D block model

The average potential on the epicardium was used as the reference potential. The ST potential distributions on the epicardium, the endocardium and a cross-section of the left ventricular wall in the two small sizes of OM ischaemia (OM 1.28 & OM 3.52) are shown in Figure 6.4. The comparison among the four different sizes of ischaemia is illustrated in Figure 6.5. To assess the ST elevation distribution over the ischaemic region, a uniformness factor was defined as the ratio of central ST

elevation to maximal ST elevation. A uniformness factor of 1.0 indicates a uniform distribution and the factor decreases as the degree of uniformness reduces. The uniformness factor on the epicardium was 0.95 for OM 1.28, 0.82 for OM 3.52, 0.64 for OM 8.64, and 0.48 for OM 19.68. As shown in Figure 6.5.b, the maximal ST elevation on the ischaemic side and the maximal ST depression on the normal side of the ischaemic boundary varied with the ischaemic size. Regarding endocardial ST potentials, uniform ST elevation appeared over the ischaemic region, and its amplitude only slightly varied with the ischaemic size (Figure 6.5.a).

6.5.1.2 Isolated heart model

The data were presented against the reference potential, the average potential on the epicardium. ST potentials from the simulation of OM transmural ischaemia in the isolated heart model are shown in Figures 6.6, 6.7 & 6.8. For OM 1.28 ischaemia, epicardial ST elevation appeared over the ischaemic region with ST elevation in a range of 12-13mV, and the surrounding ST depression in a range of -1 to -2mV. For OM 2.40 ischaemia, the corresponding values were 10-12mV for ST elevation, and -2 to -3mV for surrounding ST depression. As shown in Figure 6.8, epicardial ST elevation on the centre of the ischaemic region was slightly lower than that on the boundary, with a uniformness factor of 0.96 for OM 1.28 ischaemia and 0.87 for OM 2.40 ischaemia. On the endocardium, ST potentials showed a monophasic distribution with ST elevation appearing over the ischaemic region (Figure 6.6 bottom). The amplitude of endocardial ST elevation was in the order of 6-7mV, with ST elevation in OM 1.28 ischaemia being slightly greater than that in OM 2.40 ischaemia. The current density plots on a cross-section during these two ischaemia are shown in Figure 6.9.

6.5.1.3 Torso model

The average potential on the torso surface was used as the reference potential for data presentation. The simulated ST potentials in OM transmural ischaemia are shown in Figure 6.10. For OM 1.28 ischaemia, a localised ST elevation appeared

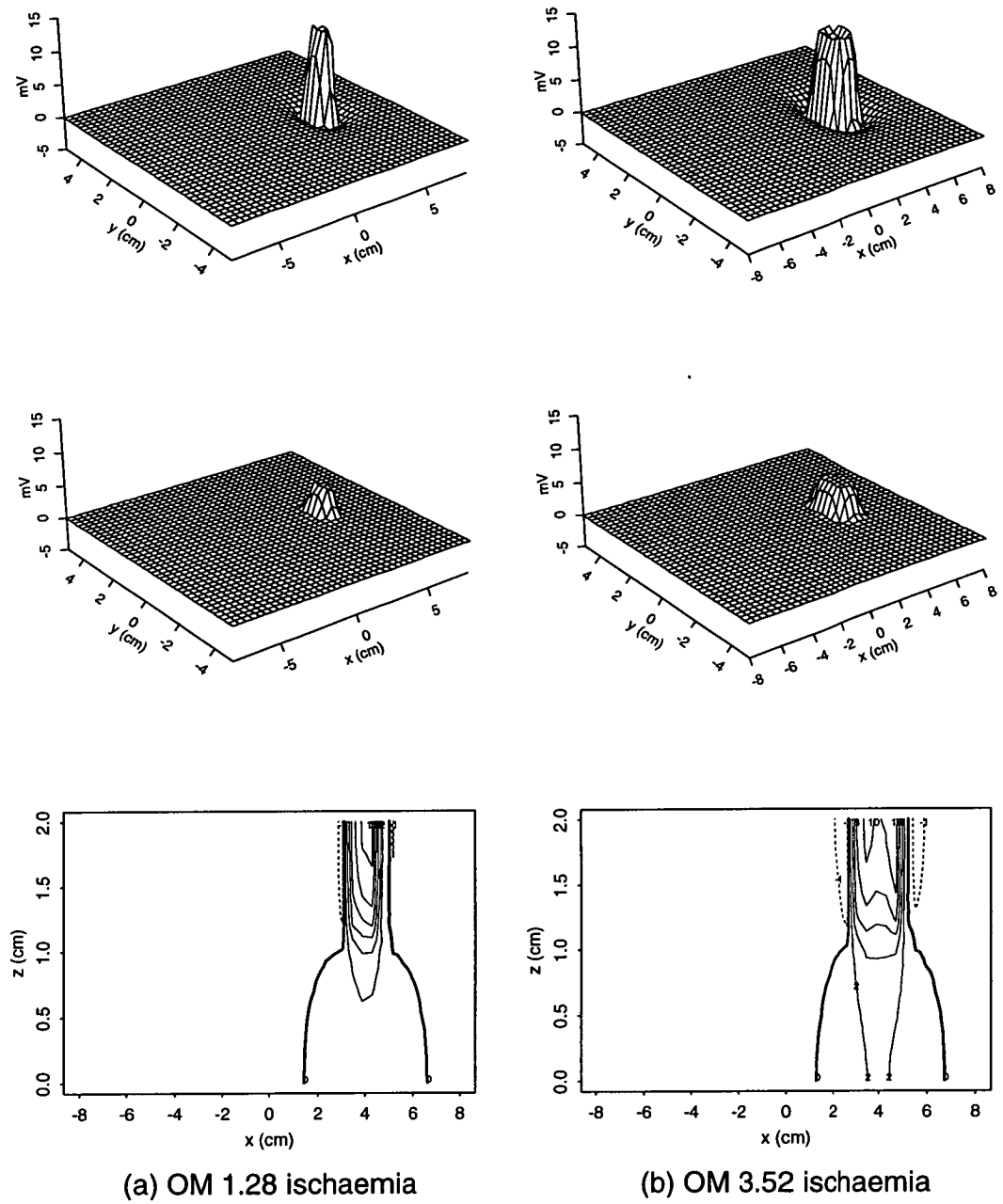

Figure 6.4: *Contour plots of ST potential distributions from simulations of OM 1.28 and OM 3.52 ischaemia in the 3D block model. Diagram (a) represents the smaller size ischaemia and diagram (b) the ischaemia of the larger size. The top, middle and bottom plots represent the potentials on the epicardium, endocardium and a cross-section (xz plane) of the left ventricular wall, respectively. For the bottom panels, the area from z=0 to z=1 represents the left ventricular cavity and the area from z=1 to z=2 the left ventricular muscle. The thick solid lines represent zero potential, thin solid lines positive potentials, and dashed lines negative potentials. The contour interval is 2mV.*

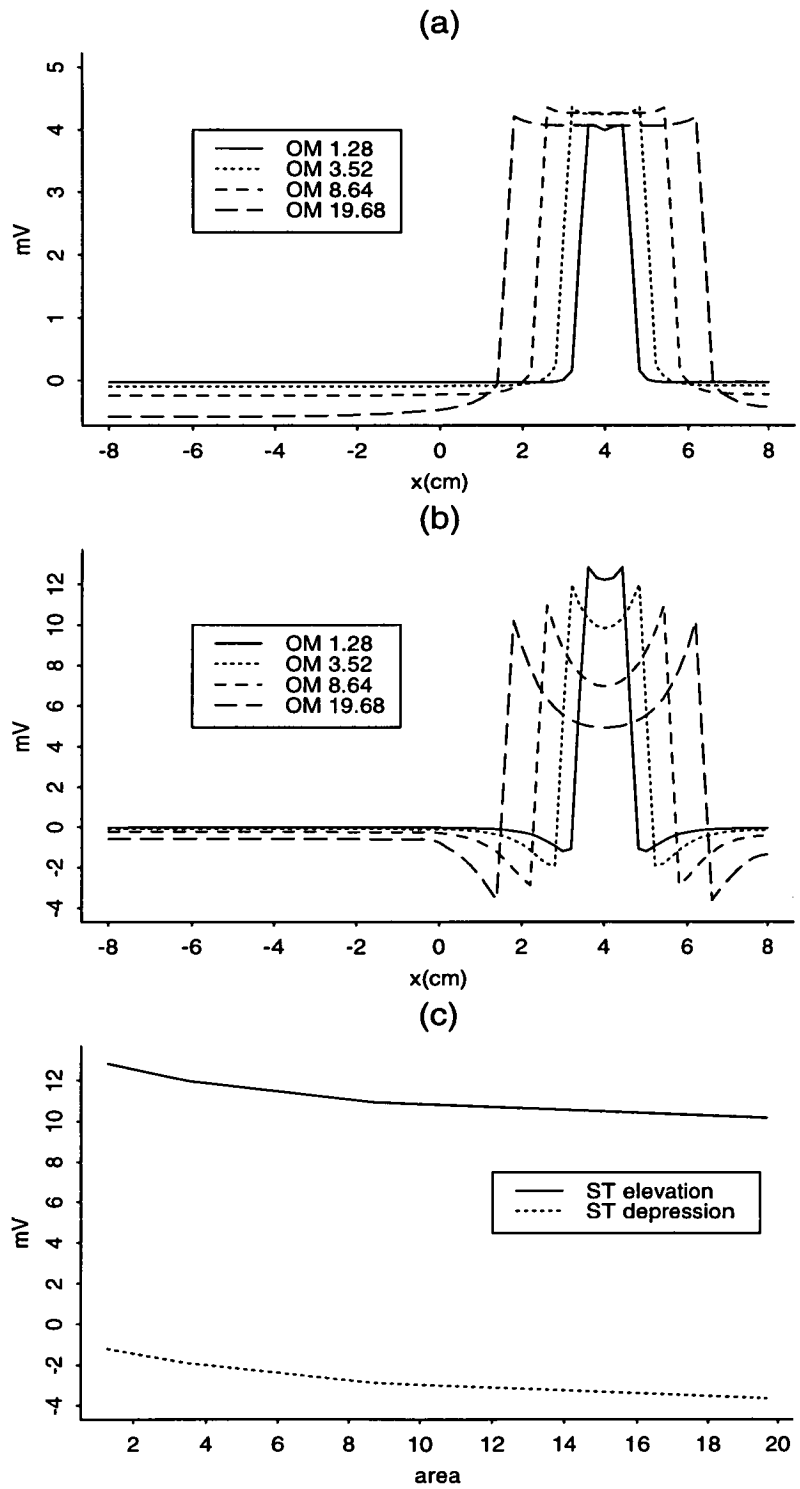

Figure 6.5: *Comparison of epicardial and endocardial ST changes along the x axis crossing the ischaemic region among different sizes of ischaemia in the 3D block model. Panel (a) represents endocardial potentials, panel (b) epicardial potentials, panel (c) the peak epicardial ST elevation (solid line) and the peak epicardial ST depression (dashed line).*

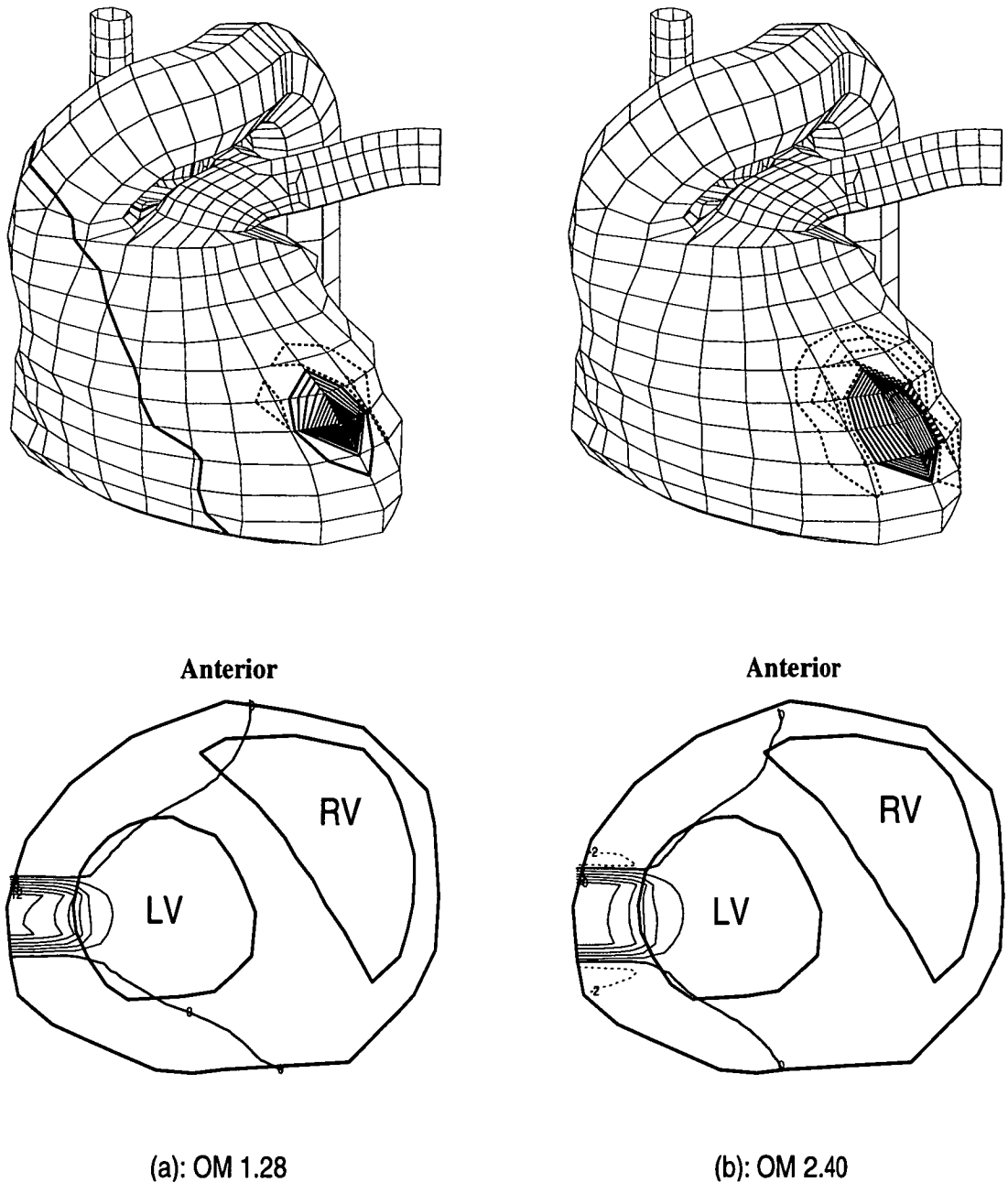

Figure 6.6: *Contour plots of ST potential distribution on the epicardium (top) and a cross-section of the isolated heart (bottom) during OM transmural ischaemia in the isolated heart model. The left and right ventricular cavities are represented by LV and RV outlined by the heavy lines. The thick solid lines represent zero potentials, the thin solid lines positive potentials, and the dashed lines negative potentials. The contour interval is 1mV for top plots and 2mV for bottom plots. The left plots (a) are for OM 1.28 and the right (b) for OM 2.40.*

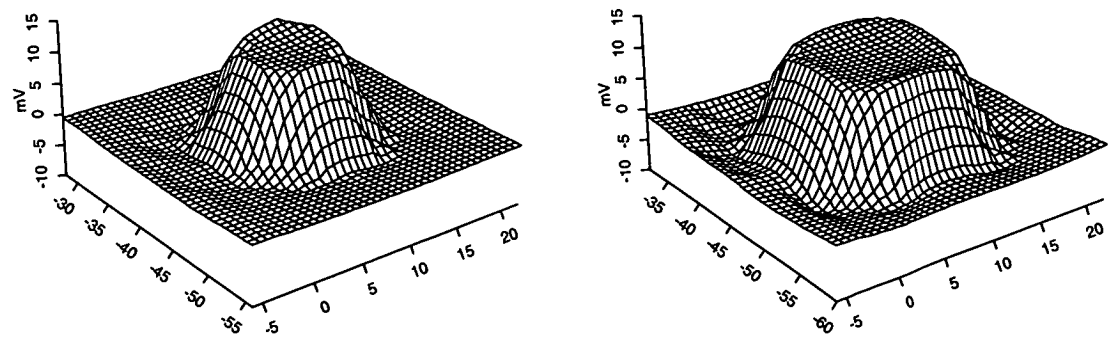

(a) OM 1.28 (b) OM 2.40

Figure 6.7: *Contour plots of epicardial potential distributions on the ischaemic region and its periphery in the isolated heart model. The left plot represents OM 1.28 and the right plot OM 2.40.*

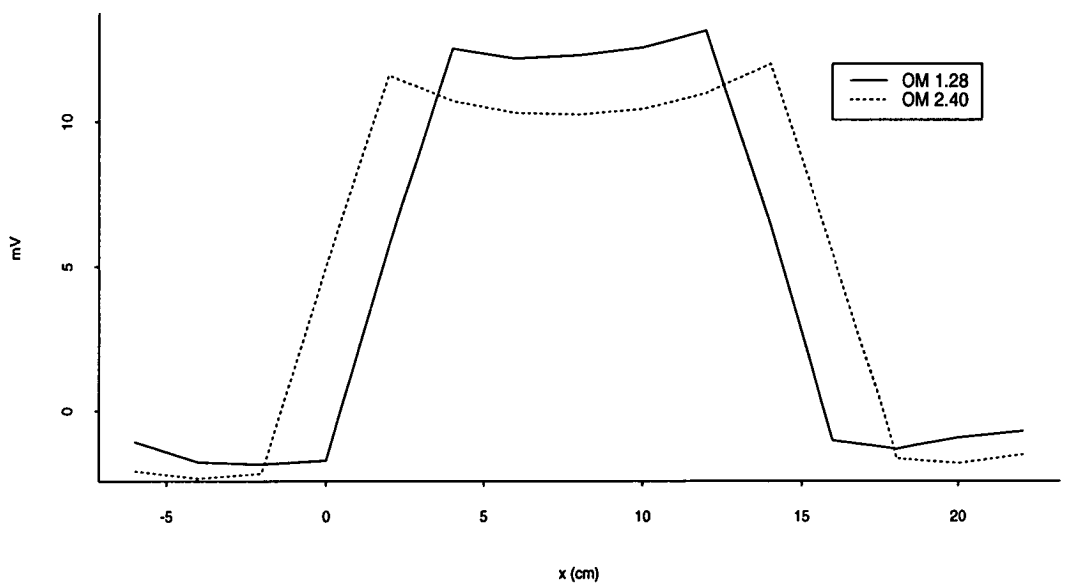

Figure 6.8: *Epicardial ST potential distributions on a line crossing the ischaemic region during OM 1.28 (solid line) and OM 2.40 (dashed line) transmural ischaemia in the isolated heart model. The ischaemic centre is located at x=8.*

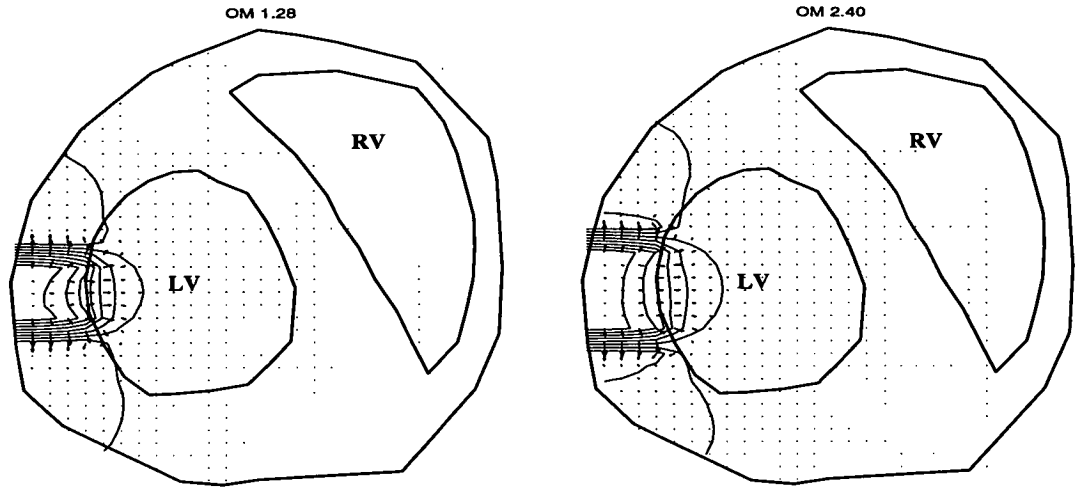

Figure 6.9: *Direction of current flow on a cross-section during OM ischaemia in the isolated heart model. Thin lines represent the isopotential lines and arrows the direction of current flow. Thick solid lines represent the outlines of the left ventricle (LV) and right ventricle (RV).*

on the epicardium over the ischaemic region with a maximum of 7.42mV; epicardial ST depression with a much lower amplitude (the peak of -1.42mV) appeared at the normal side of the ischaemic boundary. On the torso surface, the maxima of ST changes were 8μV and -18μV with ST elevation indicating the ischaemic region. For OM 2.40 ischaemia, the epicardial ST maxima were 6.85mV for ST elevation and -2.91mV for ST depression, and the maxima of ST changes on the torso surface were 15μV for ST elevation and -34μV for ST depression.

6.5.2 Transmural ischaemia of a large region

6.5.2.1 3D block model

For transmural ischaemia of a large region, a strong dipole of ST depression and ST elevation appeared over the lateral area (x=4) of the left ventricle with ST elevation on the ischaemic side and ST depression on the normal side (Figures 6.11 & 6.12); the amplitude of ST potential in this dipole was in a range of $\pm$(7-8)mV. ST elevation extended over the ischaemic region and ST depression over the normal region. The amplitude of ST potentials was reduced towards the ischaemic boundary.

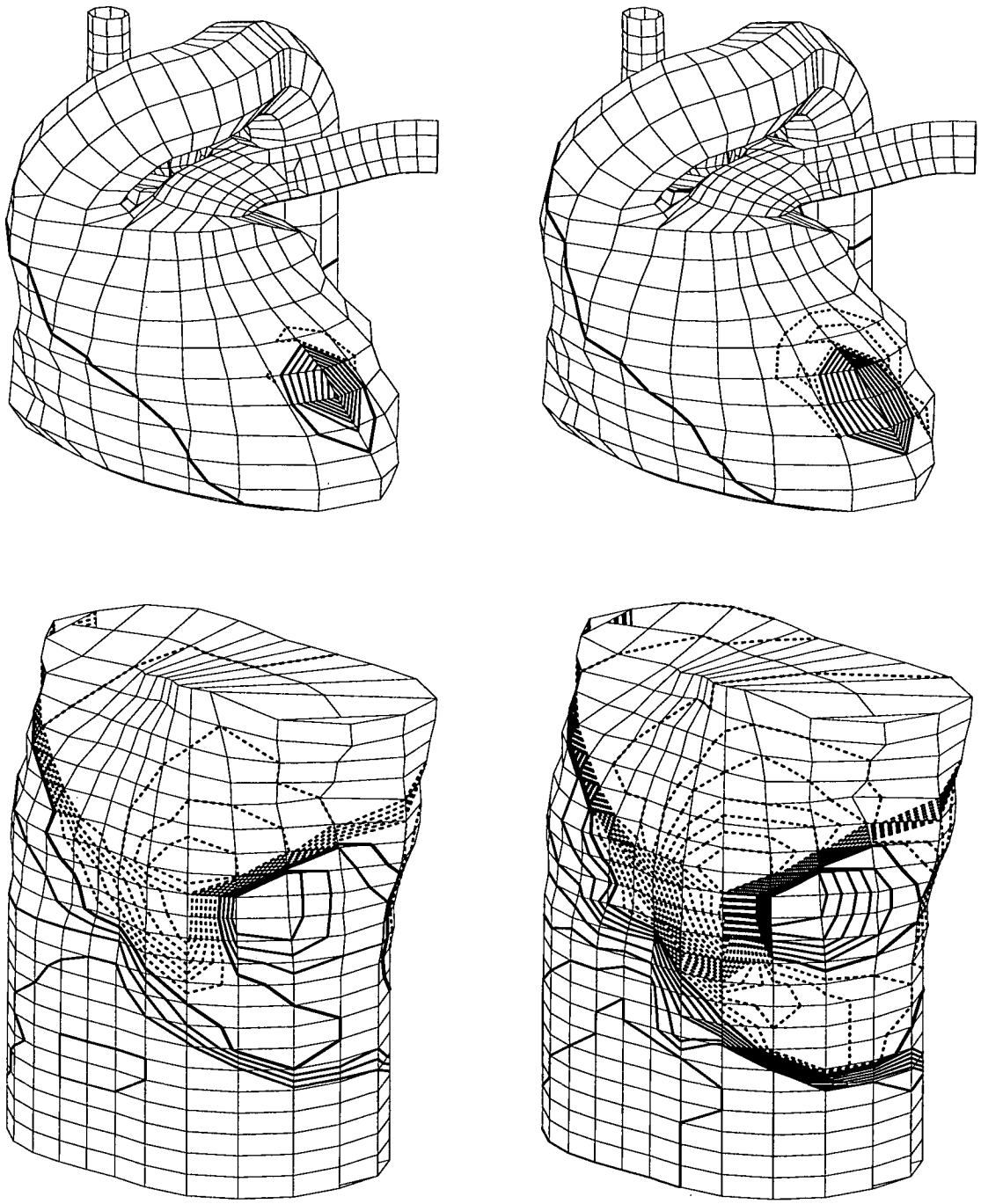

(a) OM 1.28 **(b) OM 2.40**

Figure 6.10: *ST potentials (a) in OM 1.28 ischaemia, (b) in OM 2.40 ischaemia from the torso simulation. The top diagrams represent ST isopotential contours on the epicardium and the bottom plots ST potential distribution on the torso surface. The contour interval is 1 mV in the top plots and 2μV in the bottom plots. The thick solid lines represent zero potentials, the thin solid lines positive potentials, and the dashed lines negative potentials.*

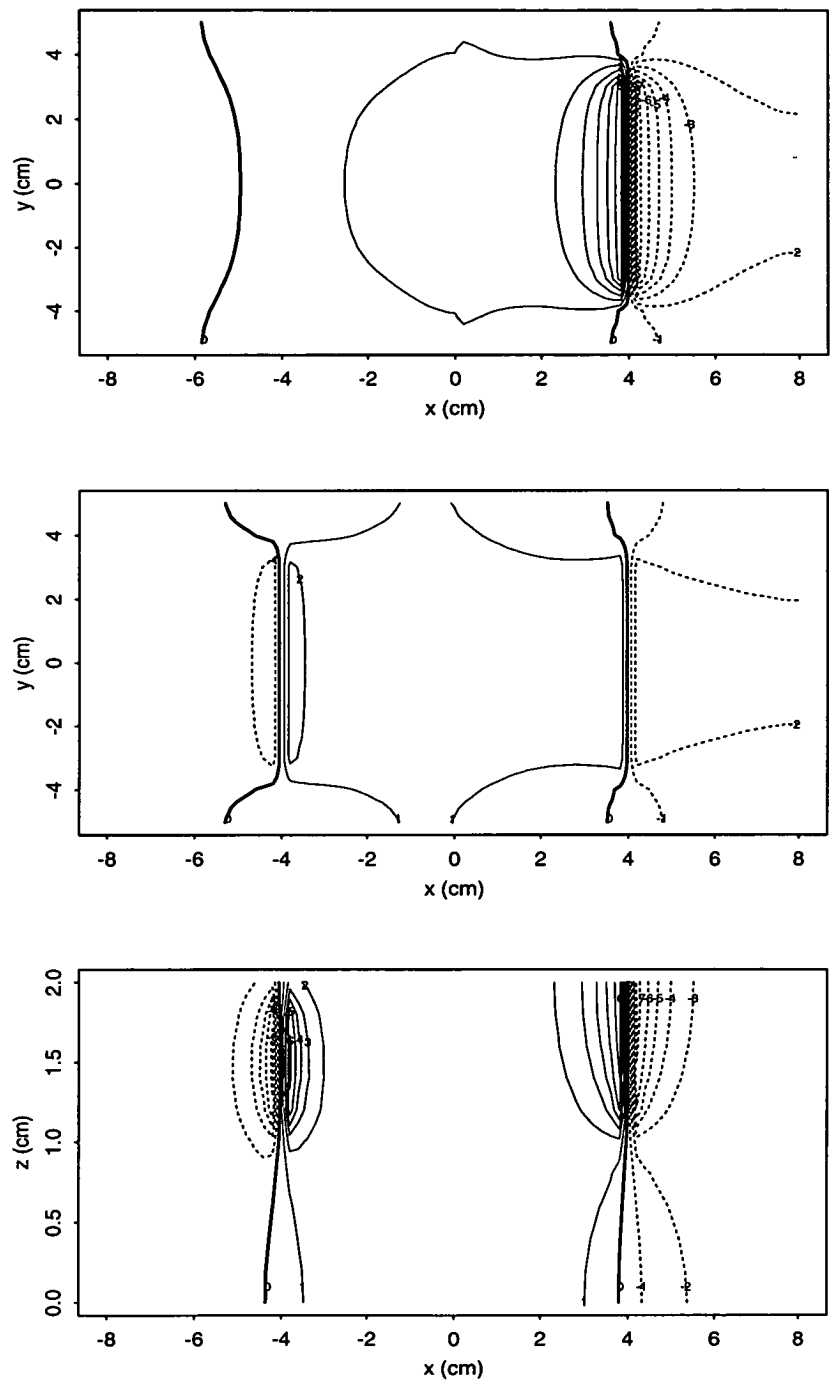

Figure 6.11: *Contour plots of ST potentials on the epicardium (top), the endocardium (middle) and a cross-section of the left ventricle (bottom) during ischaemia of a large region in the 3D block model. The contour interval is 1mV. The thick solid lines represent zero potentials, the thin solid lines positive potentials, and the dashed lines negative potentials.*

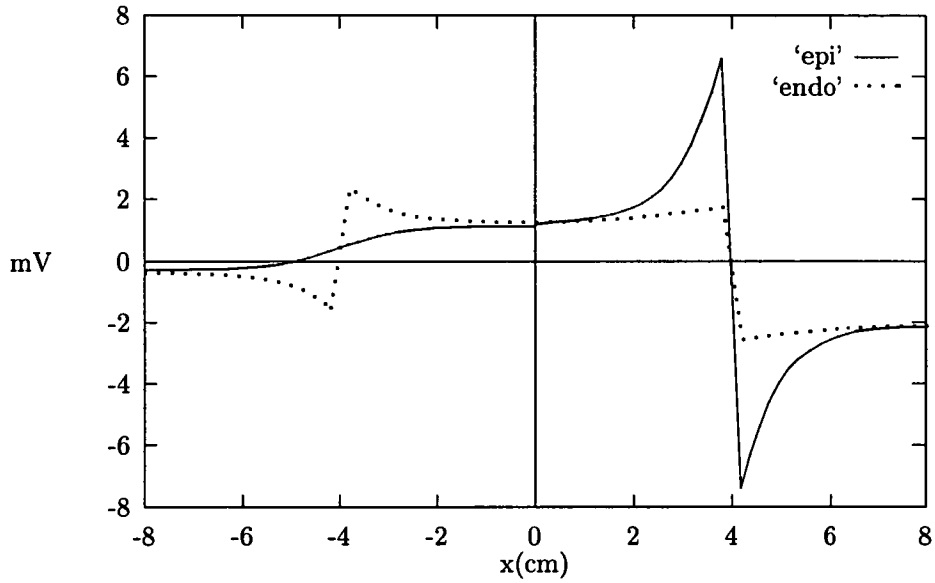

Figure 6.12: *ST potentials along the x axis across the ischaemic region on the epicardium (solid line) and the endocardium (dotted line) in the 3D block model of transmural ischaemia of a large region.*

On the endocardium, ST elevation appeared over the ischaemic region with a lower amplitude of about 2mV, and ST depression occurred on the normal region with an amplitude of about -2mV. Two weak dipoles of ST changes appeared over the ischaemic boundaries (x=-4, x=4) on the endocardium.

6.5.2.2 Isolated heart model

The ST potential distribution on the epicardium and a cross-section of the heart during transmural ischaemia of a large region from the isolated heart model are shown in Figure 6.13. A strong dipole of ST changes appeared on the epicardium over the lateral region of the left ventricle with ST elevation on the ischaemic side and ST depression on the normal side of the ischaemic boundary. The amplitude of the dipole was in the order of ±(6-7)mV. On the cross section, there were two dipoles of ST changes: one in the left lateral region and the other in the septum. The dipole source in the left ventricular wall gave rise to ST elevation at the ischaemic side and ST depression at the normal side, with their maxima appearing on the epicardium. However, the dipole source in the septum did not extend its dipole potentials to the epicardium, with the maxima appearing at the centre of the ischaemic boundary in

the septum. On the endocardium, ST elevation appeared over the ischaemic region and ST depression over the normal region with a lower amplitude, and two dipoles of ST changes appeared on the ischaemic boundaries, with an amplitude in the range of ±(3-4)mV. The current density of ST potential was calculated from that on the cross-section, and the direction of the current density on the cross-section is shown in Figure 6.14.

6.5.2.3 Torso model

The ST potentials during transmural ischaemia of a large region in the torso simulation are shown in Figure 6.15. On the epicardium, a dipole of peak ST changes with an amplitude of about ±(2-3)mV appeared over the left lateral region, with ST elevation on the ischaemic side and ST depression on the normal side of the ischaemic boundary (Figure 6.15 top). On the torso surface, the peak ST changes shifted away from the ischaemic boundary, with maximal ST elevation indicating the centre of the ischaemic region and maximal ST depression occurring on the opposite side of the torso (Figure 6.15 bottom). The amplitude of ST changes on the torso surface was in a range of ±(300-500)μV.

6.6 Discussions

6.6.1 Current source

The intensity of current source varies with the ischaemic size at constant ischaemic severity. As shown in equation (4.1), the current source due to ischaemia is derived from the spatial gradient of transmembrane potential. During the ST segment, this gradient produces a positive source at the ischaemic side of the ischaemic boundary and a negative source at the normal side (Figure 4.6). For transmural ischaemia of a small region, the ischaemic region occupies less space than the normal region, rendering the positive source more intensive than the negative source. This finding is also confirmed by the Laplacian map of ST potential in pigs [8], where the current

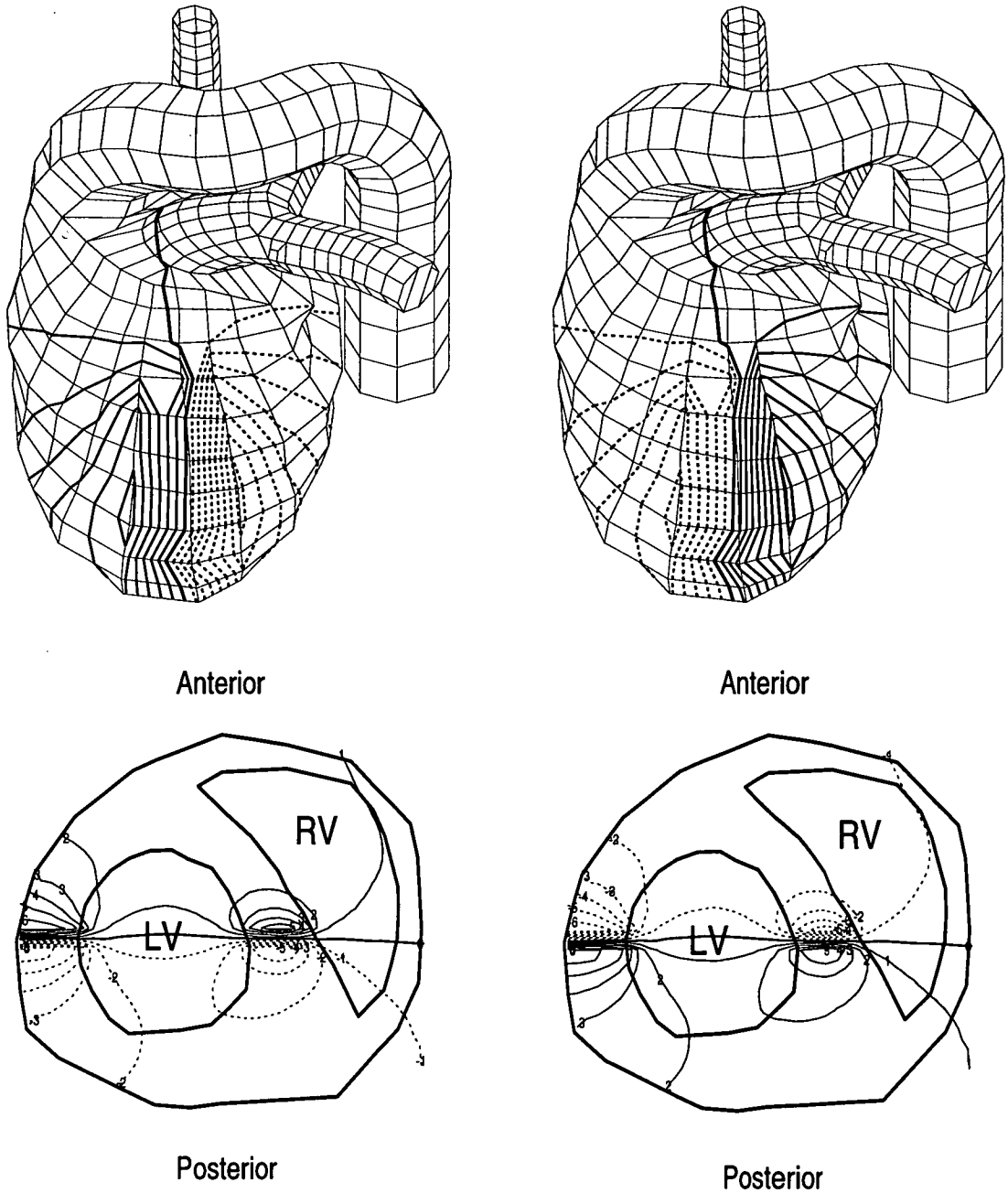

(a) LAD transmural ischaemia **(b) LCX transmural ischaemia**

Figure 6.13: *ST potentials during transmural ischaemia in the LAD territory (a) and the LCX territory (b) in an isolated heart model. The top diagrams represent ST isopotential contours on the epicardium. The bottom plots represent ST potential distribution on a cross section of the heart. The thick solid lines represent zero potentials, the thin solid lines positive potentials, and the dashed lines negative potentials. The contour interval is 1mV.*

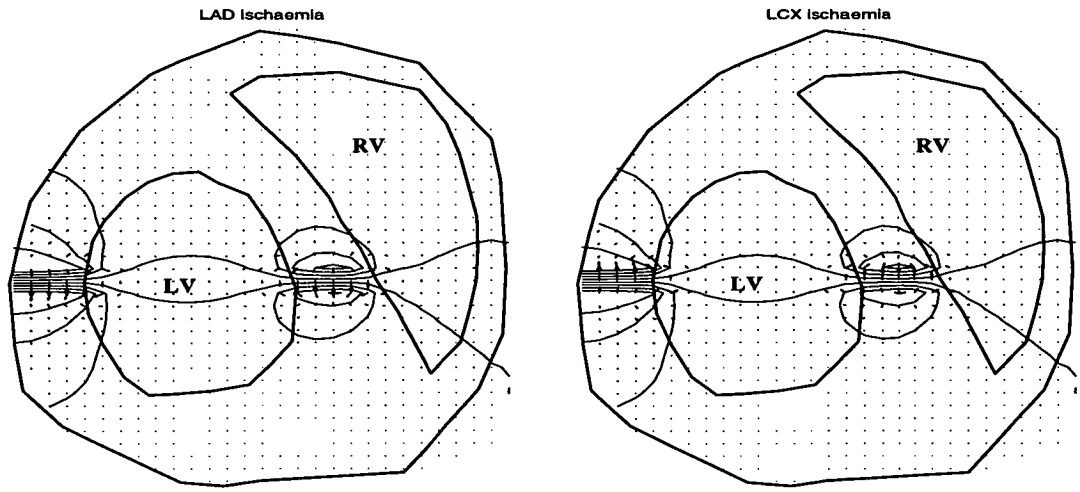

Figure 6.14: *Direction of current flow on a cross-section of the heart during LAD and LCX large regions of ischaemia in the isolated heart model. Thin lines indicate isopotential lines and arrows the direction of current flow. Thick solid lines represent the outlines of the left ventricle (LV) and right ventricle (RV).*

source (positive source) has a density of $1.0\mu A/mm^3$ and the sink a density of $0.6\mu A/mm^3$ (negative source) after 15 minutes of ischaemia. With an increase in size of the ischaemic region, the difference in density between the positive and the negative sources is reduced (Tables 6.1 & 6.2). When the LAD or the LCX territory is involved, ischaemic and non-ischaemic regions occupy almost the same space in the left ventricle, hence the positive and the negative sources are of the same intensity. As discussed in Section 6.3, both the LAD and LCX territories share the same boundary in the left lateral region at one side and in the septum at the other. Therefore the current sources originate only in the left lateral region and the septum (Figures 6.11 & 6.13).

The source intensity is also affected by the severity of ischaemia. As discussed in Section 4.4.1.3, the source intensity was proportional to the difference in the transmembrane potential between ischaemic and normal tissues at an isotropic intracellular conductivity (equation 4.12). Thus, a severe ischaemia creates an intensive current source. The governing equation for ST potentials (equation 4.1) is a linear equation at a constant myocardial conductivity, hence, ST potential is proportional to the source intensity. Therefore the potential amplitude increases linearly with

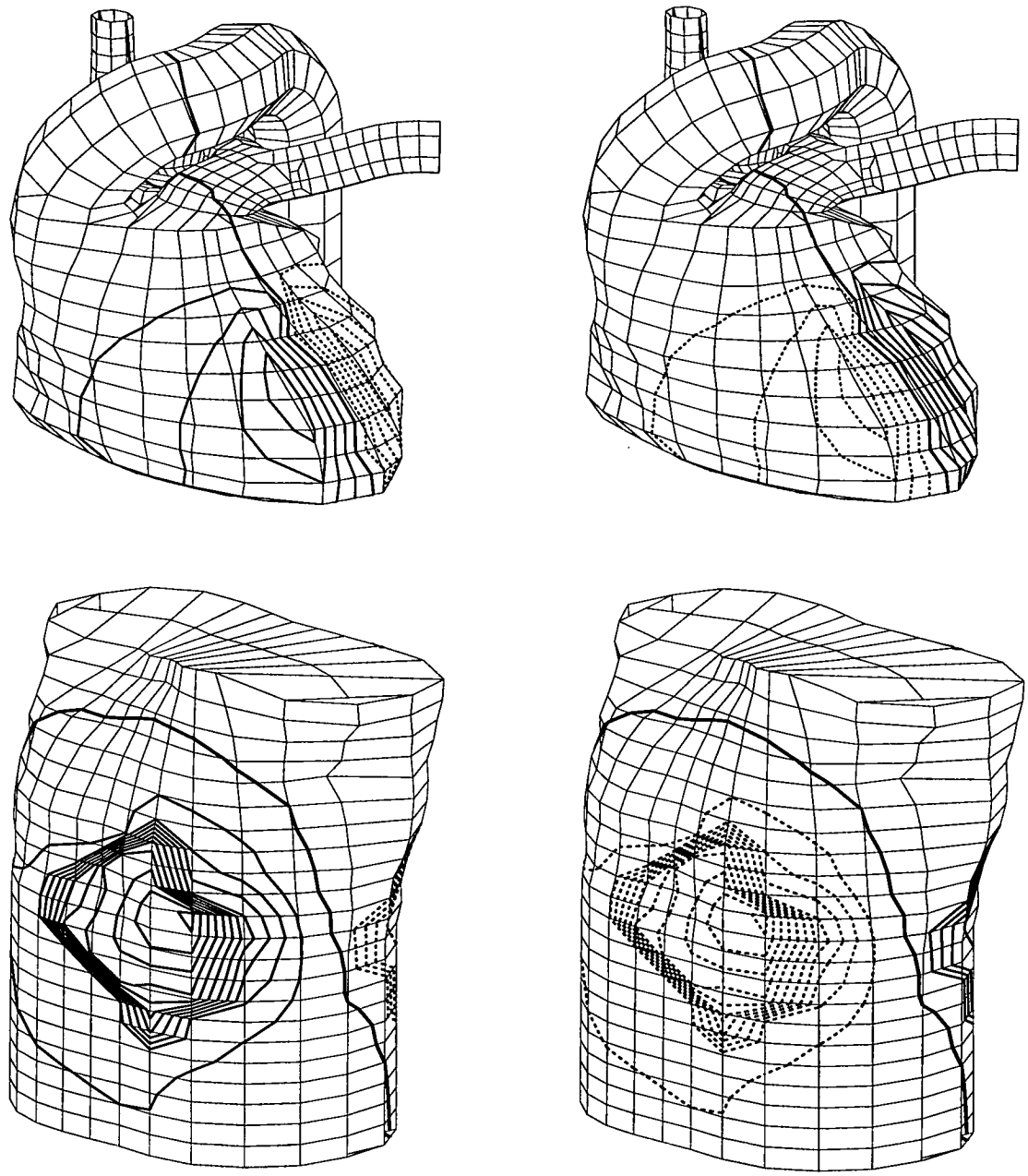

(a) LAD transmural ischaemia **(b) LCX transmural ischaemia**

Figure 6.15: *ST potentials during transmural ischaemia in the LAD territory (a) and the LCX territory (b) from the torso simulation. The top diagrams represent ST isopotential contours on the epicardium and the bottom plots ST potential distribution on the torso surface. The contour interval is 0.5 mV in top plots and 50μV in bottom plots. The thick solid lines represent zero potentials, the thin solid lines positive potentials, and the dashed lines negative potentials.*

the severity of ischaemia at a constant isotropic myocardial conductivity.

6.6.2 Current path

In an isolated heart, current flows from positive to negative source not only by crossing the ischaemic boundary but also through the cavities. For a small region of ischaemia, a positive source originating at the ischaemic side has a higher current density than a negative source at the normal side. This current pattern produces a potential difference not only tangentially but also transmurally (Figures 6.4 & 6.9). For the source closer to the endocardium, more current flows through the surrounding media, which gives rise to a lower potential difference across the ischaemic boundary. For instance, OM 3.52 ischaemia in the 3D block model showed a potential difference of 13.89mV across the ischaemic boundary on the epicardium and 4.14mV on the endocardium (Figure 6.5). The existence of transmural current was shown by a potential difference between the epicardium and the endocardium in the ischaemic region, i.e. a potential difference of 5.56mV existed at the centre of the ischaemic region. Kleber *et al.* [8] confirmed the tangential potential difference on the epicardium after LAD occlusion in pigs, although no major transmural potential gradient was found in the ischaemia. However, this absence of transmural potential gradients could be due to the tube used in Kleber's study, which had a diameter of $0.7mm$ and carried the intracellular wick electrodes, causing extra injury when it was driven through the ventricular wall. The current flows transmurally from the epicardium to the endocardium in the ischaemic region, from the endocardium to the epicardium in the normal region, and tangentially across the ischaemic boundary.

Similarly, both transmural and tangential currents exist in large regions of transmural ischaemia. The transmural current flows from the ischaemic side of the boundary to the normal side through the intracavitary blood, and the tangential current flows across the ischaemic boundary (Figure 6.14). The pattern of current flow around the boundary in the left lateral region is different from that around the boundary in the septum. In the left lateral region, no current can flow out of the heart (in the torso, only a limited amount of current flows out of the heart because of the low

conductivity of its adjacent region, i.e. the left lung), thus the transmural current mainly flows through the left intracavitary blood, which produces a great potential difference across the ischaemic boundary on the epicardium and a small difference on the endocardium. For instance, a difference of 14.01mV appeared on the epicardium and 4.29mV on the endocardium over the lateral region of the left free wall in the 3D block model (Figure 6.12). However, for the ischaemic boundary in the septum, transmural current can flow through the blood in both the left and right cavities, giving rise to a small potential difference across the boundary on both sides, i.e. 3.86mV on the left side (z=1) and 3.81mV on the right side (z=2) in the 3D block model (Figure 6.11). As a result, there is a strong dipole pattern of ST changes on the epicardium in the left lateral region, with ST elevation on the ischaemic side and ST depression on the normal side of the ischaemic boundary. Meanwhile, the endocardial ST potential shows a similar pattern but with a lower amplitude (Figure 6.12). This pattern of ST potential distribution is in good agreement with epicardial and endocardial maps in sheep, in which a strong dipole of ST change appeared on the epicardium over the left lateral region, with ST depression on the non-ischaemic area and ST elevation on the ischaemic area, and a similar pattern on the endocardium with a much lower amplitude occurred during either LAD or LCX ligation [9, 21].

In the torso, current flows in a way similar to that in the isolated heart except for a small amount of current flowing out of the heart. The epicardial potential is reduced with its distribution pattern unchanged. For example, with the same ischaemic configuration for OM 1.28, the peak epicardial ST elevation was about 12mV in the isolated heart while it was reduced to about 7mV in the torso simulation. This tendency was clearly demonstrated in transmural ischaemia of a large region, with a dipole of $\pm$(6-7)mV on the epicardium in the isolated heart and of $\pm$(2-3)mV in the torso model. As confirmed by Green *et al.* [131], the amplitude of epicardial potentials from isolated dog hearts during the QRS was markedly higher when the heart was surrounded by an insulating medium, but potential patterns were less affected by the surrounding medium.

6.6.3 ST elevation distribution over ischaemic region

6.6.3.1 Epicardial ST elevation

The distribution of epicardial ST elevation over the ischaemic region varies with the size of the ischaemic region. ST elevation decreases towards the centre of the ischaemic region with its maximum on the ischaemic side of the ischaemic boundary. For transmural ischaemia of a small region such as the ischaemia produced by OM artery ligation, epicardial ST segment is almost uniformly elevated over the ischaemic region, with a uniformness factor of about 1 (Figures 6.4 & 6.6). As the size of the ischaemic region is increased, the uniformness factor decreases, namely ST elevation at the centre of ischaemia was smaller than that at the ischaemic boundary (Figure 6.5). For transmural ischaemia of a large region, such as ischaemia in the LAD or LCX territory, the uniformness was reduced to about 0.17 in both the 3D block and the isolated heart simulations (Figures 6.11 & 6.13). These results closely agree with the measurements in the studies in sheep by Li [21], in which simultaneous epicardial and endocardial ST mapping was performed during transmural ischaemia of various sizes. It was shown that the epicardium in small infarcts had uniform ST elevation over the infarcted region and little ST changes elsewhere, while with large infarcts there was a strong bipolar pattern between the infarcted region (ST elevation) and the normal myocardium (ST depression), with the extremes appearing on the ischaemic boundary over the left lateral region.

Transmural ischaemia of a small region tends to produce a uniform ST elevation on the epicardium over the ischaemic region. Transmural ischaemia produced by occluding the distal third of the LAD in baboons [7] showed a uniform ST elevation over the ischaemic region with a little ST depression over the adjacent normal area. Transmural ischaemia of a small region induced by occluding a diagonal branch of the LAD in baboons produced a localised ST elevation over the ischaemic region [145]. Kleber *et al.* [8] showed that a similar epicardial ST elevation pattern occurred over the ischaemic area with ST elevation at the boundary slightly greater than that over the central region; also there was little ST depression on the immediate normal area. However, there were reports that the higher ST segment elevation tended

to occur in the central region of ischaemia during transmural ischaemia of a small region [118, 114, 21]. This epicardial ST pattern could be explained by the polarised volume model of Smith *et al.* [119], who assumed that the severity of ischaemia was not uniform in the ischaemic region and increased towards the centre. Similar results were obtained in Tung's simulation using the bidomain model when the ischaemic boundary was assumed to be diffusive. However, a spatially linear change of severity will not produce a current source (equation 4.1). Moreover, if this severity gradient had existed in the ischaemic region, the epicardial ST potential patterns associated with large infarction [10, 114, 21] would not be explained. There are two possible reasons for this discrepancy. The distribution of ischaemic severity may vary with the size of ischaemia. A small region of ischaemia is produced by narrowing a branch of a major coronary artery, which may produce an ischaemic region with a diffusive ischaemic boundary [105]. The ligation of a major coronary artery may produce an ischaemic region with a sharp boundary [107, 102]. The effects of the myocardial anisotropy may also be responsible, as will be discussed in Chapter 7.

With an increase in size of the ischaemic region, there is an increase in the difference between ST elevation at the centre and that at the boundary. As shown in Figure 6.4, the uniformness factor decreases with an increase in size of the ischaemic region. A moderate region of transmural ischaemia induced by distal LCX occlusion in dogs [114] showed epicardial ST elevation on the ischaemic zone and ST depression on the non-ischaemic zone. The degrees of ST elevation and ST depression were prominent near the ischaemic border, that is, the epicardial ST elevation had the higher ST amplitude near the ischaemic boundary, decreasing gradually towards the centre of the ischaemic region.

The distribution of epicardial ST elevation is not an indicator of the ischaemic location for transmural ischaemia of a large size. As discussed above, ST elevation does not appear uniformly over the ischaemic region, instead it has a much lower amplitude at the centre than at the boundary. Some studies have provided evidence for the poor correlation between epicardial ST elevation with other ischaemic markers such as blood flow [12, 13]. Irvin and Cobb [13] reported a good correlation between the RMBF and the severity of myocardial infarction, while epicardial ST elevation

was not correlated with either of these two markers of ischaemia. In some studies, ST elevation did not appear over the infarcted region when the coronary artery was occluded more proximally [61, 10]. Li [21] found that the greatest epicardial ST elevation appeared on the lowest flow region in LAD or LCX infarction.

6.6.3.2 Endocardial ST elevation

Endocardial ST elevation shows a distribution pattern similar to that on the epicardium but with a less abrupt change at the ischaemic boundary. With a small size of transmural ischaemia, ST elevation had a monophasic distribution and no ST depression appeared on the normal side of the boundary (Figure 6.5.a). For transmural ischaemia of a large region, endocardial ST elevation showed a pattern similar to that on the epicardium except that the strong dipole of ST changes did not occur on the left lateral region (Figure 6.12), and the amplitude of ST elevation was much lower. This is consistent with the measurements from endocardial ST potential mapping with 40 electrodes during transmural ischaemia in either LAD or LCX territory in sheep by Li [21]. However, no endocardial measurement is available during transmural ischaemia of a small region.

6.6.3.3 Body surface ST elevation

ST elevation on the body surface indicates the underlying transmural ischaemia. The maximal ST elevation on the body surface appears over the portion of the torso facing the ischaemic region (Figures 6.10 & 6.15). In the torso, the current can flow out of the heart from the positive source to the negative source in the myocardium through other regions in the torso. This current flow gives rise to the maximal ST elevation at the centre of ischaemia on the torso surface. This pattern in transmural ischaemia of large region was well observed in the clinic [16, 136] and laboratory [60, 114]. Other computer simulations of transmural ischaemia shared the same conclusion [60, 70, 121].

ST elevation on the body surface indicates the general location of transmural ischaemia. However, some ST elevation on the body surface could also be seen during

subendocardial ischaemia (Figure 5.14). Therefore it is important to perform an inverse transformation to obtain the epicardial potentials to further identify the ischaemic type and location.

6.6.4 Amplitude of ST elevation and size of ischaemic region

6.6.4.1 Epicardial ST elevation

The amplitude of epicardial ST elevation decreases as the size of the ischaemic region increases. When the severity of ischaemia is constant, ST potentials decrease with the size of ischaemia (Figure 6.5); in particular, epicardial ST elevation at the centre of the ischaemic area was significantly reduced with an increase in size of the ischaemic region. For example, ST elevation at the centre was only 9.82mV for small region (OM 3.52) and 1.15mV for large region of ischaemia in the 3D block model, while ST elevation at the boundary was 11.97mV and 6.60mV respectively. Similar findings were made in animal studies on ST elevation at the ischaemic centre [10, 61].

However, experimental observations showed that transmural ischaemia of large regions were always associated with high amplitude epicardial ST elevation [104, 118, 119]. Although Smith *et al.* [119] explained these observations by the polarised volume model, the assumption of the diffusive distribution of the ischaemic severity in the ischaemic region was not confirmed by any measurements. Moreover the ischaemic severity in ischaemia of different sizes was not necessarily the same. Transmural ischaemia of a large region may be associated with more severe ischaemia. As shown in the sheep studies by Li [21], the OM ligation caused a reduction in flow to about 40% of the normal flow in the ischaemic region, while either LAD or LCX ligation caused a flow reduction to less than 20% of the normal flow in the ischaemic region at 20 minutes of ischaemia.

6.6.4.2 Body surface ST elevation

ST elevation on the body surface increases with the size of the ischaemic region. As shown in Figures 6.10 & 6.15, maximal ST elevation on the body surface was $8\mu V$ for OM 1.28, $15\mu V$ for OM 2.40 and about $300\mu V$ for either LAD or LCX ischaemia. The overall source intensity in ischaemia of a small region is less than that in transmural ischaemia of a large region, thus the current which can reach the torso surface is smaller during ischaemia of small regions than large regions. When the severity of ischaemia is constant, the maximal ST elevation on the body surface over the ischaemic region increases with an increase in size of the ischaemic region. The same conclusion was drawn using solid angle theory [61] and validated experimentally [114]. Thus ST elevation on the body surface is an indicator of transmural ischaemia for both the severity and the location.

6.6.5 ST depression in transmural ischaemia

6.6.5.1 Epicardial ST depression

Epicardial ST depression on the normal side of the ischaemic boundary increases with the size of the ischaemic region. For transmural ischaemia of small regions, little ST depression appeared on the normal side of the ischaemic boundary (Figure 6.5), while epicardial ST depression on the normal side became as strong as ST elevation on the ischaemic side of the ischaemic boundary in ischaemia in the LAD or LCX territory (Figures 6.11 & 6.13). The maximal ST depression was -1.10mV for small regions of ischaemia (OM 1.28) and -7.0mV for either the LAD or LCX ischaemia of large regions in the 3D block model. These ST changes formed a strong dipole of ST changes on the epicardium over the lateral region of the left ventricular free wall. Experimental studies also support this change of ST depression with the size of ischaemia. OM ligation in sheep produced a uniform ST elevation on the epicardium over the ischaemic region with little ST depression on the normal region [9]. Kleber *et al.* [8] showed a similar finding in transmural ischaemia of a small region in pigs. In transmural ischaemia produced by ligation of a branch of the LAD, ST depression

had a much lower amplitude than ST elevation [7]. A relatively lower amplitude of ST depression than that of ST elevation was observed in a middle size transmural ischaemia [114]. Li and co-workers [9] found that there was a strong dipole of ST changes on the epicardium over the left lateral region with ST depression occurring on the non-ischaemic region during either LAD or LCX total ligation in a sheep model. Therefore ST depression in transmural ischaemia is associated with the size of ischaemia and is thus a good indicator of the ischaemic size.

Epicardial ST depression is derived from the negative element of the current source and is thus an integral part of the current source associated with ischaemia of large sizes. Although Li [9] suggested that epicardial ST depression might have resulted from remote subendocardial ischaemia because of the reduction of blood flow to normal myocardium, no endocardial ST elevation was observed to support the suggestion.

6.6.5.2 Endocardial ST depression

Endocardial ST depression also appears over the normal region in transmural ischaemia of large regions. ST depression did not appear in ischaemia of small regions (Figure 6.5) but in ischaemia of large regions, ST depression was seen but had a much smaller amplitude than that on the epicardium (Figure 6.12). This lower amplitude of endocardial ST depression was confirmed by Li's study of either LAD or LCX transmural ischaemia [21]. However, no endocardial ST potential mapping during transmural ischaemia of a small region was available to compare with the simulated results. This endocardial ST depression over the normal region provided direct evidence to support the hypothesis that ST depression in transmural ischaemia was an integral part of the current source. As discussed above, although a reduction in blood flow was found in the non-infarcted region, no endocardial ST elevation was observed to confirm that subendocardial ischaemia was developed in the non-infarcted region [21].

6.6.5.3 Body surface ST depression

ST depression on the body surface is an integral part of the current source during transmural ischaemia. The distribution pattern of ST depression changes with the size of the ischaemic region. During transmural ischaemia of a small region, ST depression appears over the normal region adjacent to the ischaemic region. For instance, an OM ischaemia produced ST elevation over the left lateral region and ST depression over the anterior and posterior non-ischaemic regions (Figure 6.10). Because the current source was fairly close to the anterior surface, ST depression had a higher amplitude than that on the posterior torso surface, therefore a bipolar pattern of ST changes was formed in the lateral anterior region. Miller and Geselowitz [70] demonstrated similar results for transmural ischaemia located in the lateral wall of the left ventricle. They pointed out that the opposing maxima and minima in transmural ischaemia were not necessarily on opposite sides of the torso, and the exact locations of these maxima and minima were dependent on both the location of the injuries and their distance from the torso surface. However, transmural ischaemia of a large region showed ST depression appearing opposite the ST elevation sites which indicated the ischaemic location (Figure 6.15). A similar conclusion for LAD or LCX ischaemia was reached by a computer simulation in a detailed torso model [121]. This ST depression in transmural ischaemia of a large region was also confirmed experimentally [17, 136], where the myocardium facing precordial ST depression had no indication of being ischaemic on the basis of regional left ventricular wall motion. Therefore ST depression over the normal region in transmural ischaemia is a part of the current source.

6.6.6 Comparison with previous models

6.6.6.1 Solid angle model

As discussed in Section 5.5.7, solid angle theory is not valid for the near field. Using a constant potential difference to represent the cardiac source in ischaemia leads to a potential jump across the ischaemic boundary on the epicardium and the endo-

cardium. This abrupt change in potential appeared as maximal ST elevation and maximal ST depression in the model region. In transmural ischaemia, this potential jump would appear at the ischaemic boundary both on the epicardium and endocardium. Simulations in this study did not show this potential jump at the ischaemic boundary in either small or large regions of ischaemia. In particular, endocardial ST actually showed a monophasic distribution in small scale ischaemia (Figure 6.4). This is also confirmed by ST potential measurements [15, 114]. Regarding ST elevation on the body surface, the same conclusion was drawn as in the present study, that is, ST elevation on the body surface indicates the ischaemic region and its maximum appears at the centre of ischaemia.

6.6.6.2 Miller and Geselowitz's model

Miller and Geselowitz's model provides an excellent simulation of body surface potential using the bidomain model. In the model, the current source was calculated using the bidomain model [70]. The source for the extracellular potential was represented by the intracellular dipole moment density ($\vec{J}_i$), which in turn was derived from the first gradient of intracellular potentials (equation 6.1). However, it was not clear how to obtain the intracellular potentials from the known transmembrane potentials and activation times. In fact, transmembrane potentials were used in the place of intracellular potentials in the model, which happened to lead to an equation which resembled the governing equation (equation 6.2) in the bidomain model except for the different conductivity of the myocardium.

$$\sigma_e \nabla^2 \Phi_e = \nabla \cdot \vec{J}_i = -\sigma_i \nabla^2 \Phi_i \tag{6.1}$$

$$\sigma \nabla^2 \Phi_e = -\sigma_i \nabla^2 \Phi_m \tag{6.2}$$

In their model, ischaemia in three locations (anterior, lateral and inferior walls of the left ventricle) were simulated. Their calculated ST potentials on the body surface matched with clinical observations, i.e. a maximal ST elevation appeared on the torso facing the ischaemic region. Their results were similar to those obtained in this study, especially for OM transmural ischaemia (equivalent to the lateral ischaemia). Although a detailed heart geometry was used in their simulation, no

torso inhomogeneity was considered. No comparison was made between ischaemia of different sizes. No epicardial or endocardial potentials were available to further compare with experimental epicardial and endocardial ST recordings.

6.6.6.3 Tung's model

Tung's model only provides a basic information of ST segment changes in transmural ischaemia. Tung employed the same equation as used in the present study to simulate DC potentials in ischaemia, i.e. the ischaemic current source was expressed as current density per volume, which was derived from the spatial gradient of transmembrane potentials. Thus the monophasic endocardial TQ potential distribution was reported in the simulation of transmural ischaemia. However, an over-simplified heart model was used, which represented the heart by a sphere of a certain thickness. The right ventricle was ignored in his study. Also the heart model was placed in a semi-infinite media. Only one size of transmural ischaemia was simulated, which represented a typical medium size of transmural ischaemia located in the left free wall. Hence transmural ischaemic zones with abrupt borders would yield a decreasing epicardial potential towards the centre of the zone; the epicardial potential distribution would be biphasic with reversal in polarity at the border. Meanwhile, endocardial TQ potential showed a monophasic distribution with a much lower amplitude than epicardial potentials. No simulation was performed to address ST potentials on the body surface.

6.6.7 Clinical implications

Epicardial ST potential pattern is more reliable than its amplitude to indicate the location of ischaemia, and epicardial ST depression is a good indicator of the size of ischaemia. Uniform epicardial ST elevation with little surrounding ST depression localises the underlying transmural ischaemia of a small region. A strong dipole of ST changes on the left lateral region indicates transmural ischaemia of a large region in the left ventricle with ST elevation on the ischaemic side, and ST depression on the normal side of the boundary and an additional boundary in the septum. ST

depression during acute myocardial infarction is an integral part of the current source rather than from a remote subendocardial ischaemia.

6.6.8 Limitations

As shown in Figure 6.3, the boundary between the ischaemic region at the left ventricular wall and the normal region at the right ventricle in ischaemia in either the LAD or LCX territory was ignored in this study. No estimation could be made because there was no information available about this boundary. In addition, simulation of ischaemia in the territory of the right coronary artery territory was not performed because no measured data were available to confirm the ischaemic region.

Chapter 7

Effects of myocardial anisotropy

7.1 Introduction

Myocardial anisotropy is one of the most important characteristics of the heart muscle. The influence of myocardial anisotropy on excitation wavefront and extracellular potentials during ectopic stimulation has been widely studied by using the bidomain model [86, 65, 35]. These simulations were generally carried out in a 3D block model. It was found that myocardial anisotropy did affect the excitation wavefront and potential distribution patterns on the endocardium and the epicardium. Some investigators employing a detailed realistically shaped 3D heart model suggested that myocardial anisotropy of conduction velocity and intracellular conductivity did not change body surface ECGs significantly [87]. Other studies indicated that simulation of normal activation and transmural ischaemia matched well with the observations when myocardial anisotropy was taken into account [88, 121]. However no comparison with a simulation of the isotropic conductivity was made to enable a conclusion to be drawn as to the effects of anisotropy.

This chapter presents results from simulation of ischaemia in various locations when myocardial anisotropy is taken into account to study the effects of anisotropy on ST potential distribution. As shown in equation (4.1), myocardial anisotropy affects the potential distribution in two aspects: the source and the conductivity of a part of the volume conductor. These two aspects were studied separately. Subendocardial

ischaemia from two different arterial territories (LAD and LCX) were simulated. Transmural ischaemia of a small region in OM territory and transmural ischaemia of large regions in either LAD or LCX territory were also simulated.

7.2 Myocardial anisotropy

As defined in Section 4.3.4.1, the longitudinal direction is parallel to the fibre axes (x axis) and the transverse direction (y and z axes) transverse to the fibre axes. The following four different combinations of the intracellular (σ_i) and the bulk myocardial (σ) conductivities were used in the simulation. The following conductivity values are in units of Siemens per meter (S/m).

1. Isotropic σ_i, isotropic σ:

$$\sigma_i = 0.174, \quad \sigma = 0.236$$

2. Isotropic σ_i, anisotropic σ:

$$\sigma_i = 0.174, \quad \sigma = \begin{pmatrix} 0.236 & 0 & 0 \\ 0 & 0.0429 & 0 \\ 0 & 0 & 0.0429 \end{pmatrix}$$

3. Anisotropic σ_i, isotropic σ:

$$\sigma_i = \begin{pmatrix} 0.174 & 0 & 0 \\ 0 & 0.0193 & 0 \\ 0 & 0 & 0.0193 \end{pmatrix}, \quad \sigma = 0.236$$

4. Anisotropic σ_i, anisotropic σ:

$$\sigma_i = \begin{pmatrix} 0.174 & 0 & 0 \\ 0 & 0.0193 & 0 \\ 0 & 0 & 0.0193 \end{pmatrix}, \quad \sigma = \begin{pmatrix} 0.236 & 0 & 0 \\ 0 & 0.0429 & 0 \\ 0 & 0 & 0.0429 \end{pmatrix}$$

With the above values of the anisotropic intracellular conductivity (σ_i), the ratio of the longitudinal to the transverse conductivity (σ_{il}/σ_{it}) is about 9. As a result, the

source density at the longitudinal direction should be 9 times that in the transverse direction for an anisotropic σ_i. The corresponding sources were calculated in the following way:

To be compatible with the source densities used in the simulation with the isotropic intracellular conductivity: σ_i=0.174S/m, $\sigma_i \nabla^2 \Phi_m = \pm 1.0 \mu A/mm^3$, the source at the longitudinal ischaemic boundary which is perpendicular to the x axis ($\sigma_{il} \nabla^2 \Phi_m$) would have a density of about $\pm 1.0 \mu A/mm^3$ and the source at transverse ischaemic boundary which is perpendicular to the y or z axes ($\sigma_{it} \nabla^2 \Phi_m$) would be $\pm 0.111 \mu A/mm^3$.

The effect of bulk myocardial conductivity (σ) on ST potential distribution was studied by assigning the anisotropic conductivity to the myocardium.

7.3 Simulations

In this chapter, all simulations were carried out in the 3D block model representing the isolated heart. The details of the 3D block model were described in Section 4.2.1.

7.3.1 Subendocardial ischaemia

Subendocardial ischaemia in either the LAD or LCX territory was simulated. The details of the ischaemic configuration and the model geometry were described in Section 5.2.1. The following four simulations with different myocardial conductivities were performed.

7.3.1.1 Isotropic σ_i, isotropic σ

As discussed in Section 5.2.1.1, when the intracellular myocardial conductivity (σ_i) was assumed to be isotropic, the positive source had a density of 1.0 $\mu A/mm^3$ and the negative source -0.913 $\mu A/mm^3$. The value of isotropic conductivity of σ=0.236 was assigned to the myocardium.

7.3.1.2 Isotropic σ_i, anisotropic σ

The same source densities as the above (section 7.3.1.1) were used, and the myocardium had the anisotropic conductivity of σ_{xx}=0.236, σ_{yy}=σ_{zz}=0.0429.

7.3.1.3 Anisotropic σ_i, isotropic σ

The sources at the lateral boundary had the densities of $\pm 1.0 \mu A/mm^3$ and those at the transverse boundary $\pm 0.111 \mu A/mm^3$. The isotropic conductivity σ=0.236 was assigned to the myocardium.

7.3.1.4 Anisotropic σ_i, anisotropic σ

The same source densities as the above (Section 7.3.1.3) were used, and the anisotropic conductivity of σ_{xx}=0.236, σ_{yy}=σ_{zz}=0.0429 was assigned to the myocardium.

7.3.2 Transmural ischaemia of a small region

Transmural ischaemia of a small region was considered, which was located in the OM artery supplied territory and had a volume of $1.28 cm^3$ (OM 1.28). The detailed description of OM transmural modelling in the 3D block was discussed in Section 6.2.1.

7.3.2.1 Isotropic σ_i, isotropic σ

As discussed in Section 6.2.1, the current densities were $1.0 \mu A/mm^3$ for the positive source and -$0.75 \mu A/mm^3$ for the negative source. The myocardium had an isotropic conductivity of σ=0.236.

7.3.2.2 Isotropic σ_i, anisotropic σ

The same source densities as above (Section 7.3.2.1) were used, and the myocardium was assumed to have an anisotropic conductivity of σ_{xx}=0.236, σ_{yy}=σ_{zz}=0.0429.

7.3.2.3 Anisotropic σ_i, isotropic σ

In this section, the source densities at the longitudinal boundary were in the order of $\pm 1.0 \mu A/mm^3$ while the source densities at the transverse boundary were in the order of $\pm 0.111 \mu A/mm^3$. The myocardium had an isotropic conductivity of σ = 0.236.

7.3.2.4 Anisotropic σ_i, anisotropic σ

The same source densities as in Section 7.3.2.3 were used, and the anisotropic conductivity of σ_{xx}=0.236, σ_{yy}=σ_{zz}=0.0429 was assigned to the myocardium.

7.3.3 Transmural ischaemia of a large region

Transmural ischaemia of a large region was simulated, in which the ischaemic region was located in either the LAD or the LCX territory. The details of the 3D block model for transmural ischaemia of a large region were described in Section 6.3.1. As there are only longitudinal boundaries in ischaemia of a large region, the source is proportional to the longitudinal intracellular conductivity. Furthermore, the governing equation (equation 4.1) is a linear equation at a constant myocardial conductivity, thus the ST potentials are proportional to the longitudinal σ_{il}. Therefore only the following two simulations were performed to study the effects of the anisotropic property of the myocardium, a part of the volume conductor.

7.3.3.1 Isotropic σ_i, isotropic σ

As discussed in Section 6.3.1, the source densities were $\pm 1.0 \mu A/mm^3$. The myocardium had an isotropic conductivity of σ=0.236.

7.3.3.2 Isotropic σ_i, anisotropic σ

The same source densities as above (Section 7.3.3.1) were used, and the myocardium was assumed to have an anisotropic conductivity of σ_{xx}=0.236, σ_{yy}=σ_{zz}=0.0429.

7.4 FIDAP solution

After the source densities were assigned to the corresponding elements, the governing equation was solved by the finite element method package FIDAP. The details of solving the equation were described in Section 4.4. Displays of the simulated data were provided in Section 4.5.

7.5 Results

7.5.1 Subendocardial ischaemia

The simulated ST potentials in subendocardial ischaemia are shown in Figures 7.1 & 7.2. For isotropic σ_i and σ, ST depression mainly appeared over the left free wall on the epicardium, with the maximal ST depression of about -10mV at the ischaemic boundary (x=4.0cm). On the endocardium, ST elevation appeared over the ischaemic region with the maximal ST elevation (16mV) at the centre of the ischaemic region (x=0, y=0). This pattern was further shown in Figure 7.3. On the cross section of the left ventricle (y=0), ST depression mainly occurred in the normal region where the lateral and transmural boundaries meet, while ST elevation occurred at the ischaemic endocardium. The anisotropic conductivity of the myocardium (σ), as the conductive property of a part of the volume conductor, in-

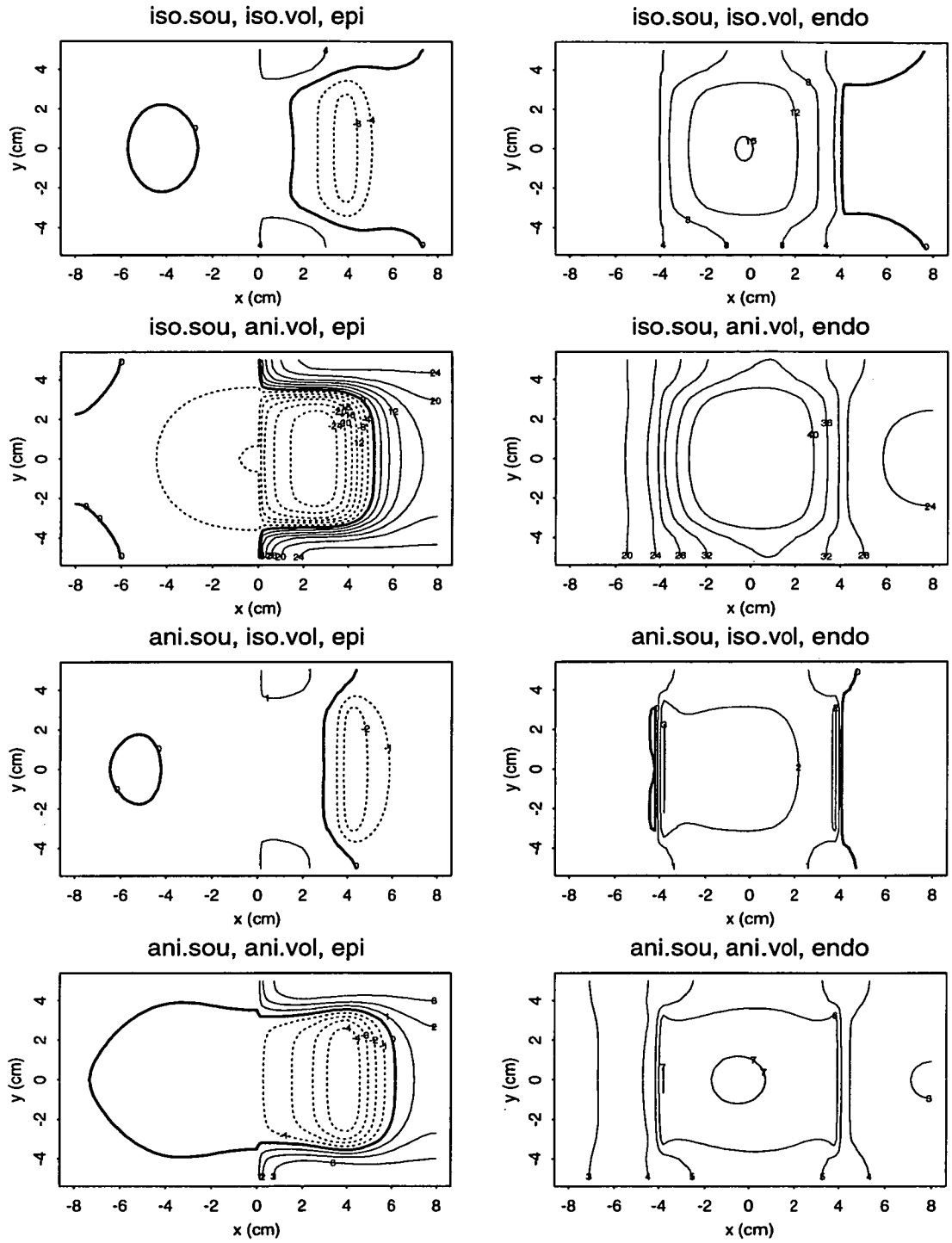

Figure 7.1: *Epicardial (left) and endocardial (right) ST potentials in simulations of endocardial ischaemia with anisotropic myocardial conductivities. Iso.sou indicates that the isotropic σ_i is used to calculate the source and ani.sou the anisotropic σ_i. Iso.vol indicates that the isotropic σ is used for the myocardium as a part of the volume conductor and ani.vol the anisotropic σ. The contour interval is 4mV in the top four plots and 1mV in the bottom four plots.*

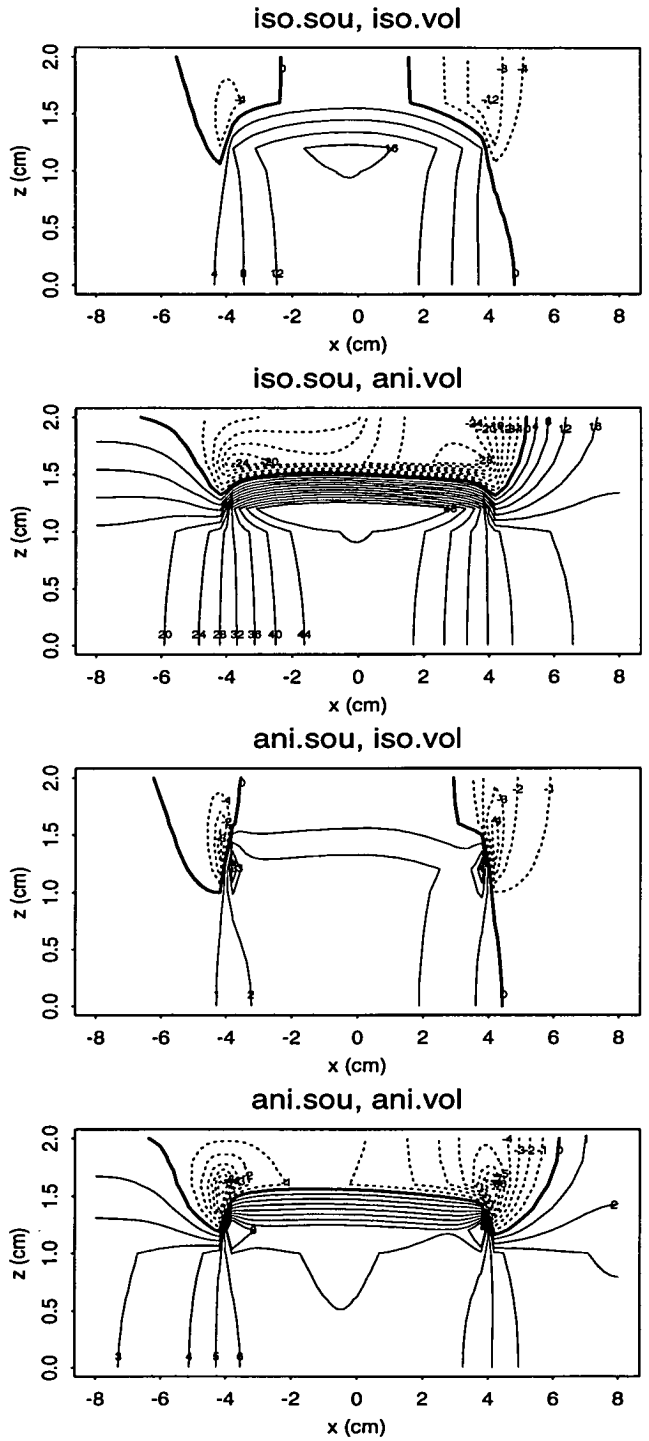

Figure 7.2: *ST potentials on a cross section of the heart (y=0) in simulations of subendocardial ischaemia with anisotropic myocardial conductivities. Iso.sou indicates that the isotropic σ_i is used to calculate the source and ani.sou the anisotropic σ_i. Iso.vol indicates that the isotropic σ is used for the myocardium as a part of the volume conductor and ani.vol the anisotropic σ. The contour interval is 4mV in the top two panels and 1mV in the bottom two panels.*

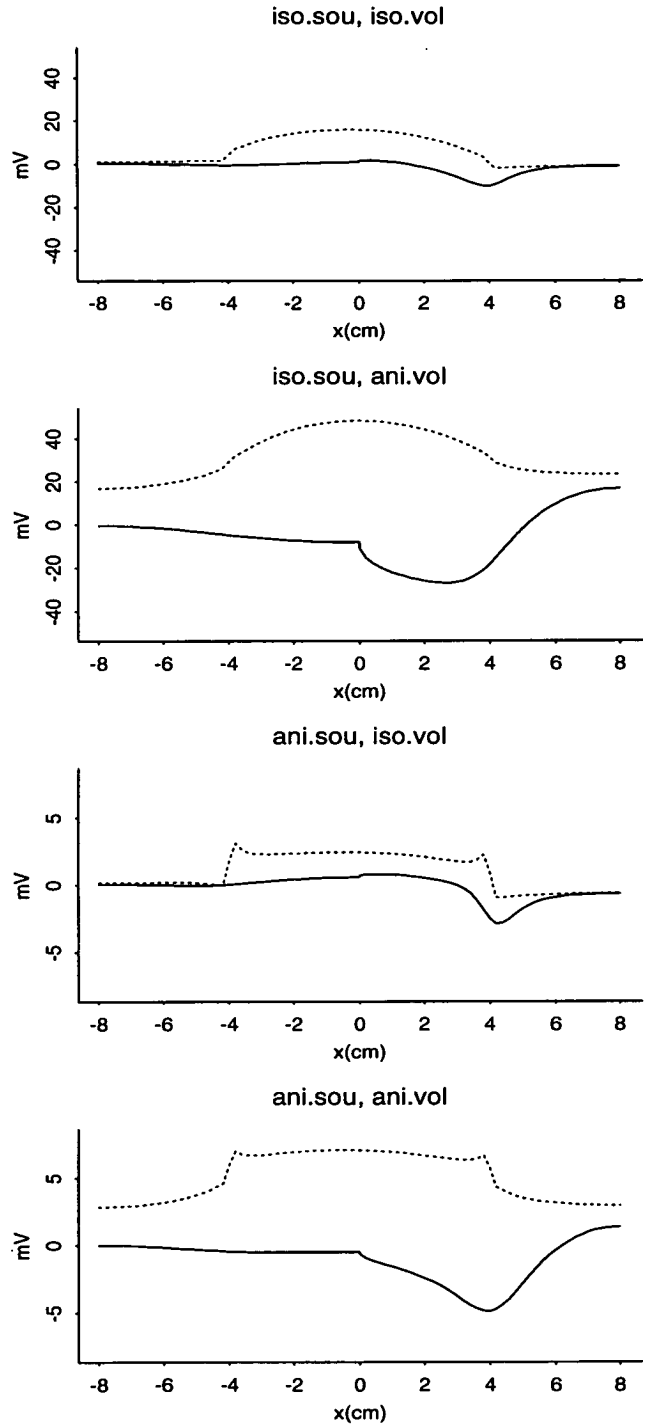

Figure 7.3: *ST potentials along the x axis on the epicardium (solid line) and the endocardium (dashed line) in simulations of subendocardial ischaemia with anisotropic myocardial conductivities. Iso.sou indicates that the isotropic σ_i is used to calculate the source and ani.sou the anisotropic σ_i. Iso.vol indicates that the isotropic σ is used for the myocardium as a part of the volume conductor and ani.vol the anisotropic σ.*

creased the amplitude of ST potentials and changed their distribution patterns. The amplitude of ST potentials on the epicardium was increased by more than 100% and the same increase occurred to ST potentials on the endocardium. ST depression on the epicardium became more spread and the position of its maximum was shifted towards the centre of the ischaemic region.

When the anisotropic intracellular conductivity was taken into account for the source calculation, the ST potential patterns were similar to that with isotropic σ_i, with ST depression maximum of -2.90mV shifted slightly towards the normal side of the lateral ischaemic boundary. The amplitude of ST potentials could not be directly compared with that in the simulation with the isotropic σ_i because the isotropic σ_i was assumed to be the same as the longitudinal conductivity. However, if the transverse conductivity was assumed to be the same as the isotropic value used in the simulation of isotropic σ_i, the source would be 9 times that used in the simulation of the anisotropic σ_i (ani σ_i), thus the potentials would be also 9 times. The maximal ST depression on the epicardium would be about -26mV, compared with -10mV for the isotropic σ_i. Furthermore, when the anisotropy was considered in both the source and the volume conductor, maximal ST depression appeared over the left lateral region and spread over the left ventricular wall on the epicardium, while ST elevation appeared on the left ventricular endocardium with higher amplitude covering the ischaemic region. Similarly the anisotropic σ dramatically increased the potential amplitude by nearly 100%. These pattern changes are clearly shown in Figure 7.3.

7.5.2 Transmural ischaemia of a small region

The ST potential distribution in simulation of OM transmural ischaemia is shown in Figures 7.4 & 7.5. As discussed in Section 6.5.1.1, when σ_i and σ were isotropic, a localised ST elevation appeared over the ischaemic region on both the epicardium (11-12mV) and the endocardium (3-4mV), while ST depression surrounding the ischaemic region had an amplitude of -1 to -2mV on the epicardium and -0.05mV on the endocardium. The anisotropic σ affected epicardial ST elevation significantly,

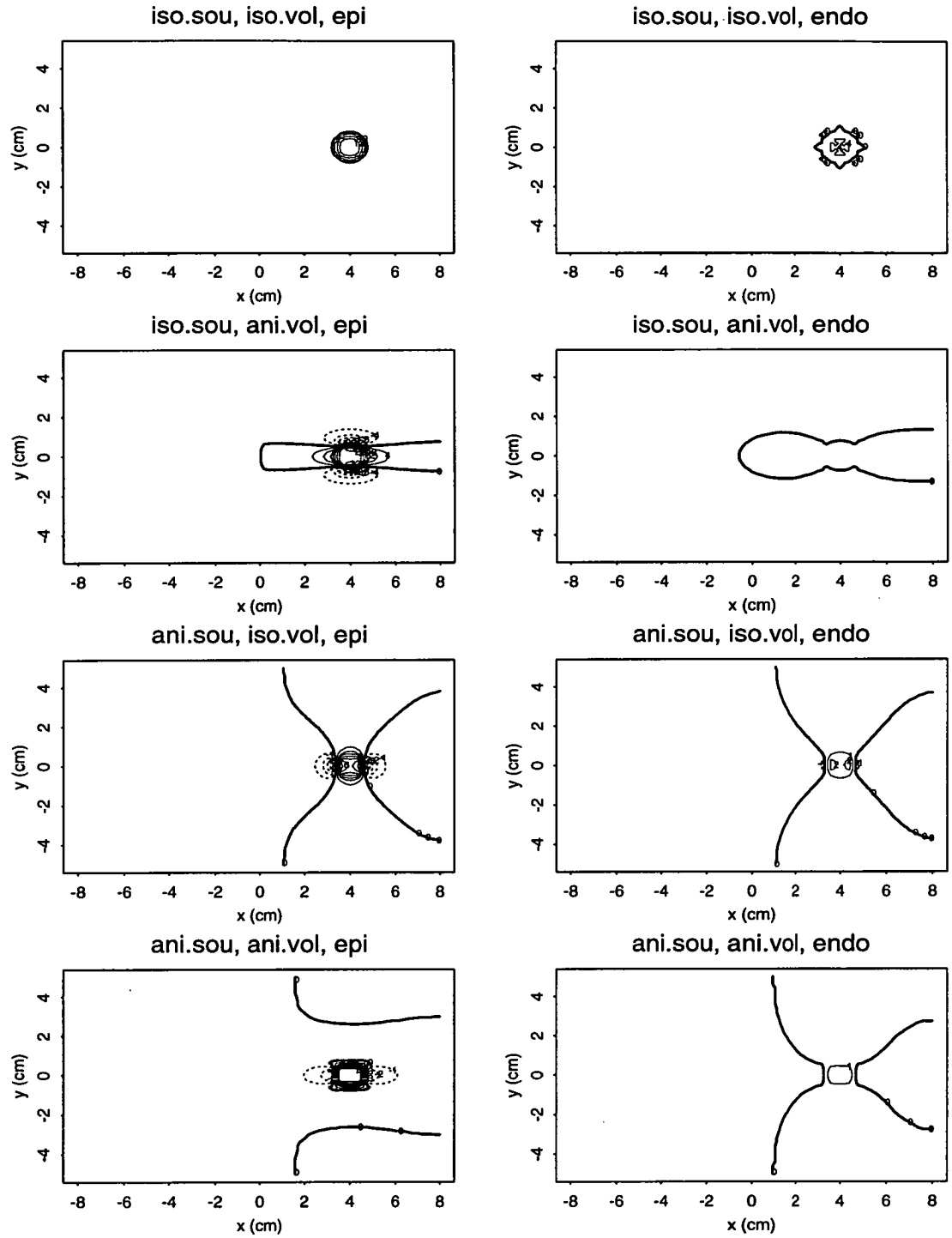

Figure 7.4: *Epicardial (left) and endocardial (right) ST potentials in simulation of OM transmural ischaemia with anisotropic myocardial conductivities. Iso.sou indicates that the isotropic σ_i is used to calculate the source and ani.sou the anisotropic σ_i. Iso.vol indicates that the isotropic σ is used for the myocardium as a part of the volume conductor and ani.vol the anisotropic σ. The contour interval is 4mV in the top four panels and 1mV in the bottom four panels.*

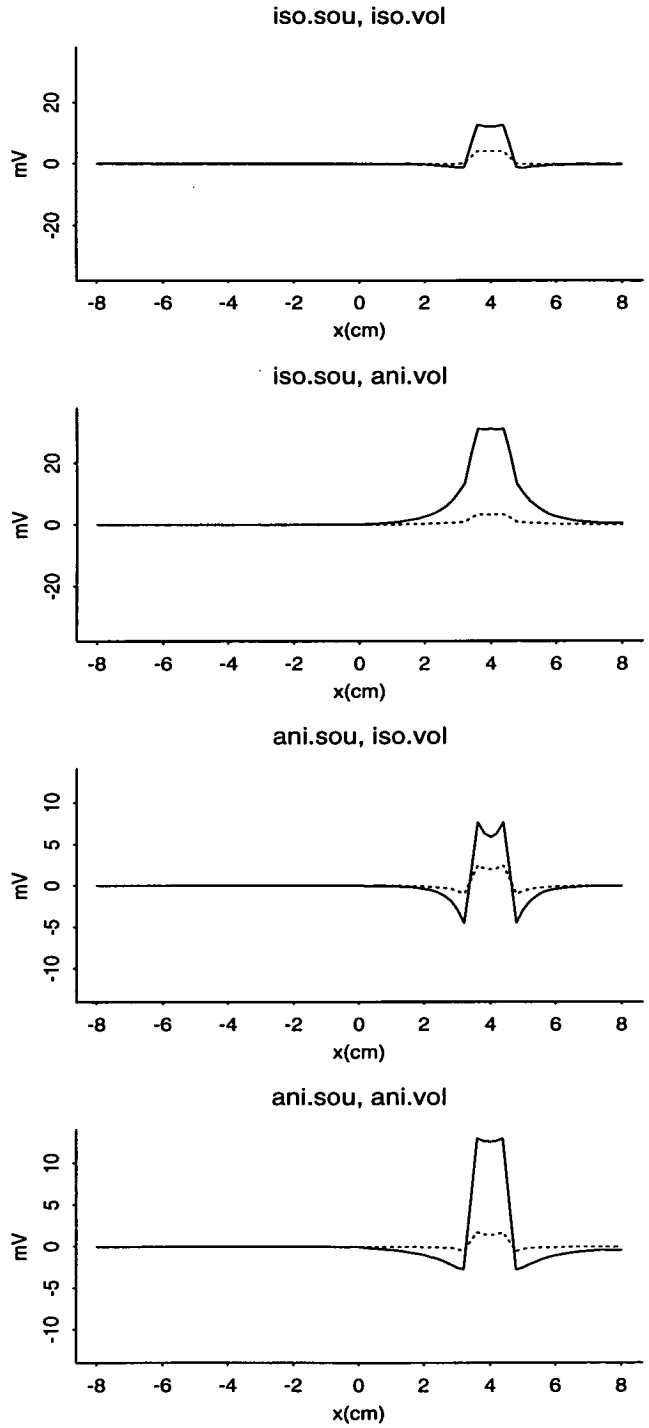

Figure 7.5: *ST potentials along a circumferential direction (x axis) on the epicardium (solid line) and the endocardium (dashed line) in simulation of OM transmural ischaemia with anisotropic myocardial conductivities. Iso.sou represents the isotropic σ_i used to calculate the source and ani.sou for anisotropic σ_i. Iso.vol represents an isotropic σ used for the myocardium as a part of the volume conductor and ani.vol for anisotropic σ.*

increasing its amplitude by nearly 200% (33-34mV maximum) and making ST elevation spread along the longitudinal direction. Meanwhile epicardial ST depression appeared on the normal side of the transverse boundary, with a maximal ST depression of about -18mV. The anisotropic σ did not greatly affect endocardial ST potentials, only slightly decreasing its amplitude.

When the anisotropic σ_i was taken into account, epicardial ST elevation (6-7mV) still appeared over the ischaemic region while ST depression occurred on the normal side of the longitudinal boundary, with an amplitude of -4 to -5mV. Endocardial ST potentials showed a similar distribution but a lower amplitude, with the extremes of -1.06mV for ST depression and 2.33mV for ST elevation. Furthermore, when the anisotropic σ was also taken into account, epicardial ST elevation was increased to 12-13mV over the ischaemic region, while the amplitude of epicardial ST depression was reduced to about -2 to -3mV. On the endocardium, the amplitudes of both ST elevation and ST depression were reduced, with the extremes of -0.55mV for ST depression and 1.70mV for ST elevation.

7.5.3 Transmural ischaemia of a large region

ST potentials in the simulation of transmural ischaemia of a large region are shown in Figures 7.6 & 7.7. As discussed in Section 6.5.2.1, a dipole pattern of ST changes appeared over the ischaemic boundary in the left ventricular wall on both the epicardium and the endocardium when both σ_i and σ were isotropic. The dipole of ST changes on the epicardium was in the range of $\pm$(7-8)mV while the dipole on the endocardium was in the range of $\pm$(2-3)mV. The anisotropic σ increased the potential amplitude and made the dipole more spread on the epicardium (Figure 7.7), but did not change the potential distribution patterns. The amplitude of the maximal epicardial ST changes was increased by 12.5% and its dipole pattern on the epicardium was extended to the whole left ventricular wall. However, the endocardial ST potentials were not greatly affected by the anisotropy (Figure 7.7).

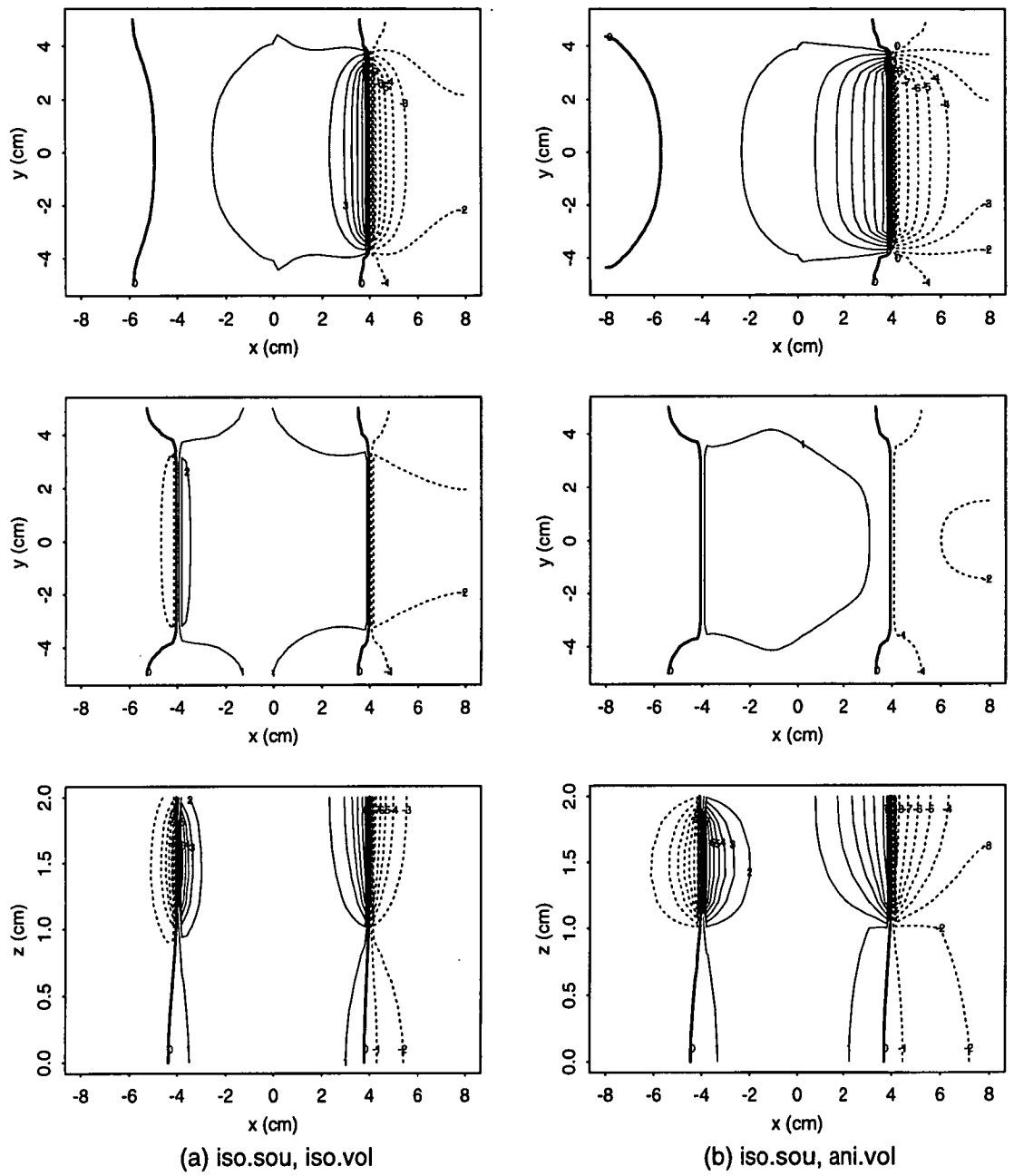

Figure 7.6: *ST potentials on the epicardium (top), the endocardium (middle) and a cross section of the heart (bottom) in simulations of transmural ischaemia of large regions with anisotropic myocardial conductivities. Diagram (a) represents the simulation with the isotropic σ_i for the source and the isotropic σ for the volume conductor. Diagram (b) represents the simulation with the isotropic σ_i for the source and the anisotropic σ for the volume conductor. The contour interval is 1mV.*

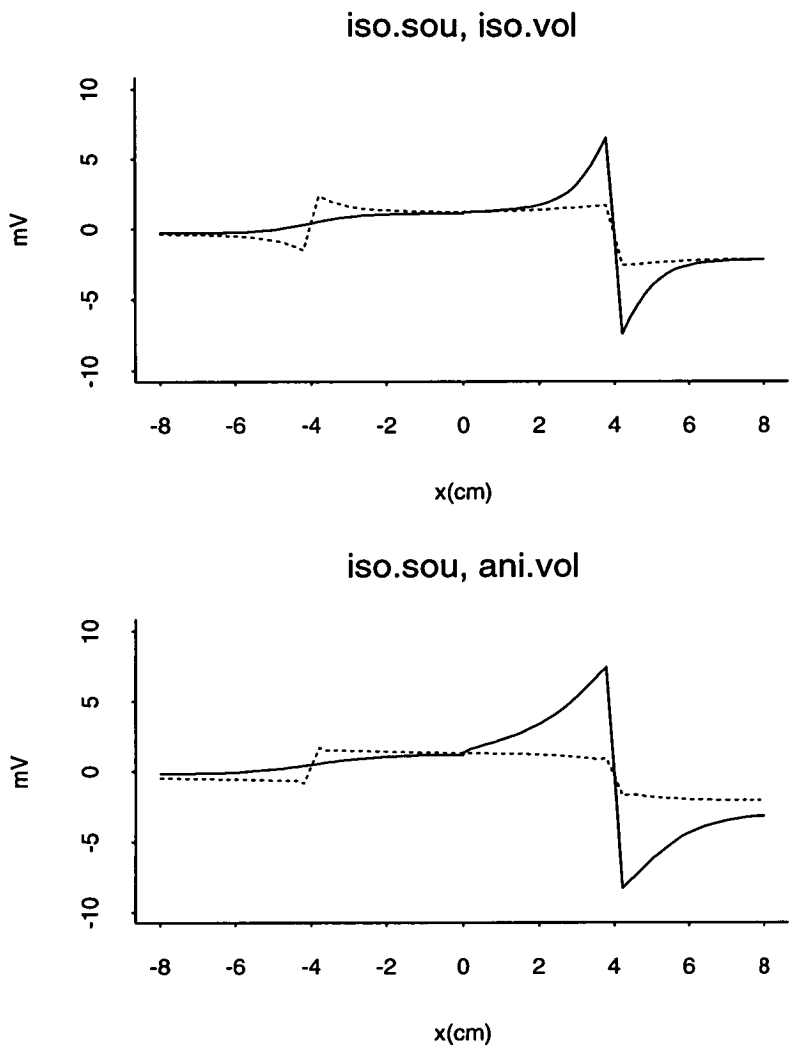

Figure 7.7: *ST potentials on a line crossing the ischaemic region in simulation of transmural ischaemia of a large region with anisotropic myocardial conductivities. Top diagram represents the simulation with the isotropic σ_i and the isotropic σ, with solid line representing epicardial potentials and dashed line endocardial potentials. Bottom diagram represents the simulation with the isotropic σ_i and the anisotropic σ, with solid line representing epicardial potentials and dashed line endocardial potentials.*

7.6 Discussion

7.6.1 Current source

7.6.1.1 Subendocardial ischaemia

Myocardial anisotropy enhances the epicardial ST depression over the lateral region of the left free wall. In the bidomain model, the cardiac source in ischaemia is proportional to σ_i when σ_i is constant. In subendocardial ischaemia, the lateral ischaemic boundary is perpendicular to the longitudinal direction of the fibres while the transmural ischaemic boundary is perpendicular to the transverse direction. When σ_i was assumed to be isotropic, the source was uniformly distributed at the ischaemic boundary and ST depression appeared over the non-ischaemic region where the lateral and transmural boundaries met (Figure 7.2). For an anisotropic σ_i, the ratio of the longitudinal to the transverse conductivities in the intracellular space is generally greater than one [77]. The density of current source produced at the lateral boundary is greater than that produced at the transmural boundary. Thus ST depression is enhanced in the non-ischaemic region of the lateral boundary. Consequently ST depression over the left region on the epicardium is increased. Although the fibre rotation is ignored, this effect of anisotropic σ_i on the source during subendocardial ischaemia is considered to be acceptable because the middle layer of the myocardial muscle, where most of the current source is generated, has the fibre orientation as assumed in the present study [76].

Although Plonsey and Barr [86] did not study the effect of myocardial anisotropy on the ST potential, they showed that the computed results from anisotropic myocardium were in conflict with many reports which assumed isotropic conductivity, and that the current flow patterns in the wavefront were complicated and dependent on the values of myocardial anisotropy.

7.6.1.2 Transmural ischaemia of a small region

Myocardial anisotropy increases the longitudinal source density and then causes an inequality of ST changes around the ischaemic boundary. In a simplified assumption, the ischaemic boundary for transmural ischaemia of a small region has both the longitudinal and transverse aspects. As discussed in Section 6.6.1, when σ_i was isotropic, the current sources were uniformly distributed at the ischaemic boundary with the density of the positive source larger than that of the negative source. Therefore localised ST elevation appeared over the ischaemic region with little ST depression over the adjacent non-ischaemic region. The anisotropic σ_i causes the source originating at the longitudinal boundary to be much intensive than that at the transverse boundary, which in turn increases ST potential at the longitudinal boundary. As shown in Figure 7.4, epicardial ST depression appeared on the non-ischaemic side of the longitudinal boundary, but not of the transverse boundary. This effect of σ_i may not be observed because of the fibre rotation across the ventricular wall [76].

7.6.1.3 Transmural ischaemia of a large region

Under the simplified assumption of no fibre rotation, there is only a longitudinal ischaemic boundary perpendicular to the endocardium in transmural ischaemia of large regions, thus the source is proportional to the longitudinal conductivity (σ_{il}). Therefore the amplitude of ST potentials would increase. However, when the fibre rotation is taken into account, the ischaemic boundary is not necessarily perpendicular to the fibre direction. Particularly the boundary at the subepicardium and subendocardium is actually parallel to the fibre direction [76]. Thus the intracellular anisotropy may not dramatically increase the source in transmural ischaemia. As shown in the study of Wei *et al.* [87], there was no significant differences in global excitation sequences of the heart and body surface ECGs when only the intracellular anisotropy was considered. They suggested that two reasons may be responsible: firstly, the function of the Purkinje fibres which were assumed to be isotropic in their study, and secondly the rotation of the fibre orientation which was assumed

to be about 90^o between the epicardium and the endocardium. This rotation may cause the effect of anisotropy to be averaged to some extent, thus the anisotropic heart model behaved isotropically as a whole.

7.6.2 Volume conductor

7.6.2.1 Subendocardial ischaemia

The electrical conductivity of the myocardium, which is a part of the volume conductor, affects the potential distribution when the source is constant. It increases the amplitude and spreads the distribution of epicardial ST depression. When the conductivity is isotropic, the current flows equally in all directions. However, when the conductivity is anisotropic with the longitudinal value much greater than the transverse value, the current flows more easily along the longitudinal than the transverse direction. As a result, the potential difference in the transverse direction is greater than that in the longitudinal direction. This effect was shown in the simulation in which the amplitude of ST potentials on either the epicardium or the endocardium was increased and the ST potentials along the longitudinal direction changed less rapidly (Figure 7.3). Also the spread of ST depression on the epicardium can be explained by the greater longitudinal conductivity. As discussed in Section 5.5.1, this wide spread of ST depression on the left lateral region matched well with the measured epicardial ST depression during subendocardial ischaemia in sheep [21].

7.6.2.2 Transmural ischaemia of a small region

In transmural ischaemia of a small region, the anisotropic σ increases epicardial and endocardial ST potentials when the source is uniform at the ischaemic boundary. ST depression at the non-ischaemic side of the longitudinal boundary disappears because of the high longitudinal conductivity, meanwhile the low transverse σ increases ST depression in the transverse direction (Figure 7.4). When the anisotropic σ_i is taken into account, the effect of σ was similar, i.e. epicardial ST elevation is increased by nearly 50% and ST depression at the longitudinal boundary is reduced. The

endocardial ST potential is also affected in the same way.

7.6.2.3 Transmural ischaemia of a large region

The anisotropic σ affects the potential distribution in the same way as that in subendocardial ischaemia (Section 7.6.2.1). The anisotropic σ increases the amplitude of ST potentials on the epicardium and makes ST changes spread over the left ventricular wall with ST depression on the non-ischaemic region and ST elevation on the ischaemic region (Figure 7.6). This wide spreading of ST changes over the left ventricular wall is in good agreement with the observation by Li [21]. However, endocardial potentials are not markedly affected by the anisotropic σ.

As shown in other studies [86, 65, 35], myocardial anisotropy affects the wavefront and the epicardial potential distribution during the heart activation, although the effects of σ_i and σ are not studied separately. The simulation in this study supports this view. Although Dube *et al.* [121] did not compare the difference between the isotropy and the anisotropy, their study of ST potentials on the body surface in PTCA with the anisotropy correlated well with the observations when the source was derived from an isotropic intracellular conductivity. As shown in this study, the extracellular anisotropy affects the potential distribution significantly as it represents the conductive property of a part of the volume conductor. The influence of anisotropy on the epicardial potentials is very important for the inverse transformation of ECGs to provide an accurate diagnostic basis. Therefore anisotropy must be taken into account for the epicardial potentials in the forward problem of electrocardiology.

7.6.3 Conclusions

The classic models, such as the dipole, multiple dipoles and solid angle models, are based on the assumption that the myocardium is isotropic and therefore can not predict the effects of anisotropy. The bidomain model can take the realistic factors of the heart into account, such as the anisotropic conductivity, the finite space and

the inhomogeneity. The simulated epicardial potentials with anisotropy are closer to Li's observations [21], therefore it is important to include myocardial anisotropy in the ECG modelling.

7.6.4 Limitations

The fibre rotation was ignored in this study to simplify the computations. When the fibre rotation is considered, it will increase the difficulty not only in calculating the source, but also in solving the equation. Although the simulation with anisotropy was not carried out in a realistic heart model, the results obtained in the 3D block model were acceptable to represent the basic features of the effect of anisotropy on ST changes in ischaemia because they were indeed closer to Li's observations [21]. In addition, the effect of anisotropy on the body surface ECGs has not been performed in this study because of the computation difficulty in including the anisotropic property in the equation.

Chapter 8

Conclusions

8.1 General Conclusions

The aim of this thesis was to establish a computer model of electrocardiographic ST segment shift during ischaemia to explain ST changes with both subendocardial an full thickness ischaemia and to establish the relationship between the 3D ST potential and the underlying ischaemia.

8.1.1 Subendocardial ischaemia

The current source in the myocardium was established by giving ischaemic cells an altered transmembrane potential. This resulted in a region of ischemia which was positive compared to normal muscle during the ST segment. The effect of this source in the 3D heart is to cause ST depression on the epicardium located over the lateral ischaemic boundary, normal to the endocardium. At the transmural boundary between normal and ischaemic muscle, parallel to the endocardium, the current flow is highly localised and is not seen on the epicardium. On the endocardium ST elevation is seen over the ischaemic region. Because the LAD and LCX territories share the same lateral boundary at the left free wall and at the septum, a similar epicardial ST depression pattern appears over the left lateral region with ischaemia in either territory. The source at the septum does not give rise to ST depression

on the epicardium because it is surrounded by the highly conductive intracavitary blood. These results explain why ST depression is a poor locator of subendocardial ischaemia. Clinically the spatial and temporal gradients of the ST segment may help to differentiate the ischaemic source.

The bidomain model reproduces clinical and experimental observations satisfactorily for subendocardial ischaemia.

8.1.2 Transmural ischaemia

The results of full thickness ischaemia in three locations, the OM, LAD and LCX, were compared. The ischaemic region located in the OM territory only occupies a small volume of the ventricle, and results in a localised and almost uniform ST elevation on both the myocardium and the endocardium over the ischaemic region with little ST depression elsewhere. With increased ischaemic size, the epicardial ST elevation at the boundary becomes larger than that at the centre of the ischaemic region, and ST depression on the immediate non-ischaemic region is enhanced. Because the endocardium comes into direct contact with the intracavitary blood, a large amount of current flows through the cavity and produces a lower amplitude of endocardial ST elevation. On the body surface, ST elevation appears over the portion of the torso facing the ischaemic region with its maximum appearing at the centre; ST depression appears over the non-ischaemic region with its maximum not necessarily appearing at the opposite side of the location of the maximal ST elevation.

For transmural ischaemia of large regions, such as LAD or LCX ischaemia, there is a strong dipole of ST changes on the left lateral region on the epicardium with ST elevation on the ischaemic side and ST depression on the non-ischaemic side of the ischaemic boundary. The amplitude of ST change decreases towards the centre. A similar pattern of ST change appears on the endocardium with a lower amplitude because of immediate contact with the intracavitary blood. The source at the left lateral region gives rise to the dipole pattern of ST changes on the epicardium because only a limited amount of current can flow out of the heart, while the source at

the septum is not shown on the epicardium because it is surrounded by the intracavitary blood. On the body surface, ST elevation indicates the location of ischaemia with ST depression appearing at the opposite side of the torso. This ST depression is part of the source and also appears on the endocardium over the ischaemic region. If ST depression resulted from remote subendocardial ischaemia in the non-infarcted region, endocardial ST elevation would occur. Thus ST depression in transmural ischaemia is an integral part of the ischaemic source. Additional subendocardial ischaemia may coexist but would produce subendocardial ST elevation.

In conclusion:

1. ST depression is secondary to the current source at the lateral boundary of subendocardial ischaemia and thus does not localise the source.
2. ST depression associated with full thickness ischaemia is generated at the non-ischaemic side of the ischaemic boundary and is a part of the source.
3. The amount of epicardial ST depression with transmural ischaemia is related to the amount of the myocardium involved and is thus an excellent indicator of the ischaemic size.
4. Myocardial anisotropy does contribute to the observed ST changes.

8.2 Further work

There are a number of developments that can be considered for future work.

8.2.1 Effect of the narrow lateral boundary in torso model

In subendocardial ischaemia, the lateral ischaemic boundary has a narrower width than does the transmural boundary. Its effect is to increase the lateral source, thus increasing the amplitude of the ST depression over the left lateral region, as demonstrated in the 3D block model. It is expected that the same effect will occur on the ST depression on the body surface, although such a simulation was not performed

in the present study. This could be studied in the future when the myocardium is meshed into even smaller elements.

8.2.2 Distribution of transmembrane potential

The distribution of the transmembrane potential in the ischaemic region was assumed to be uniform in subendocardial and transmural ischaemia based on blood flow measurements. However, blood flow may not directly reflect the change in transmembrane potentials. There are also reports stating that a gradient in the ischaemic severity exists in the ischaemic region in terms of the transmembrane potentials. A further study could be carried out if the distribution of transmembrane potentials in ischaemia becomes available.

8.2.3 Anisotropy in a realistic geometry

The effect of the myocardial anisotropy on ST potential was studied in a simplified way, i.e. the myocardium was assumed to be in a 2D anisotropy and have no fibre rotations, and the heart was represented by a 3D block model. Although it was shown that the inclusion of anisotropy indeed makes the simulated results closer to the observations, myocardial anisotropy was not included in the realistic geometry, such as the isolated heart and the torso models. The following methods of including anisotropy may be used in the future. The myocardium is considered to have a 3D anisotropy and be formed from fibres of tissue constructed in spiral formations and forming sheets running parallel to the endocardium and epicardium. The conductivity of the myocardium is assumed to be 0.5, 0.2, and 0.08S/m in the fibre, sheet and cross-sheet directions respectively, from the literature. Elements having a similar direction can be gathered into one group which has an anisotropic conductivity. The direction of anisotropy for each finite element can be either obtained from fibre measurements or approximated from available data [154].

8.2.4 Other studies

As shown in this study, the myocardium can be precisely represented by the bidomain model in terms of the current source and the potential distribution. Thus it can be used to study QRS complex if the myocardium is meshed into fine elements to accurately define the wavefront. The bidomain model can also be used to study other components of the ECG in macroscopic level, such as T wave, TQ segment in normal and abnormal hearts.

Appendix A

Image presentation of ST potential

A.1 Subendocardial ischaemia

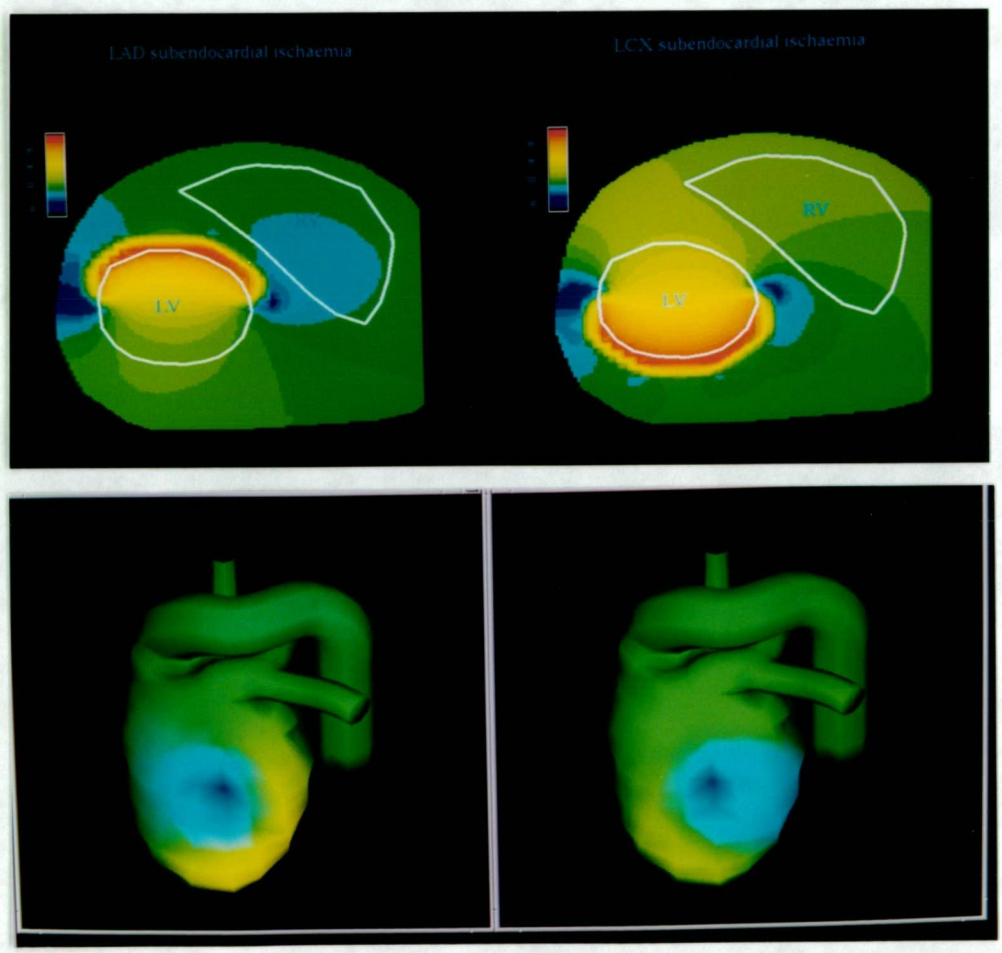

ST potential distribution on a cross-section of the heart (top) and on the epicardium (bottom) during LAD and LCX subendocardial ischaemia. Red colour indicates ST elevation, green colour zero potential, and blue colour ST depression.

A.2 Transmural ischaemia of small regions

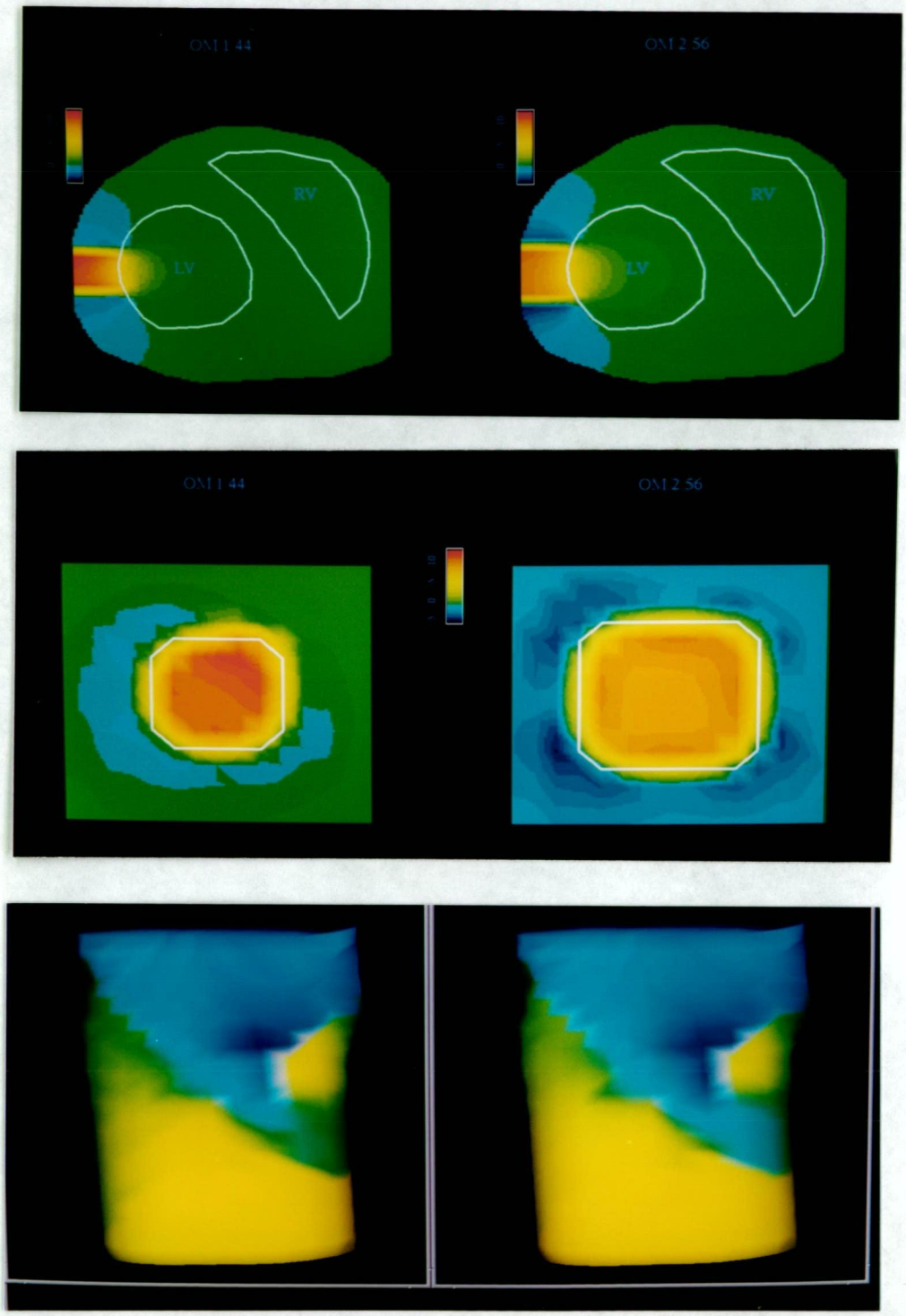

ST potential distribution on a cross-section of the heart (top), on the epicardial patch (middle) and on the body surface (bottom) during transmural ischaemia of a small region. Red colour indicates ST elevation, green colour zero potential, and blue colour ST depression.

A.3 Transmural ischaemia of large regions

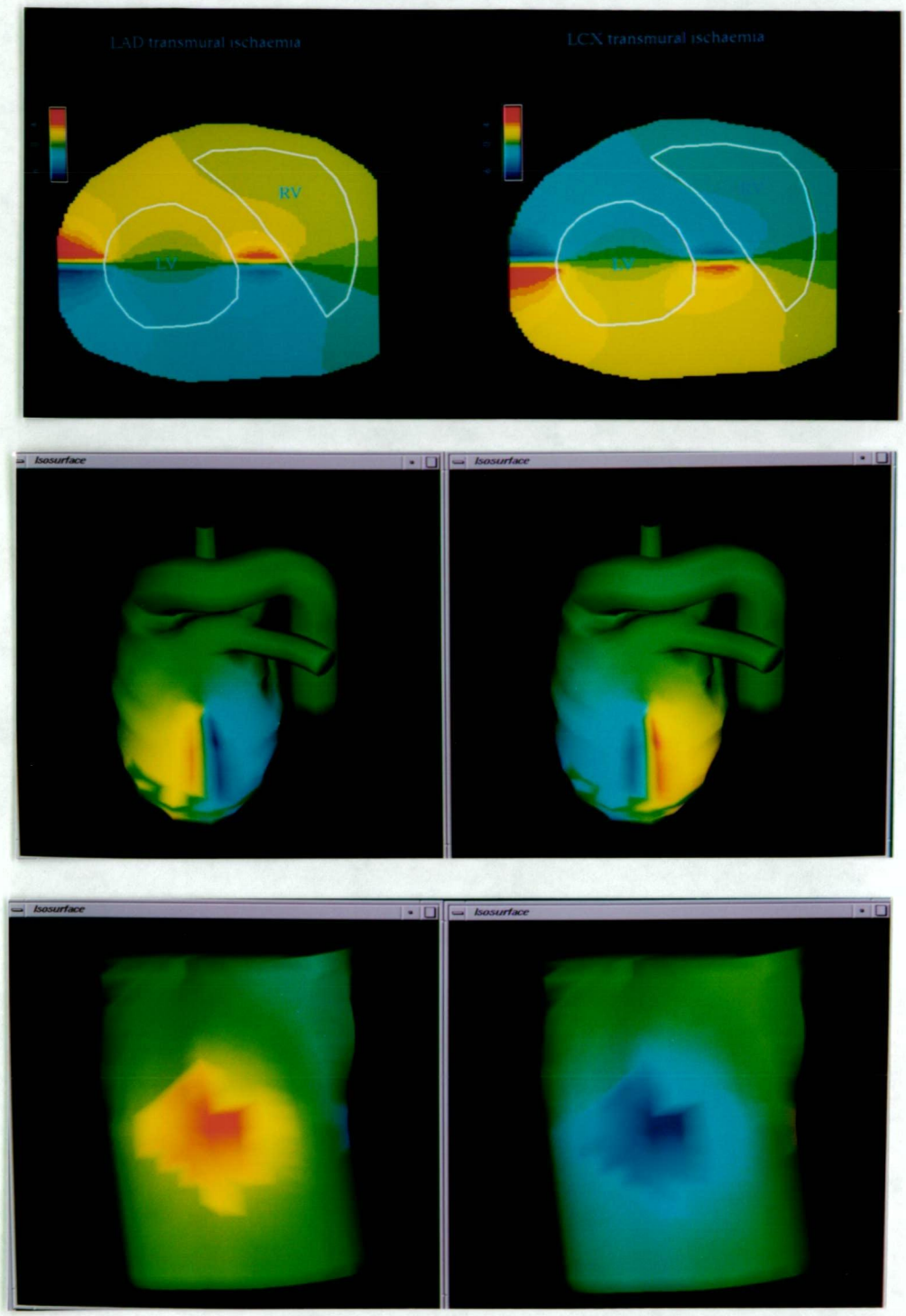

ST potential distribution on a cross-section of the heart (top), on the epicardium (middle) and on the body surface (bottom) during LAD and LCX transmural ischaemia. Red colour indicates ST elevation, green colour zero potential, and blue colour ST depression.

Bibliography

[1] R. F. Dunn, B. Freeman, I. K. Bailey, R. F. Uren, and D. T. Kelly. "Localisation of coronary artery disease with exercise electrocardiography" Correlation with thallium-201 myocardial perfusion scanning. *Am. J. Cardiol.*, 48:837–843, 1981.

[2] D. B. Mark, M. A. Hlatky, K. L. Lee, F. E. Harrell, Jr, R. M. Califf, and D. B. Pryor. Localising coronary artery obstructions with the exercise treadmill test. *Ann. Intern. Med.*, 106(1):53–55, Janurary 1987.

[3] I. Kubota, K. Ikeda, T. Ohyama M. Yamaki, S. Kawashima, A. Igarashi, K. Tsuiki, and Shoji Yasui. Body surface distribution of ST segment changes after exercise in effort angina pectoris without myocardial infarction. *Am. Heart J.*, 110(5):949–955, November 1985.

[4] D. S. Li, A. C. Yong, W. K. Pluta, and D. Kilpatrick. Origin of epicardial ST in the ischaemic sheep model. *Medical and Biological Engineering and Computing*, 34 (Suppl. 1)(2):101–102, 1996.

[5] D. Kilpatrick, S. J. Walker, and A. J. Bell. Importance of the great vessels in the genesis of the electrocardiogram. *Circ. Res.*, 66(4):1081–1087, April 1990.

[6] J. E. Muller, P. R. Maroko, and E. Braunwald. Precordial electrocardiographic mapping. A technique to assess the efficacy of interventions designed to limit infarct size. *Circulation*, 57(1):1–18, January 1978.

[7] K. J. J. Bruyneel. Use of moving epicardial electrodes in defining ST-segment changes after acute coronary occlusion in the baboon. Relation to primary ventricular fibrillation. *Am. Heart J.*, 89(6):731–741, June 1975.

[8] A. G. Kleber, M. J. Janse, F. J. L. van Capelle, and D. Durrer. Mechanism and time course of ST and TQ segment change during acute regional myocardial ischaemia in the pig heart determined by extracellular and intracellular recordings. *Circ. Res.*, 42(5):603–613, May 1978.

[9] D. S. Li, A. C. Yong, W. K. Pluta, and D. Kilpatrick. Epicardial and endocardial potential mapping of ST elevation in experimental myocardial infarction. *Medical and Biological Engineering and Computing*, 34 (Suppl. 1)(2):111–112, 1996.

[10] M. V. Cohen and E. S. Kirk. Reduction of epicardial ST-segment elevation following increased myocardial ischaemia: Experimental and theoretical demonstration. *Clin. Res.*, (abstr) 22:269A, 1974.

[11] H. J. Smith, B. N. Singh, R. M. Norris, M. B. John, and P. J. Hurley. Changes in myocardial blood flow and S-T segment elevation following coronary occlusion in dogs. *Circ. Res.*, 36:697–705, June 1975.

[12] M. K. Heng, B. N. Singh, R. M. Norris, M. B. John, and R. Elliot. Relationship between epicardial ST-segment elevation and myocardial ischaemic damage after experimental coronary artery occlusion in dogs. *J. Clin. Invest.*, 58:1317–1326, December 1976.

[13] R. G. Irvin and F. R. Cobb. Relationship between epicardial ST-segment elevation, regional myocardial blood flow, and extent of myocardial infarction in awake dogs. *Circulation*, 55(6):825–832, June 1977.

[14] C. C. Wolferth, S. Bellet, M. M. Livezey, and F. D. Murphy. Negative displacement of the RS-T segment in the electrocardiogram and its relationship to positive displacement: an experimental study. *Am. Heart J.*, 29:220–245, 1945.

[15] J. F. Richeson, T. Akiyama, and E. Schenk. A solid angle analysis of epicardial ischaemic TQ-ST deflection in the pig: A theoretical and experimental study. *Circ. Res.*, 43(6):879–888, December 1978.

[16] R. S. Gibson, R. S. Crampton, D. D. Watson, G. J. Taylor, B. A. Carabello, N. D. Holt, and G. A. Beller. Precordial ST-segment depression during acute inferior myocardial infarction: Clinical, scintigraphic and angiographic correlations. *Circulation*, 66(4):732–741, October 1982.

[17] M. S. Norell, J. P. Lyons, J. E. Gardener, C. A. Layton, and R. Balcon. Significance of "reciprocal" ST segment depression: Left ventriculographic observations during left anterior descending coronary angioplasty. *J. Am. Coll. Cardiol.*, 13(6):1270–1274, May 1989.

[18] E. H. Schuster and B. H. Bulkley. Ischaemia at a distance after acute myocardial infarction: A cause of early post-infarction angina. *Circulation*, 62(3):509–515, September 1980.

[19] K. Jennings, D. S. Reid, and D. G. Julian. "Reciprocal" depression of the ST segment in acute myocardial infarction. *Br. Med. J.*, 287:634–637, 1983.

[20] D. M. Mirvis. Physiologic bases for anterior ST segment depression in patients with acute inferior wall myocardial infarction. *Am. Heart J.*, 116(5):1308–1322, November 1988.

[21] D. S. Li. *Epicardial and endocardial ST potential mapping in ischaemia.* PhD thesis, University of Tasmania, Hobart, Tasmania, Australia, February 1997.

[22] R. M. Berne and M. N. Levy. *Cardiovasc. Physiol.*, chapter 2, pages 5–52. Mosby - Year Book, sixth edition, 1992.

[23] D. P. Zipes and J. Jalife, editors. *Cardiac electrophysiology: From cell to bedside*, chapter 8-10, pages 65–82. W. B. Sauders Company, The Curtis Centre, Independence Square West, Philadelphia, Pennsylvania 19106, USA, second edition, 1995.

[24] F. N. Wilson and R. H. Bayley. The electric field of an eccentric dipole in a homogeneous spherical conducting medium. *Circulation*, 1:84–92, 1950.

[25] E. Frank. Electric potential produced by two point current sources in a homogeneous conducting sphere. *J. Appl. Phys.*, 23:1225–1228, 1952.

[26] H. C. Burger, H. A. Tolhoek, and F. G. Backbier. The potential distribution on the body surface caused by a heart vector. Calculations on some simple models. *Am. Heart J.*, 48:249–263, 1954.

[27] R. M. Gulrajani. Models of the electrical activity of the heart and computer simulation of the electrocardiogram. *CRC Critical Reviews in Biomedical Engineering*, 16(1):1–66, 1988.

[28] A. M. Scher and A. C. Young. Frequency analysis of the electrocardiogram. *Circ. Res.*, 8:344–346, March 1960.

[29] A. S. Berson, F. Y. K. Lau, J. M. Wojick, and H. V. Pipberger. Distortions in infant electrocardiograms caused by inadequate high-frequency response. *Am. Heart. J.*, 93(6):730–734, 1977.

[30] Robert Plonsey. *Bioelectric Phenomena*, chapter 5, pages 202–275. McGraw-Hill Book Company, first edition, 1969.

[31] F. N. Wilson, A. G. Macleod, and P. S. Barker. The distribution of the currents of action and of injury displayed by heart muscle and other excitable tissues. *University of Michigan Studies (Scientific Series)*, 10:1–59, 1933.

[32] E. Frank. A comparative analysis of the eccentric double-layer representation of the human heart. *Am. Heart J.*, 46:364–378, 1953.

[33] A. van Oosterom. *Cardiac potential distributions.* PhD thesis, University of Amsterdam, Amsterdam, The Netherlands, 1978.

[34] W. T. Miller and D. B. Geselowitz. Simulation studies of the electrocardiology. I: The normal heart. *Circ. Res.*, 43(2):301–315, August 1978.

[35] A. E. Pollard, M. J. Burgess, and K. W. Spitzer. Computer simulations of three-dimension propagation in ventricular myocardium. *Circ. Res.*, 72(4):744–756, October 1993.

[36] W. Einthoven, G. Fahr, Translated by H. E. Hoff A. de Waart, and P. Sekelj. On the direction and manifest size of the variations of potential in the human heart and on the influence of the position of the heart on the form of the electrocardiogram. *Am. Heart J.*, 40(2):163–197, August 1950.

[37] B. Taccardi. La distribution spatiale des potentiels cardiaques (Spatial distribution of cardiac potentials). *Acta Cardiologica*, 13(2):173–189, 1958.

[38] H. A. Haus and J. R. Melcher. *Electromagnetic Fields and Energy*, chapter 4, pages 109–111. Prentice-Hall. Inc., Englewood Cliffs, New Jersey 07632, USA, 1989.

[39] B. Taccardi. Distribution of heart potentials on the thoracic surface of normal human subjects. *Circ. Res.*, 12:341–352, 1963.

[40] R. H. Selvester, J. C. Solomon, and T. L. Gillespie. Digital computer model of a total body electrocardiographic surface map: An adult male-torso simulation with lungs. *Circ. Res.*, 38:684–690, October 1968.

[41] D. B. Geselowitz. Multipole representation for an equivalent cardiac generator. *Proc. Inst. Radio Engrs.*, 48:75–79, 1960.

[42] R. H. Okada. A critical review of vector electrocardiography. *IEEE Trans. Biomed. Eng.*, 10(1):95–98, July 1963.

[43] D. Gabor and C. V. Nelson. Determination of the resultant dipole of the heart from measurements on the body surface. *J. Applied Physics*, 25(4):413–416, April 1954.

[44] R. H. Selvester, C. R. Collier, and R. B. Pearson. Analog computer model of vectorcardiogram. *Circulation*, 31:45–53, January 1965.

[45] R. H. Selvester, R. Kalaba, C. R. Collier, and R. Bellmanand H. Kagiwada. A digital computer model of the vectorcardiogram with distance and boundary effects: simulated myocardial infarction. *Am. Heart J.*, 74(6):792–808, December 1967.

[46] A. M. Scher and A. C. Young. The pathway of ventricular depolarisation in the dog. *Circ. Res.*, 4:461–469, 1956.

[47] H. L. Gelernter and J. C. Swihart. A mathematical-physical model of the genesis of the electrocardiogram. *Biophys. J.*, 4:285–301, 1964.

[48] P .S. Thiry and R. M. Rosenberg. On electrophysiological activity of the normal heart. *J. Franlin Inst.*, 297(5):377–396, May 1974.

[49] D. Durrer, R. T. Dam, G E. Freud, M. J. Janse, F. L. Meijler, and R. C. Arzbecher. Total excitation of the isolated human heart. *Circulation*, 41:899–912, June 1970.

[50] B. N. Cuffin and D. B. Geselowitz. Studies of the electrocardiogram using realistic cardiac and torso models. *IEEE Trans. Biomed. Eng.*, 24(3):242–252, May 1977.

[51] A. C. Barnard, I. M. Duck, M. S. Lynn, and W. P. Timlake. The application of electromagnetic theory to electrocardiology. II. Numerical solution of the integral equations. *Biophys. J.*, 7(5):463–491, 1967.

[52] J. M. Hlavin and P. Plonsey. An experimental determination of a multipole representation of a turtle heart. *IEEE Trans. Biomed. Eng.*, 10:98–105, July 1963.

[53] D. B. Geselowitz. On bioelectric potentials in an inhomogeneous volume conductor. *Biophys. J.*, 7:1–11, 1967.

[54] R. M. Arthur, D. B. Geselowitz, S. A. Briller, and R. F. Trost. Quadrupole components of the human surface electrocardiogram. *Am. Heart J.*, 83(5):663–677, May 1972.

[55] P. Savard, F. A. Roberge, J. Perry, and R. A. Nadeau. Representation of cardiac electrical activity by a moving dipole for normal and ectopic beats in the intact dog. *Circ. Res.*, 46:415–425, 1980.

[56] P. Savard, A. Ackaoui, R. M. Gulrajani, R. A. Nadeau, F. A. Roberge, R. Guardo, and B. Dube. Localisation of cardiac ectopic activity in man by a single moving dipole. Comparison of different computation techniques. *J. Electrocardiol.*, 18(3):211–222, 1985.

[57] Y. Rudy and R. Plonsey. The eccentric spheres model as a basis for a study of the role of geometry and inhomogeneities in electrocardiography. *IEEE Trans. Biomed. Eng.*, 26(7):392–399, 1979.

[58] J. C. Solomon and R. H. Selvester. Current dipole moment density of the heart. *Am. Heart J.*, 81(3):351–360, March 1971.

[59] A. van Oosterom and R. T. van Dam. Potential distribution in the left ventricular wall during depolarisation. *Adv. Cardiol.*, 16:27–31, 1976.

[60] R. P. Holland and H. Brooks. Precordial and epicardial surface potentials during myocardial ischaemia in the pig: A theoretical and experimental analysis of TQ and ST segments. *Circ. Res.*, 37:471–480, October 1975.

[61] R. P. Holland, H. Brooks, and B. Lidl. Spatial and nonspatial influences on the TQ-ST segment deflection of ischaemia. *J. Clin. Invest.*, 60:197–214, July 1977.

[62] L. Tung. *A bidomain model for describing ischaemic myocardial DC potentials.* PhD thesis, M.I.T., Cambridge, Massachusetts, USA, 1978.

[63] B. J. Roth and J. P. Wikswo. A bidomain model for the extracellular potential and magnetic field of cardiac tissue. *IEEE Trans. Biomed. Eng.*, 33(4):467–469, April 1986.

[64] J. P. Barach and J. Wikswo. Magnetic fields from simulated cardiac action currents. *IEEE Trans. Biomed. Eng.*, 41(10):969–974, October 1994.

[65] P. Colli-Franzone, L. Guerri, and B. Taccardi. Potential distributions generated by point stimulation in a myocardial volume: Simulation studies in a model of anisotropic ventricular muscle. *J. Cardiovasc. Electrophysiol.*, 4(4):438–458, August 1993.

[66] N. G. Sepulveda, B. J. Roth, and J. P. Wikswo. Current injection into a two-dimensional anisotropic bidomain. *Biophys. J.*, 55:987–999, May 1989.

[67] B. J. Roth. Action potential propagation in a thick strand of cardiac muscle. *Circ. Res.*, 68(1):162–173, January 1991.

[68] N. A. Trayanova and T. C. Pilkington. A bidomain model with periodic intracellular junctions: a one-dimension analysis. *IEEE Trans. Biomed. Eng.*, 40(5):424–433, May 1993.

[69] N. A. Trayanova, B. J. Roth, and L. J. Malden. The response of a spherical heart to a uniform electric field: a bidomain analysis of cardiac stimulation. *IEEE Trans. Biomed. Eng.*, 40(9):899–908, September 1993.

[70] W. T. Miller and D. B. Geselowitz. Simulation studies of the electrocardiogram. II: Ischaemia and infarction. *Circ. Res.*, 43(2):315–323, August 1978.

[71] M. Aoki, Y. Okamoto, T. Musha, and K. I. Harumi. Three-dimensional simulation of the ventricular depolarisation and repolarisation processes and body surface potentials: normal heart and bundle branch block. *IEEE Trans. Biomed. Eng.*, 34(6):455–462, June 1987.

[72] M. S. Spach, R. C. Barr, G. A. Koostey, and E. A. Johnson. Extracellular potentials related to intracellular action potential in the dog Purkinje system. *Circ. Res.*, 30:505–519, 1972.

[73] M. S. Spach and R. C. Barr. Origin of epicardial ST-T wave potentials in the intact dog. *Circ. Res.*, 39:475–487, 1976.

[74] Stanley Rush, J. A. Abildskov, and Richard Mcfee. Resistivity of body tissues at low frequencies. *Circ. Res.*, 12:40–50, January 1963.

[75] L. Clerc. Directional difference of impulse spread in trabecular muscle from mammalian heart. *J. Physiol.*, 255:335–346, 1976.

[76] D. D. Streeter, H. M. Spotnitz, D. P. Patel, J. Ross, Jr, and E. H. Sonnenblick. Fibre orientation in canine left ventricle during diastole and systole. *Circ. Res.*, 24:339–347, March 1969.

[77] B. J. Roth. Electrical conductivity values used with the bidomain model of cardiac tissue. *IEEE Trans. Biomed. Eng.*, 44(4):325–328, April 1977.

[78] A.G. Kleber, C. B. Riegger, and M. J. Janse. Electrical uncoupling and increase of extracellular resistance after induction of ischaemia in isolated, arterially perfused rabbit papillary muscle. *Circ. Res.*, 61(2):271–279, August 1987.

[79] D. E. Roberts and A. M. Scher. Effect of tissue anisotropy on extracellular potential fields in canine myocardium in situ. *Circ. Res.*, 50(3):342–351, March 1982.

[80] D. E. Roberts, L. T. Hersh, and A. M. Scher. Influence of cardiac fibre orientation on wavefront voltage, conduction velocity, and tissue resistivity in the dog. *Circ. Res.*, 44(5):701–712, May 1979.

[81] D. E. Roberts, L. T. Hersh, and A. M. Scher. Influence of cardiac fibre orientation on wavefront voltage, conduction velocity, and tissue resistivity in the dog. *Circ. Res.*, 44(5):701–712, May 1979.

[82] L. V. Corbin and A. M. Scher. The canine heart as an electrocardiographic generator. Dependence on cardiac cell orientation. *Circ. Res.*, 41(1):58–67, July 1977.

[83] P. Colli-Franzone, L. Guerri, and C. Viganotti et al. Potential fields generated by oblique dipole layers modelling excitation wavefront in the anisotropic myocardium. *Circ. Res.*, 51(3):330–346, September 1982.

[84] M. S. Spach, W. T. Miller, E. Miller-Jones, R. B. Warren, and R. C. Barr. Extracellular potentials related to intracellular action potentials during impulse conduction in anisotropic canine cardiac muscle. *Circ. Res.*, 45(2):188–204, August 1979.

[85] N. G. Sepulveda and J. P. Wikswo. Electric and magnetic fields from two-dimensional anisotropic bisyncytia. *Biophys. J.*, 51:557–568, April 1987.

[86] R. Plonsey and R. C. Barr. Current flow patterns in two-dimensional anisotropic bisyncytia with normal and extreme conductivities. *Biophys. J.*, 45:557–571, March 1984.

[87] D. Wei, O. Okazaki, K. Harumi, K. Harumi, E. Harasawa, and H. Hosaka. Comparative simulation of excitation and body surface electrocardiogram with isotropic and anisotropic computer heart models. *IEEE Trans. Biomed. Eng.*, 42(4):343–357, April 1995.

[88] M. Lorange and R. M. Gulrajani. A computer heart model incorporating anisotropic propagation. *J. Electrocardiol.*, 26(4):245–261, October 1993.

[89] C. Y. Li, D. Kilpatrick, P. R. Johnston, and D. S. Li. A bidomain model of ST changes during subendocardial ischaemia. In *Bridging Disciplines For Biomedicine: 18th Annual International Conference of The IEEE Engineering in Medicine and Biology Society*, page 102, Paper number 1083, 31 October - 3 November 1996.

[90] W. E. Samson and A. M. Scher. Mechanism of ST segment alteration during acute myocardial injury. *Circ. Res.*, 8:780–787, July 1960.

[91] M. Prinzmetal, K. Ishikawa, M. Nakashima, H. Oishi, E. Ozkan, J. Wakayama, and J. Baines. Correlation between intracellular and surface electrograms in acute myocardial ischaemia. *J. Electrocardiol.*, 1(2):161–166, 1968.

[92] E. Downar, M. J. Janse, and D. Durrer. The effect of acute coronary artery occlusion on subepicardial transmembrane potentials in intact porcine heart. *Circulation*, 56(2):217–224, August 1977.

[93] M. J. Janse and Andre G. Kleber. Electrophysiological changes and ventricular arrhythmias in the early phase of regional myocardial ischaemia. *Circ. Res.*, 49(5):1069–1081, November 1981.

[94] H. Morena, M. J. Janse, J. W. T Fiolet, W. J. G. Krieger, H. Crijns, and D. Durrer. Comparison of the effects of regional ischaemia, hypoxia, hyperkalemia and acidosis on intracellular and extracellular potentials and metabolism in the isolated porcine heart. *Circ. Res.*, 46(5):634–646, May 1980.

[95] H. A. Fozzard and P. S. DasGupta. ST segment potentials and mapping: Theory and experiments. *Circulation*, 54(3):533–537, September 1976.

[96] D. Cohen, P. Savard, R. D. Difkin, E. Lepeschkin, and W. E. Strauss. Magnetic measurement of ST and TQ segment shifts in human. *Circ. Res.*, 53(2):274–279, August 1983.

[97] D. E. Euler, J. F. Spear, and E. N. Moore. Effect of coronary occlusion on arrhythmias and conduction in the ovine heart. *Am. J. Physiol.*, 245:H82–H89, 1983.

[98] L. J. Markovitz, E. B. Savage, M. B. Ratcliffe, J. E. Bavaria, G. Kreiner, R. V. Iozzo, W. C. Hargrove, III, D. K. Bogen, and L. H. Edmunds, Jr. Large animal model of left ventricular aneurysm. *Ann. Thorac. Surg.*, 48:838–845, 1989.

[99] D. J. Hearse and D. M. Yellon. The "border zone" in evolving myocardial infarction: controversy or confusion? *Am. J. Cardiol.*, 47:1321–1334, 1981.

[100] K. A. Reimer and R. B. Jennings. The "wavefront phenomenon" of myocardial ischaemic cell death. *Lab. Invest.*, 40(6):633–644, 1979.

[101] D. M. Yellon, D. J. Hearse, R. Crome, J. Grannel, and R. K. H. Wyse. Characterisation of the lateral interface between normal and ischaemic tissue in the canine heart during evolving myocardium infarction. *Am. J. Cardiol.*, 47:1233–1239, 1981.

[102] R. H. Murdock, D. M. Harlan, J. J. Morris, W. W. Pryor, and F. R. Cobb. Transitional blood flow zones between ischaemic and nonischaemic myocardium in the awake dog. *Circ. Res.*, 52(4):451–459, April 1983.

[103] M. J. Janse, J. Cinca. H. Morena, J. W. T. Fiolet, A. G. Kleber, G. P. de Vries, A . E. Becker, and D. Durrer. The "border zone" in myocardial ischaemia. An electrophysiological, metabolic, and histochemical correlation in the pig heart. *Circ. Res.*, 44(4):576–588, April 1979.

[104] P. R. Maroko, J. K. Kjekshus, B. E. Sobel, T. Watanabe, J. W. Covell, J. Ross, and E. Braunwald. Factors influencing infarct size following experimental coronary artery occlusions. *Circulation*, 43:67–82, January 1971.

[105] D. J. Hearse, L. H. Opie, I. E. Katzeff, W. F. Lubbe, T. J. van der Werff, M. Peisach, and G. Boulle. Characterisation of the "border zone" in acute regional ischaemia in the dog. *Am. J. Cardiol.*, 40:716–726, November 1977.

[106] L. C. Becker, R. Ferreira, and M. Thomas. Mapping of left ventricular blood flow with radioactive microspheres in experimental coronary artery occlusion. *Cardiovasc. Res.*, 7:391–400, 1973.

[107] M. L. Marcus, R. E. Kerber, and J. Ehrhardt. Three dimensional geometry of acutely ischaemic myocardium. *Circulation*, 52:254–263, August 1975.

[108] D. S. Li, A. C. Yong, and D. Kilpatrick. Validation of a subendocardial ischaemia sheep model by intra-coronary fluorescent microspheres. *Clin. Exp. Pharmacol. Physiol.*, 23:111–118, 1996.

[109] F. N. Wilson, I. G. W. Hill, and F. D. Johnston. The interpretation of the galvanometric curves obtained when one electrode is distant from the heart and the other near or in contact with the ventricular surface. I. Observation on the cold-blood heart. *Am. Heart J.*, 10:163–175, 1934.

[110] F. N. Wilson, F. D. Johnston, and I. G. W. Hill. The interpretation of the galvanometric curves obtained when one electrode is distant from the heart and the other near or in contact with the ventricular surface. II. Observation on the mammalian heart. *Am. Heart J.*, 10:176–189, 1934.

[111] R. D. Pruitt, R. M. Rochester, and F. Valencia. Immediate electrocardiographic effects of circumscribed myocardial injuries; An experimental study. *Am. Heart J.*, 35(2):161–197, February 1948.

[112] L. Rakita, J. L. Borduas, S. Rothman, and M. Prinzmetal. Studies on the mechanism of ventricular activity. XII. Early changes in the RS-T segment

and QRS complex following acute coronary artery occlusion: experimental study and clinical applications. *Am. Heart J.*, 48:351–372, 1954.

[113] D. M. Mirvis, F. W. Keller, R. E. Ideker, D. G. Zettergren, and R. F. Dowdie. Equivalent generator properties of acute ischaemic lesions in the isolated rabbit heart. *Circ. Res.*, 42(5):676–685, May 1978.

[114] K. Maehara, H. Kyona, S. Kitaoka, Y. Shimizu, Y. Maruyama, K. Ashikawa E. Eiji-Oka, and T. Takishima. A comparison of ST segment deviation and calculated solid angle during acute regional ischaemia in the isolated canine heart at precordial, epicardial and intramyocardial lead surfaces. *J. Electrocardiol.*, 19(3):235–246, 1986.

[115] P. S. Thiry, R. M. Rosenberg, and J. A. Abbott. A mechanism for the electrocardiogram response to left ventricular hypertrophy and acute ischaemia. *Circ. Res.*, 36:92–104, January 1975.

[116] R. P. Holland and H. Brooks. TQ-ST segment mapping: Critical review and analysis of current concepts. *Am. J. Cardiol.*, 40:110–133, July 1977.

[117] R. P. Holland and M. F. Arnsdorf. Solid angle theory and the electrocardiogram: Physiologic and quantitative interpretations. *Prog. Cardiol. Dise.*, 19:431–457, 1977.

[118] G. T. Smith, G. Geary, W. Ruf, T. H. Roelofs, and J. J. McNamara. Epicardial mapping and electrocardiographic models of myocardial ischaemic injury. *Circulation*, 60(4):930–938, October 1979.

[119] G. T. Smith, G. G. Geary, W. Blanchard, T. H. Roelofs, W. Ruf, and J. J. McNamara. An electrocardiographic model of myocardial ischaemic injury. *J. Electrocardiology*, 16(3):223–233, 1983.

[120] J. Hyttinen. *Development of regional aimed ECG leads especially for myocardial ischaemia diagnosis.* PhD thesis, Tampere University of Technology, Tampere, Finland, 1994.

[121] B. Dube, R. M. Gulrajani, M. Lorange, A. R. Leblanc, J. Nasmith, and R. A. Nadeau. A computer heart model incorporating anisotropic propagation. 4. Simulation of regional myocardial ischaemia. *J. Electrocardiol.*, 29(2):91–103, 1996.

[122] R. A. Guyton, J. H. Mcclenathan, G. E. Newman, and L. L. Michaelis. Significance of subendocardial ST segment elevation caused by coronary stenosis in the dog: Epicardial ST segment depression, local ischaemia and subsequent necrosis. *Am. J. Cardiol.*, 40:373–380, September 1977.

[123] G. M. Vincent, J. A. Abildskov, and M. J. Burgess. Mechanism of ischaemic ST segment displacement. *Circulation*, 56(4):559–566, October 1977.

[124] D. M. Mirvis. Differential electrocardiographic effects of myocardial ischaemia induced by atrial pacing in dogs with various locations of coronary stenosis. *Circulation*, 68(5):1116–1126, November 1983.

[125] D. M. Mirvis, K. B. Ramanathan, and J. L. Wilson. Regional blood flow correlates of ST segment depression in tachycardia-induced myocardial ischaemia. *Circulation*, 73(2):365–373, February 1986.

[126] R. M. Fuchs, S. C. Achuff, L. Grunwald, F. C. P. Tin, and L. S. C. Griffith. Electrocardiographic localisation of coronary artery narrowing: Studies during myocardial ischaemia and infarction in patients with one-vessel disease. *Circulation*, 66(6):1168–1176, December 1982.

[127] T. Nakajima, K. Kawakubo, I. Toda, S. Mashima, T. Ohtake, M. Iio, and T. Sugimoto. ST-T isointegral analysis of exercise stress body surface mapping for identifying ischaemic areas in patients with angina pectoris. *Am. Heart J.*, 115(5):1013–1021, May 1988.

[128] I. Kubota, K. Hanashima, K. Ikeda, K. Tsuiki, and Shoji Yasui. Detection of diseased coronary artery by exercise ST-T maps in patients with effort angina pectoris, single-vessel disease, and normal ST-T wave on electrocardiogram at rest. *Circulation*, 80(1):120–127, July 1989.

[129] S. J. Walker and D. Kilpatrick. Forward and inverse electrocardiographic calculations using resistor network models of the human torso. *Circ. Res.*, 61(4):504–513, October 1987.

[130] D. Kilpatrick and S. J. Walker. A validation of derived epicardial potential distributions by prediction of the coronary artery involved in acute myocardial infarction in humans. *Circulation*, 76(6):1282–1289, December 1987.

[131] L. S. Green, B. Taccardi, P. R. Ershler, and R. L. Lux. Effects of conducting media on isopotential and isochrone distributions. *Circulation*, 84(6):2513–2521, December 1991.

[132] A. H. Katcher, G. Peirce, and J. J. Sayen. Effects of experimental regional ischaemia and levarterenol on the RS-T segment and baseline of ventricular surface electrocardiograms obtained by direct-coupled amplification. *Circ. Res.*, 8:29:43, January 1960.

[133] M. Prinzmetal, H. Toyoshima, A. Ekmekci, Y. Mizuno, and T. Nagaya. Myocardial ischaemia: Nature of ischaemia electrocardiographic patterns in the mammalian ventricles as determined by intracellular electrographic and metabolic changes. *Am. J. Cardiol.*, 8:493–503, October 1961.

[134] M. H. Crawford, R. A. O'Rourke, and F. L. Grover. Mechanism of inferior electrocardiographic ST-segment depression during acute anterior myocardial infarction in a baboon model. *Am. J. Cardiol.*, 54:1114–1117, November 1984.

[135] J. F. Brymer, F. Khaja, M. Marzilli, and S. Goldstein. "Ischaemia at a distance" during intermittent coronary artery occlusion: a coronary anatomic explanation. *J. Am. Coll. Cardiol.*, 6:41–45, 1985.

[136] C. K. Wong, S. B. Freeman, G. Bautovich, B. P. Bailey, L. Bernstein, and D. T. Kelly. Mechanism and significance of precordial ST-segment depression during inferior wall acute myocardial infarction associated with severe narrowing of the dominant right coronary. *Am. J. Cardiol.*, 71:1025–1030, May 1993.

[137] C. H. Croft, W. Woodward, P. Nicod, J. R. Corbett, S. E. Lewis, J. T. Willerson, and R. E. Rude. Clinical implications of anterior ST segment depression in patients with acute inferior myocardial infarction. *Am. J. Cardiol.*, 50:428–436, September 1982.

[138] D. W. Ferguson, N. Pandian, J. M. Kioschos, M. L. Marcus, and C. W. White. Angiographic evidence that reciprocal ST-segment depression during acute myocardial infarction does not indicate remote ischaemia: Analysis of 23 patients. *Am. J. Cardiol.*, 53:55–62, January 1984.

[139] A. A. Quyyumi, T. Crake, M. B. Rubens, R. D. Levy, A. F. Rickards, and K. M. Fox. Importance of "reciprocal" electrocardiographic changes during occlusion of left anterior descending coronary artery. *The Lancet*, 15:347–350, February 1986.

[140] O. H. Kracoff, A. G. Adelman, J. F. Marquis, A. Caspi, H. E. Aldridge, and L. Schwartz. Twelve-lead electrocardiogram recording during percutaneous transluminal coronary angioplasty. *J. Electrocardiol.*, 23(3):191–198, July 1990.

[141] D. Kilpatrick, A. J. Bell, and S. J. Walker. Derived epicardial potential differentiate ischaemic ST depression from ST depression secondary to ST elevation in acute inferior myocardial infarction in humans. *J. Am. Coll. Cardiol.*, 14(3):695–702, September 1989.

[142] P. R. Maroko and E. Braunwald. Modification of myocardial infarction size after coronary occlusion. *Ann. Intern. Med.*, 79(5):720–733, November 1973.

[143] J. E. Muller, P. R. Maroko, and E. Braunwald. Evaluation of precordial electrocardiographic mapping as a means of assessing changes in myocardial ischaemic injury. *Circulation*, 52:16–27, July 1975.

[144] R. J. Capone, A. S. Most, and P. A. Sydik. Precordial ST segment mapping. A sensitive technique for the evaluation of myocardial injury? *Chest*, 67(5):577–582, May 1975.

[145] F. N. Fore, G. T. Smith, and J. J. McNamara. Prediction of infarct size with baboons. *Circ. Res.*, 43(3):455–465, September 1978.

[146] T. J. Gale. *Modelling the electric field from implantable defibrillators.* PhD thesis, University of Tasmania, Hobart, Tasmania, Australia, August 1995.

[147] R. Plonsey. Quantitative formulations of electrophysiological sources of potential fields in volume conductors. *IEEE Trans. Biomed. Eng.*, 31(12):868–872, December 1984.

[148] D. S. Li, A. C. Yong, and D. Kilpatrick. Spatial myocardial blood flow distribution in the ovine heart in pacing-induced tachycardia, subendocardial ischaemia and transmural ischaemia. In *45th Annual Scientific Meeting of the Cardiac Society of Australia and New Zealand*, page 245, 10-13 August 1997.

[149] G. Beer and J. O. Watson. *Introduction to finite and boundary element methods for engineers.* John Wiley & Sons Ltd, Baffins Lane, Chichester, West Sussex PO19 1UD, England, 1992.

[150] W. F. Ames. *Numerical methods for partial differential equations*, chapter 1, pages 15–19. Academic Press, Inc., 111 Fifth Avenue, New York, New York 10003, USA, second edition, 1977.

[151] M. J. Janse, F. J. L. van Capelle, H. Morsink, A. G. Kleber, F. Wilms-Schopman, R. Cardinal, C. N. D'Alnoncourt, and D. Durrer. Flow of "injury" current and pattern of excitation during early ventricular arrhythmias in acute regional myocardial ischaemia in isolated porcine and canine hearts: Evidence for two different arrhythmogenic mechanisms. *Circ. Res.*, 47(2):151–165, August 1980.

[152] D. A. Brody. A theoretical analysis of intracavitary blood mass influence on the heart-lead relationship. *Circ. Res.*, 4:731–738, 1956.

[153] R. M. Gulrajani and G. E. Mailloux. A simulation study of the effects of torso inhomogeneities on electrocardiographic potentials, using realistic heart and torso models. *Circ. Res.*, 52:45–56, 1983.

[154] P. M. F. Nielson, I. J. Le Crice, B. H. Smaill, and P. J. Hunter. Mathematical model of geometry and fibrous structure of the heart. *Am. J. Physiol.*, 260:H1365–H1378, 1991.